PB89-152912

Final Report

A FUNDAMENTAL STUDY OF RESPIRATORY AIR FILTRATION

Grant # 1 RO1 OHO1485-01A1
Center for Disease Control
Public Health Service
U. S. Department of Health and Human Services

Volume 2

Report Prepared by:

Benjamin Y. H. Liu and Behzad Fardi
Particle Technology Laboratory
Mechanical Engineering Department
University of Minnesota
Minneapolis, Minnesota 55455

Submitted by:

Benjamin Y. H. Liu
Principal Investigator
Telephone: 612-625-6574

Particle Technology Laboratory Publication No. 680

September, 1988

50272-101

REPORT DOCUMENTATION PAGE	1. REPORT NO.	2.	3. Recipient's Accession No. PB89 152912/AS
4. Title and Subtitle A Fundamental Study of Respiratory Air Filtration, Volume 2			5. Report Date 88/09/00
			6.
7. Author(s) Liu, B. Y. H., and B. Fardi			8. Performing Organization Rept. No.
9. Performing Organization Name and Address Mechanical Engineering Department, University of Minnesota, Minneapolis, Minnesota			10. Project/Task/Work Unit No.
			11. Contract (C) or Grant(G) No. (C) (G) R01-OH-01485
12. Sponsoring Organization Name and Address			13. Type of Report & Period Covered
			14.

15. Supplementary Notes

16. Abstract (Limit: 200 words) The purpose of this grant was to study characteristics of particulate air filters used in respiratory protective devices. In particular, efforts were made to determine the overall efficiency of the filters as a function of particle size and as a function of the velocity of air flow through the filter. A determination was also made of the resistance of the filter media to the flow of air. This specific report contained material from the final three chapters of the Grant Final Report. A numerical simulation model was designed and applied to the study of particle collection by electrically charged filter fibers. The results of dimensionless viscous drag calculations on rectangular fibers were presented along with information regarding single electret fiber capture efficiency results due to the Brownian diffusion, interception, or electrostatics. Single fiber capture efficiency was found to be proportional to 0.778, 0.54, and 0.15 powers of the solid volume fraction for the diffusion, interception, and Coulombic force interaction mechanisms, respectively, when an individual mechanism prevailed. The peak penetration of both solid monodisperse sodium-chloride particles and liquid DOP particles through respirator filters ranged from 1.2 to 30 percent at 16 liters per minute (lmp), from 3.5 to 37 percent at 28lpm, and from 6 to 45 percent at 48lpm.

17. Document Analysis a. Descriptors

b. Identifiers/Open-Ended Terms NIOSH-Publication, NIOSH-Grant, Grant-Number-R01-OH-01485, End-Date-08-30-1986, Respirators, Personal-protective-equipment, Respiratory-protective-equipment, Filter-materials, Mathematical-models

c. COSATI Field/Group

18. Availability Statement	19. Security Class (This Report)	21. No. of Pages 206
	22. Security Class (This Page)	22. Price

(See ANSI-Z39.18) *See Instructions on Reverse* OPTIONAL FORM 272(4-77) (Formerly NTIS-35) Department of Commerce

Chapter 5

NUMERICAL RESULTS

The results of calculations of the dimensionless drag and single fiber capture efficiency due to the Brownian diffusion, interception, and electrostatic mechanisms for rectangular fibers with various aspect ratios are presented and discussed below in the above-listed order. In addition, the effects of the solid-volume fraction and other dimensionless parameters corresponding to each collection mechanism on the results will be discussed also.

5.1 Results of Dimensionless Viscous Drag Calculations on Rectangular Fibers

The dimensionless drag, F^*, on a rectangular fiber was shown earlier to be functionally dependent only on α and b/w if the value of the Reynolds number based on the fiber hydraulic diameter were below 0.2 . The calculated values of F^* vs. α for several values of b/w have been tabulated in Table 5.1 and plotted in Figure 5.1. As shown, F^* is indeed a function of both parameters but its dependency on b/w is rather interesting i.e. for values of $b/w > 1$, F^* is found to be nearly independent of b/w and a function of α only

Table 5.1 Calculated values of the dimensionless drag on rectangular fibers with different aspect ratios as a function of the filter solid-volume fraction

α	F^* (Kuwabara)	F^* (b/w = 1/4)	F^* (b/w = 1/3)	F^* (b/w = 1/2)	F^* (b/w = 1/1)	F^* (b/w = 2/1)
0.005	6.599	8.524	7.908	7.245	6.542	6.256
0.008	7.515	10.256	9.396	8.486	7.521	7.111
0.020	10.250	16.545	14.556	12.582	10.616	9.779
0.050	15.762	35.494	28.377	22.346	17.179	15.130
0.070	19.380					
0.080	21.253	67.617	48.668	34.145	24.008	20.389
0.100	25.194					
0.150	36.643	365.230	154.755	78.560		35.112
0.200	51.350	2928.160	428.655	140.935	64.292	49.953
0.300	97.048					
0.400	184.405					
0.500	368.800					

Table 5.1 (continued)

α	F^* (b/w=3/1)	F^* (b/w=4/1)	F^* (b/w=5/1)	F^* (b/w=6/1)
0.005	6.245	6.326		
0.008	7.087	7.170		
0.020	9.678	9.753		
0.050	14.830	14.964		15.539
0.070			18.906	
0.080	19.901	20.201	20.894	21.740
0.100			25.310	26.960
0.150	35.113	37.775	41.961	
0.200	53.629	62.930		
0.300				
0.400				
0.500				

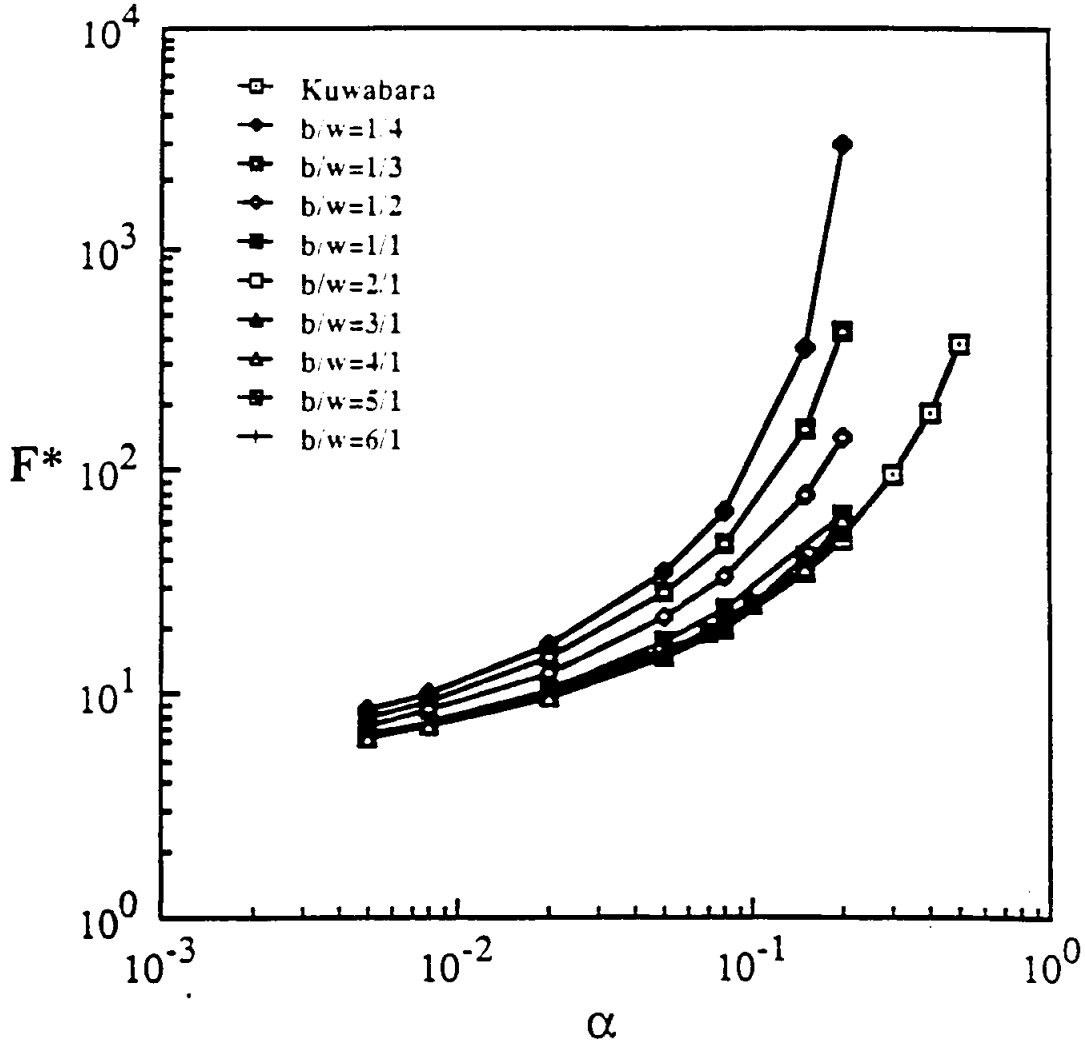

Figure 5.1 Effect of the filter solid-volume fraction on the values of F^* on rectangular fibers with different aspect ratios and for Re values below 0.2

while, for values of $b/w \leq 1$ and moderate values of α, F^* increases rapidly as b/w decreases. Furthermore, for the sake of comparison, the analytical results of Kuwabara (equation (4.24)) for the case of cylindrical fibers have also been plotted in Figure 5.1 and as seen, they appear to be in very good agreement with the F^* values obtained for the case of rectangular fibers with $b/w > 1$. Note also that all the curves corresponding to different b/w values tend to merge into one curve as the value of α decreases suggesting that the value of the dimensionless drag on a single, isolated rectangular fiber ($\alpha \rightarrow 0$) situated normal to a viscous flow with $Re \leq 0.2$ is constant and independent of the fiber aspect ratio.

5.2 Single Electret Fiber Capture Efficiency Results Due to the Brownian Diffusion

The calculation of the diffusion single fiber efficiency values was carried out assuming point-mass particles diffusing towards surface of a rectangular fiber. The single fiber efficiency values were obtained for several fibers with different aspect ratios, b/w ,ranging in value from 0.1 to 10 and for values of the Peclet number, $Pe = \frac{U_o D_h}{D}$, from 2 to 40,000 and packing density, $\alpha = 0.02, 0.08, 0.16$. The range of values considered for

each of the above dimensionless parameters should contain the values normally encountered in the experimental filtration studies.

Before presenting the results of the fiber efficiency calculations, let's consider the variation of the particle deposition rate, j, as obtained from equation (4.82) around the perimeter of a typical fiber. It is common, however, to express j in terms of the dimensionless Sherwood number, $Sh = \frac{K_m D_h}{D}$, where K_m is the mass transfer coefficient defined as $K_m = \frac{j}{N_o}$. Figure 5.2 shows a plot of the calculated values of the Sherwood number as a function of the dimensionless coordinate, S^*, for $b/w = 1$ and $Pe = 600$. The S^* parameter ranges in value from 0 to 1 and is defined as $S^* = \frac{s}{p}$, where s is the coordinate along the boundary of the fiber, originating from the forward stagnation point, and p is half the fiber perimeter equal to $w+b$. It should be mentioned once again that all the fiber-related calculations were performed on upper half of the fiber due to the symmetry considerations and therefore, the rectangle cdef, shown in Figure 5.2, is actually the upper half of a whole fiber. As illustrated, the Sherwood number or the particle flux depositing on the fiber increases with S^* along the left boundary of the fiber reaching at a maximum value in the vicinity of the left corner (point d) where the flow velocity increases as it turns around the corner. Such

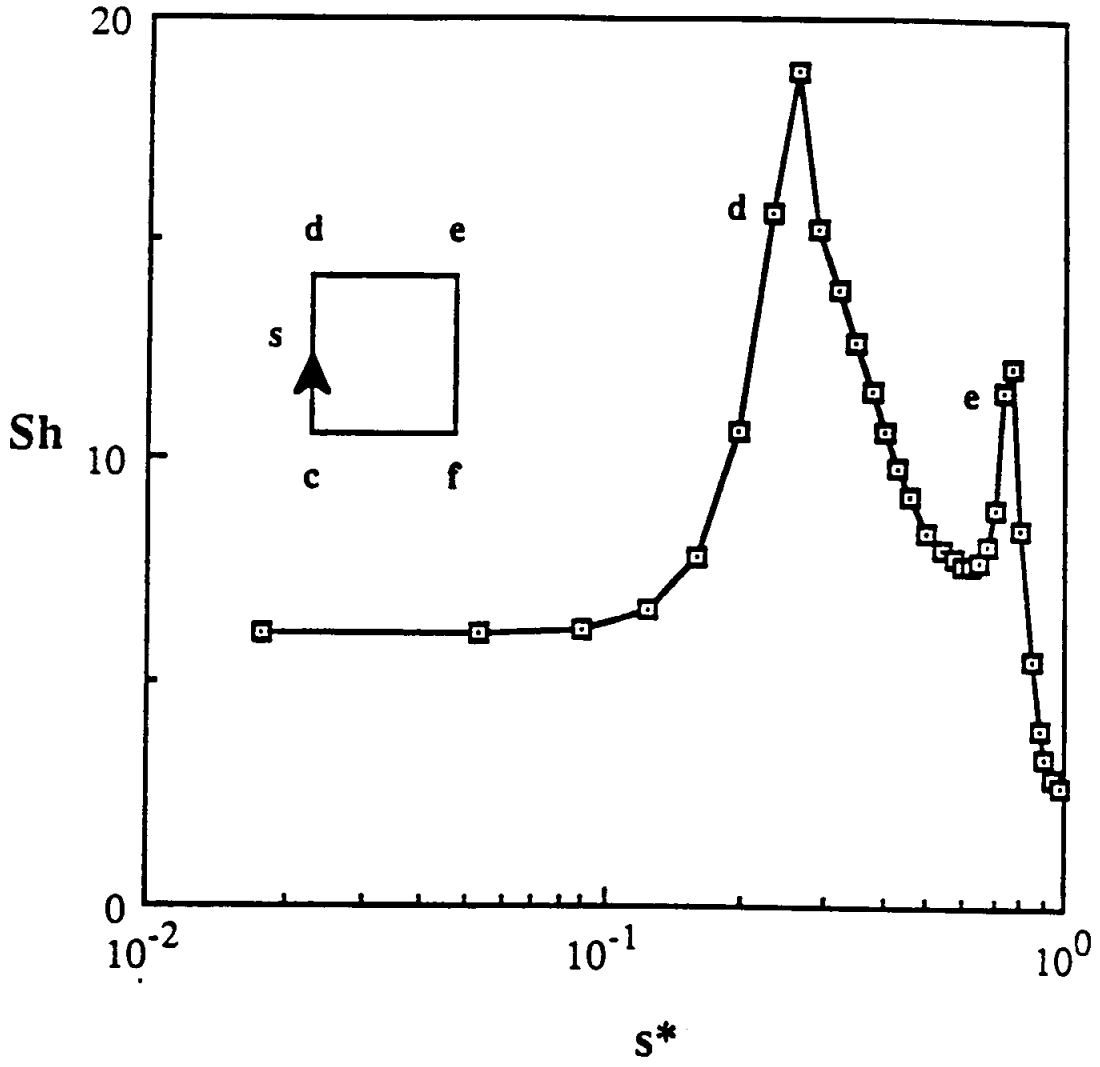

Figure 5.2 Distribution of the Sherwood number along the perimeter of upper half of a rectangular fiber with b/w=1/1 for Pe=600 and α=0.08

flow behavior is in contrast with textbook-type, end-effect-free flows which fan out from a stagnation point. For those flows, the highest value of the transfer coefficient is attained at the stagnation point and decreases with increasing distance from that point. The drop-off of the transfer coefficient is a consequence of the boundary layer growth.

But in the presence of end-effects, as the flow turns around the corner of the fiber it accelerates rapidly resulting in a decrease in the diffusion boundary layer thickness and a consequent increase in the mass transfer coefficient. These end-effects were also found to reverse the decreasing trend of Sh number with distance from the forward stagnation point as is the case in their absence.

On the top boundary of the fiber, the mass transfer coefficient decreases with increasing distance from the left corner as a consequence of the boundary layer growth. But in approaching the right corner of the fiber (point e), the air velocity increases causing the compression of the boundary layer and consequent increase in the mass transfer coefficient. As the flow turns around the corner, it decelerates allowing the boundary layer to grow once again causing the mass transfer coefficient to decrease with increasing distance from the right corner of the fiber toward the rear stagnation point. Similar characteristics

were also observed for fibers with different aspect ratios and the results for b/w = 2/1 and Pe = 600 are illustrated in Figure 5.3. Again, as shown, the maximum deposition occurs in the vicinity of the corners of the fiber.

Now let's consider the results of the single fiber efficiency calculations as described in section (4.8.1). The values of η_D obtained from equation (4.84) have been tabulated and plotted against Pe in Table 5.2 and Figure 5.4, respectively, for the case of α = 0.08 and b/w = 0.5, 1, 2. As shown by the log-log plot of Figure 5.4, for each b/w value, the corresponding results as depicted by the data symbols tend to lie along a straight line suggesting that η_D is a power-law function of Pe with the exponent being equal to the slope of the line. Also, as seen, the best-fit lines through the symbols corresponding to each b/w value tend to be parallel to each other with the slope being equal to approximately $-\frac{2}{3}$. Therefore, the following can be written

$$\eta_D = A(\alpha, b/w)\ Pe^{-2/3} \qquad (5.1)$$

where A is a proportionality coefficient being a function of b/w and α. It is important to remark that a similar expression for the case of circular fibers with proportionality factor being dependent on α only has been

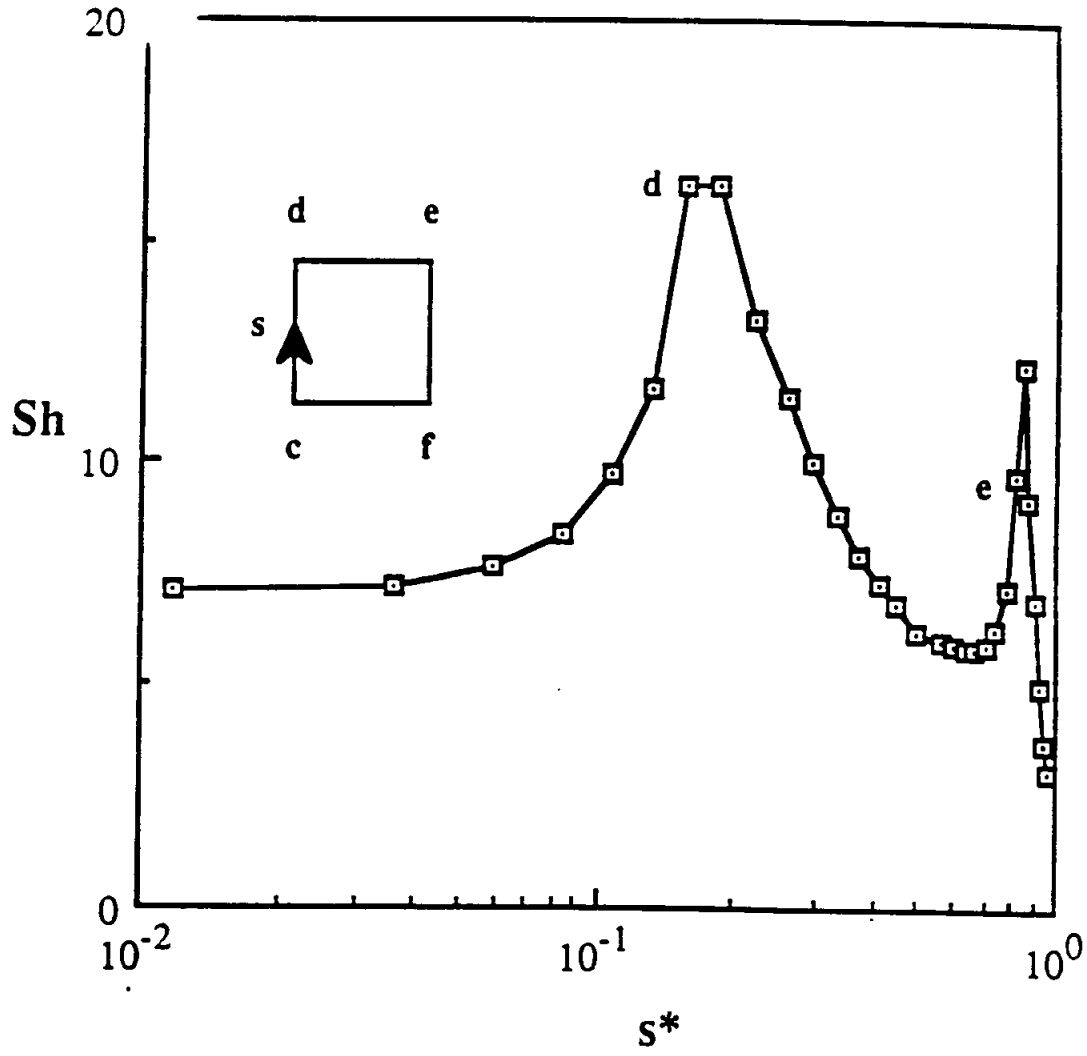

Figure 5.3 Distribution of the Sherwood number along the perimeter of upper half of a rectangular fiber with b/w=2/1 for Pe=600 and ε=0.08

Table 5.2 Calculated single fiber capture efficiency values of rectangular fibers due to the Brownian diffusion mechanism for α=0.08 and b/w=0.5, 1, and 2

Pe	η_D (b/w = 1/1)	Pe	η_D (b/w = 1/2)	Pe	η_D (b/w = 2/1)
23900.00	0.0035	15900.00	0.0041	26300.00	0.0046
2980.00	0.0208	1980.00	0.0206	3291.00	0.0281
602.00	0.0611	400.00	0.0574	663.00	0.0798
300.70	0.0935	200.00	0.0868	331.00	0.1222
60.15	0.2540	40.00	0.2310	66.30	0.3338
30.07	0.3970	20.00	0.3630	33.14	0.5220
6.02	1.1580	4.00	1.0720	6.63	1.5164
3.01	1.8080	2.00	1.5950	3.31	2.3850

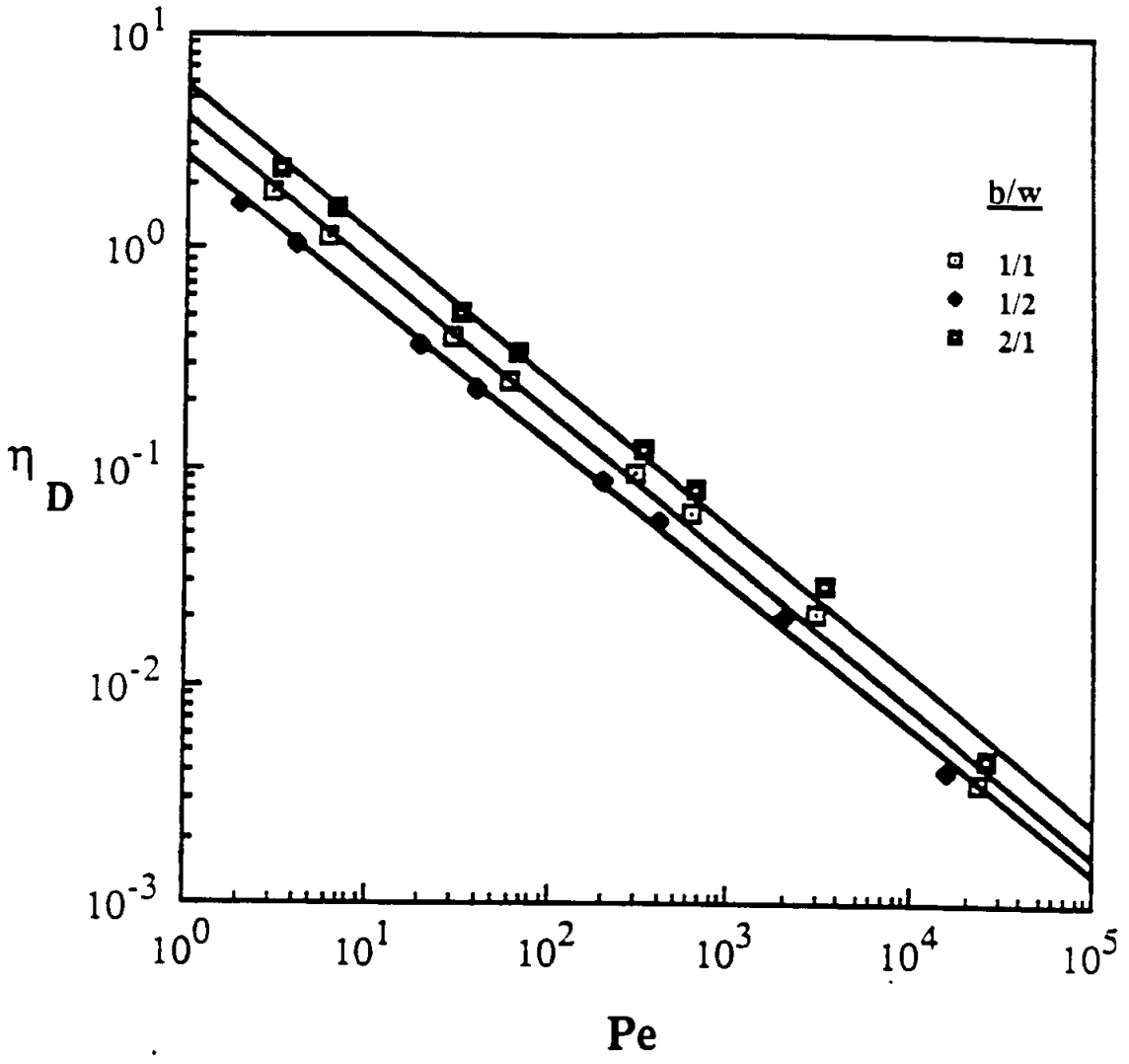

Figure 5.4 Calculated single fiber capture efficiency values of rectangular fibers due to pure diffusion for α=0.08

obtained by many investigators such as Natanson(1957), Pich (1965), Yeh (1972), Lee (1977) etc. Therefore, one may draw the conclusion that the above form of dependency between η_D and Pe is independent of the shape of fiber cross-section.

In order to determine the functional dependence of η_D on b/w and α, one should repeat the calculations of η_D for a fixed value of Pe, while holding one of the above parameters constant and varying the other. The results should be then analyzed to ascertain the relationship between η_D and b/w or α. But prior to carrying out such calculations, it was noted that expressing the total rate of particle deposition on a fiber by diffusion, J, in terms of the following new definition of the fiber efficiency would result in similar expression as equation (5.1) except that the proportionality factor would appear to be independent of b/w and a function of α only,

$$\eta_{D_h} = \frac{J}{u_o N_o h} \tag{5.2}$$

where η_{D_h} is the modified diffusion single fiber efficiency based on h which, as mentioned previously, is half the distance between centers of two successive fibers in the

staggered array model along the flow direction. Note that the denominator represents the total number of particles convected into the calculation domain (Figure (4.4)) and hence, η_{D_h} is the fraction of these particles collected by the fiber due to the Brownian diffusion of particles. It should be noted that η_{D_h} is related to η_D by

$$\eta_{D_h} = \eta_D \frac{(w/2)}{h} \tag{5.3}$$

Hence, the values of η_{D_h} corresponding to different values of b/w and $\alpha = 0.08$ were obtained from the η_D values by multiplying them by the corresponding $\frac{(w/2)}{h}$ value. The results have been tabulated against Pe in Table 5.3 and presented in graphical form in Figure 5.5. As shown, the values of η_{D_h} appear to be independent of the fiber aspect ratio and depend only on α and Pe. Except for b/w = 1/10 and large values of Pe, the logarithmic values of η_{D_h} like those of η_D are found to be a linear function of the logarithmic values of Pe with a slope of approximately $-\frac{2}{3}$. Therefore, the relationship between η_{D_h} and Pe can be expressed as

$$\eta_{D_h} = B(\alpha)\ Pe^{-2/3} \tag{5.4}$$

Table 5.3 Modified single fiber capture efficiency values of rectangular fibers due to the Brownian mechanism for several values of Pe and b/w and α=0.08

Pe	η_{D_h} (b/w = 1/1)	Pe	η_{D_h} (b/w = 1/2)	Pe	η_{D_h} (b/w = 1/5)
23900.00	0.0010	15900.00	0.0016	18410.00	0.0012
2980.00	0.0059	1980.00	0.0083	2300.00	0.0061
601.50	0.0173	400.00	0.0230	464.00	0.0212
300.70	0.0265	200.00	0.0347	232.00	0.0351
60.15	0.0719	40.00	0.0924	46.40	0.0950
30.07	0.1122	20.00	0.1450	23.20	0.1435
6.02	0.3276	4.00	0.4290	4.64	0.4020
3.01	0.5115	2.00	0.6380	2.32	0.6090
2.01	0.6353	1.33	0.7550	1.55	0.7360

Table 5.3 (continued)

Pe	η_{D_h} (b/w = 1/10)	Pe	η_{D_h} (b/w = 2/1)	Pe	η_{D_h} (b/w = 5/1)
17300.00	0.0011	26300.00	0.0009	20000.00	0.0012
2160.00	0.0065	3291.00	0.0056	2500.00	0.0066
435.00	0.0251	663.00	0.0160	742.00	0.0147
218.00	0.0444	331.00	0.0244	313.00	0.0255
43.50	0.1470	66.30	0.0668	160.10	0.0387
21.76	0.2280	33.10	0.1041	58.34	0.0723
4.35	0.5530	6.63	0.3033	25.20	0.1230
2.18	0.7630	3.31	0.4769	5.04	0.3540
1.45	0.8710	2.21	0.5994	3.15	0.4780

Pe	η_{D_h} (b/w = 10/1)
23500.00	0.0014
2940.00	0.0054
872.00	0.0122
368.00	0.0222
197.00	0.0340
42.30	0.0938
29.60	0.1181
5.93	0.3380
2.96	0.5174

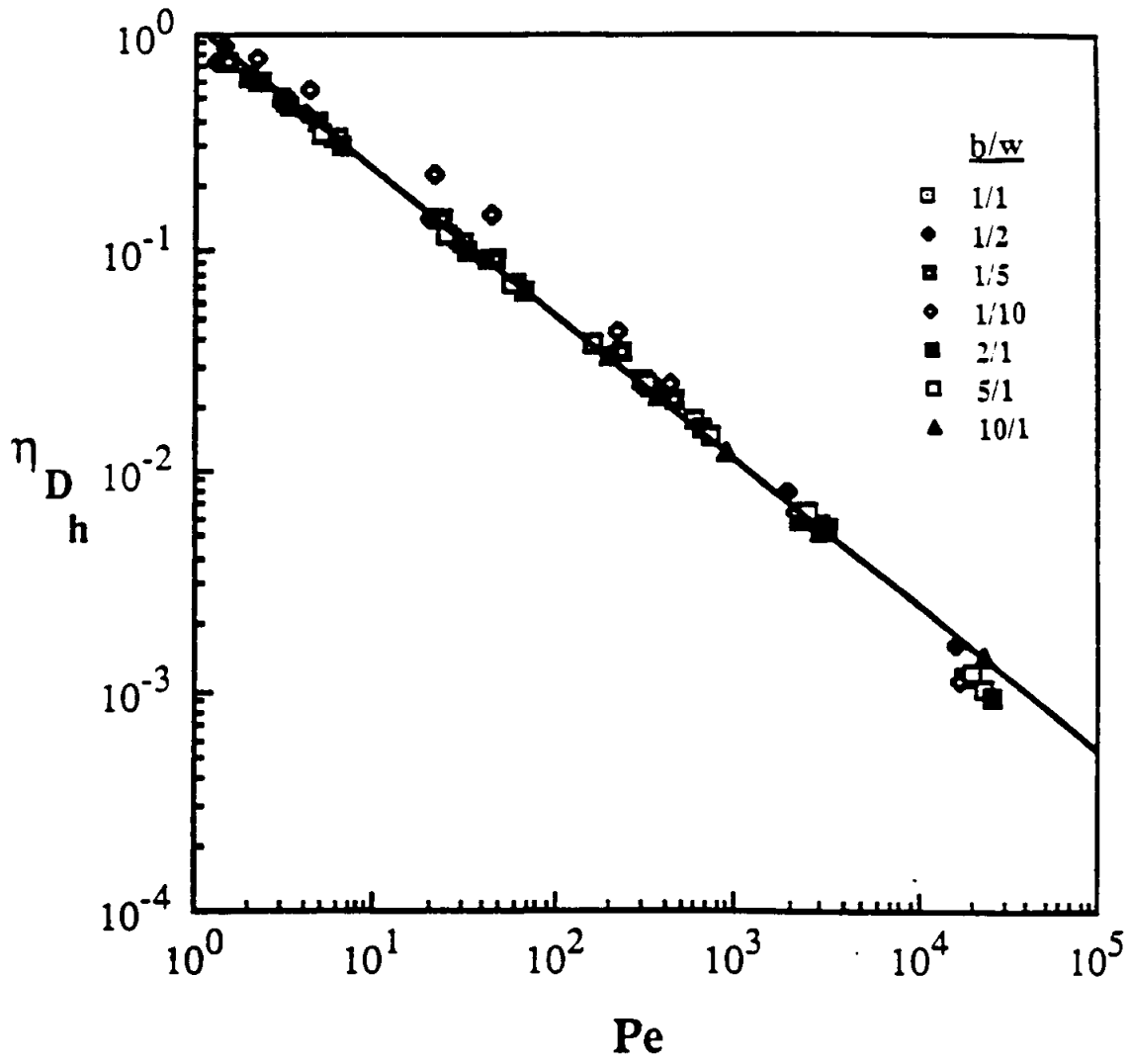

Figure 5.5 Modified single fiber efficiency values of rectangular fibers due to pure diffusion for α=0.08

where $B(\alpha)$ is the proportionality coefficient which is a function of α only. Notice that this equation is independent of the fiber aspect ratio and can be completed by determining the function B.

The diffusion single fiber efficiency calculations were also made for $\alpha = 0.02$ and $\alpha = 0.16$ to verify equation (5.4). The results expressed in terms of η_{D_h} for both values of α have been listed in Tables 5.4 and 5.5 and plotted in Figures 5.6 and 5.7, respectively. Again, the η_{D_h} values except for relatively large values of Pe appear to be independent of b/w and have a relationship with Pe similar to that shown by equation 5.4.

As seen in Figures 5.5, 5.6, and 5.7, the data tend to deviate from the best-fit line at relatively large values of Pe. The reason for such departure can be explained as follows : as described in section (4.8.1), the use of equation (4.82) instead of equation (4.81) for calculation of the local rate of particle diffusion would be free of errors if the true concentration profile were linear in the region very close to the surface of the fiber. This linear condition existed for small to moderate values of Pe as the diffusion boundary thickness was sufficiently thick so that the fine mesh around the fiber happened to be in the linear portion of the concentration profile. On the other hand, as

Table 5.4 **Modified single fiber capture efficiency values of rectangular fibers due to the Brownian mechanism for several values of Pe and b/w and α=0.02**

Pe	η_{D_h} (b/w = 1/1)	Pe	η_{D_h} (b/w = 2/1)	Pe	η_{D_h} (b/w = 5/1)
26600.00	2.40E-04	34000.00	1.86E-04	26400.00	2.40E-04
13400.00	4.61E-04	8500.00	7.25E-04	6600.00	9.16E-04
6700.00	8.92E-04	4250.00	1.40E-03	3300.00	1.73E-03
3350.00	0.0017	3400.00	0.0017	1100.00	0.0043
838.00	0.0053	850.00	0.0054	527.00	0.0072
419.00	0.0086	425.00	0.0086	330.00	0.0095
168.00	0.0150	85.00	0.0221	110.00	0.0186
55.90	0.0293	42.50	0.0348	52.70	0.0297
33.50	0.0413	34.00	0.0404	33.00	0.0407
6.70	0.1242	8.50	0.1046	11.00	0.0851
		4.25	0.1690	4.40	0.1580

Table 5.4 (continued)

Pe	η_{D_h} (b/w=10/1)	Pe	η_{D_h} (b/w=1/2)	Pe	η_{D_h} (b/w=1/5)
18400.00	3.39E-04	26800.00	2.26E-04	19170.00	3.10E-04
4600.00	1.26E-03	11170.00	5.18E-04	4790.00	1.04E-03
2300.00	2.30E-03	4470.00	1.19E-03	2400.00	1.81E-03
767.00	0.0050	2680.00	1.85E-03	960.00	0.0037
368.00	0.0084	670.00	0.0057	320.00	0.0086
230.00	0.0112	335.00	0.0094	192.00	0.0126
76.70	0.0228	134.00	0.0169	64.00	0.0262
36.80	0.0371	44.70	0.0334	32.00	0.0408
23.00	0.0507	26.80	0.0470	19.20	0.0566
9.20	0.0930	6.70	0.1210	4.80	0.1430
3.68	0.1710				

Table 5.5 Modified single fiber capture efficiency values of rectangular fibers due to the Brownian mechanism for several values of Pe and b/w and α=0.16

Pe	η_{D_h} (b/w = 1/1)	Pe	η_{D_h} (b/w = 2/1)	Pe	η_{D_h} (b/w = 4/1)
21650.00	0.0022	25500.00	0.0019	19260.00	0.0024
8660.00	0.0048	8500.00	0.0049	6420.00	0.0060
5414.00	0.0070	4250.00	0.0084	3210.00	0.0100
2707.00	0.0116	2550.00	0.0119	1926.00	0.0143
1083.00	0.0210	850.00	0.0238	642.00	0.0294
361.00	0.0406	364.00	0.0396	321.00	0.0452
216.50	0.0550	255.00	0.0490	192.60	0.0613
54.14	0.1270	63.80	0.1130	64.20	0.1180
27.07	0.2000	31.90	0.1760	32.10	0.1823
10.80	0.3650	17.00	0.2660	19.26	0.2570
3.61	0.7510	6.38	0.5230	4.81	0.6870

Table 5.5 (continued)

Pe	η_{D_h} (b/w = 1/2)	Pe	η_{D_h} (b/w = 1/4)
21560.00	0.0021	24200.00	0.0018
7190.00	0.0052	8071.00	0.0044
3600.00	0.0090	4036.00	0.0077
2160.00	0.0132	2421.00	0.0118
719.00	0.0287	807.10	0.0290
360.00	0.0441	403.60	0.0494
216.00	0.0594	242.10	0.0714
71.90	0.1130	80.71	0.1440
36.00	0.1740	40.36	0.2140
21.60	0.2410	24.21	0.2850
5.40	0.5940	6.05	0.6340

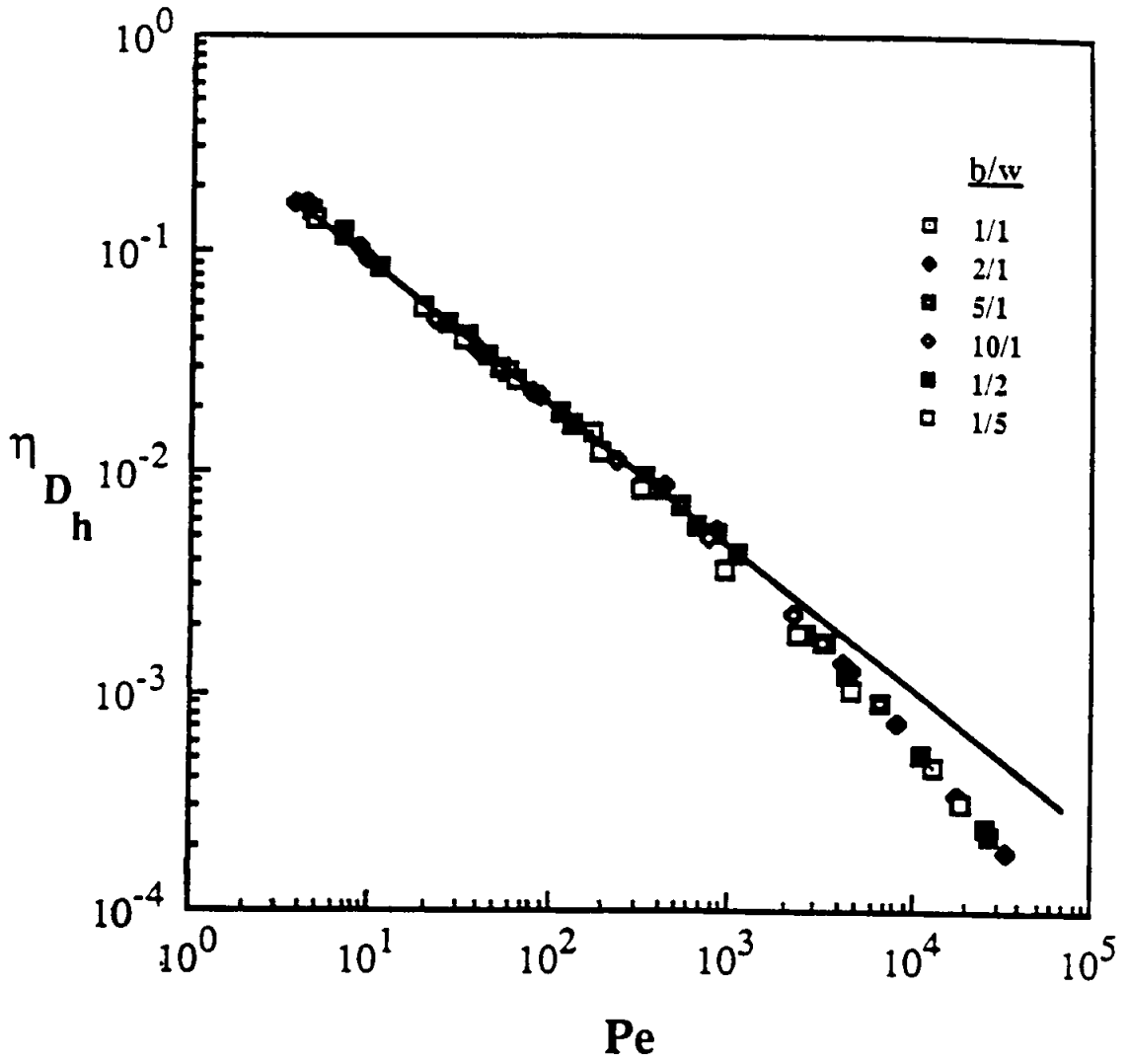

Figure 5.6 Modified single fiber efficiency values of rectangular fibers due to pure diffusion for α=0.02

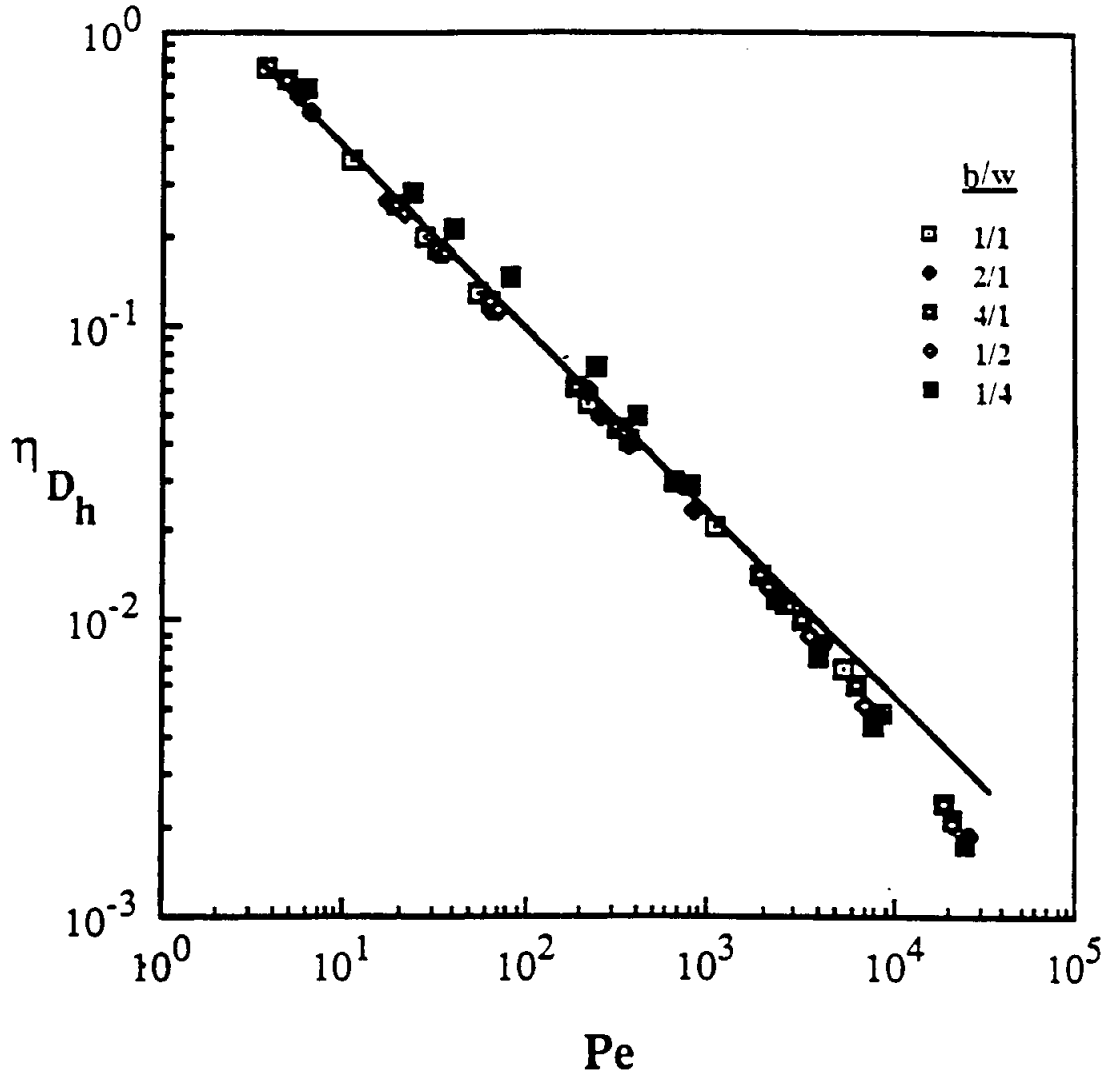

Figure 5.7 Modified single fiber efficiency values of rectangular fibers due to pure diffusion for α=0.16

the value of the Peclet number increases, the boundary layer thickness decreases thus squeezing the linear region of the concentration profile closer to the fiber. In that case, the position of the grids adjacent to the fiber may not have coincided with the linear portion of the concentration profile and therefore, the use of equation (4.82) produces inaccurate results which will reflect in the calculated values of the single fiber efficiency. The magnitude of such inaccuracies can, of course, be reduced if one employes a finer mesh than the already exisiting one in the region very close to the fiber for the larger values of Pe but that will increase the computation time and cost by a great deal. Therefore, the departure of the data from the best line at relatively large values of Pe is believed to be a consequence of the numerical errors in evaluating the concentration gradient at the surface of the fiber.

The fact that η_{D_h} can be expressed by equation (5.4) independent of the fiber aspect ratio, greatly simplifies the procedure for obtaining an empirical expression for the true single fiber efficiency, η_D, due to pure diffusion as η_{D_h} and η_D are related by equation (5.3). Combining equations (5.3) and (5.4) gives

$$\eta_D = B(\alpha)Pe^{-2/3} \frac{h}{(w/2)} \tag{5.5}$$

where $\frac{h}{(w/2)}$ can be expressed in terms of b/w and α according to

$$\alpha = \frac{wb}{4h^2} \tag{4.62}$$

which can be rearranged as follows,

$$\frac{h}{(w/2)} = \left(\frac{b/w}{\alpha}\right)^{1/2} \tag{5.6}$$

substituting equation (5.6) in equation (5.5) yields

$$\eta_D = B(\alpha)\ Pe^{-2/3} \left(\frac{b/w}{\alpha}\right)^{1/2} \tag{5.7}$$

which shows explicitly the dependence of η_D on b/w . As seen, the only unknown parameter in the above equation is the function B. A great deal of information about the behavior of this function can be obtained by calculating and plotting the values of η_{D_h} vs. α for fixed values of Pe and b/w. Hence, considering b/w =1/1 and Pe = 600, the η_{D_h} values were calculated for several values of α and the results have been tabulated in Table 5.6 and plotted in Figure 5.8. As shown, the logarithmic values of η_{D_h} and α

are found to be linearly related with a slope of approximately 0.778 .

Table 5.6 Calculated values of the modified single fiber efficiency as a function of the solid-volume fraction for Pe=600 and b/w=1/1

α	η_{D_h}
0.02	0.570
0.04	0.893
0.06	1.185
0.08	1.640
0.12	2.050
0.16	2.880

Hence, one can write the following

$$\eta_{D_h} = f(Pe)\ \alpha^{0.778} \tag{5.8}$$

where f is a function of Pe only. By comparing equations (5.4) and (5.8), the function B is determined as

$$B(\alpha) = E\ \alpha^{0.778} \tag{5.9}$$

where E is a numerical constant. Substituting the above for $B(\alpha)$ in equation (5.7) yields

$$\eta_D = E\ \alpha^{0.778}\ Pe^{-2/3}\ \left(\frac{b/w}{\alpha}\right)^{1/2} \tag{5.10}$$

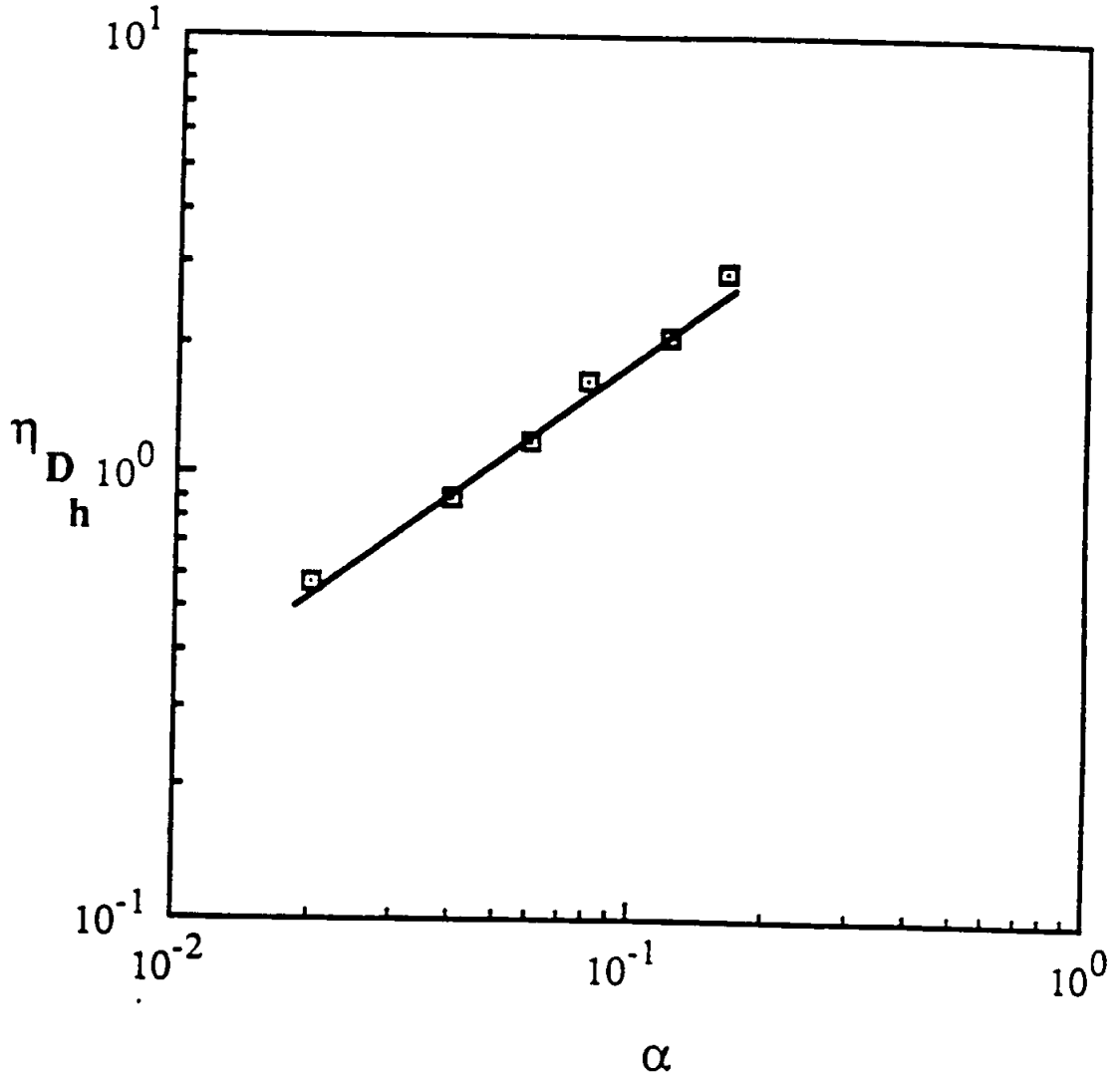

Figure 5.8 Effect of the solid-volume fraction on the modified diffusion single fiber efficiency values for fibers with b/w=1/1 and Pe=600

or

$$\eta_D = E\, \alpha^{0.278}\, Pe^{-2/3}\, (b/w)^{1/2} \qquad (5.11)$$

the value of constant E was found from the intercept of the best-fit line through the numerical data points obtained from the plot of η_D values against values of $(\alpha^{0.278}\, Pe^{-2/3}\, (b/w)^{1/2})$ for b/w =1/1 and α = 0.08, as shown in Figure 5.9. The line has a slope equal to nearly 1 and intercepts the horizontal axis at a point with the following coordinates

$$\eta_D = 0.001 \qquad (5.12a)$$

$$\alpha^{0.278}\, Pe^{-2/3}\, (b/w)^{1/2} = 0.00012 \qquad (5.12b)$$

combining equations (5.11) and (5.12) yields the following for E,

$$E = 8.33 \qquad (5.13)$$

Finally, the complete equation for determinig the single fiber collection efficiency of a rectangular fiber due to pure diffusion can be written as

$$\eta_D = 8.33\, \alpha^{0.278}\, Pe^{-2/3}\, (b/w)^{1/2} \qquad (5.14)$$

note that the efficiency increases with the square root of

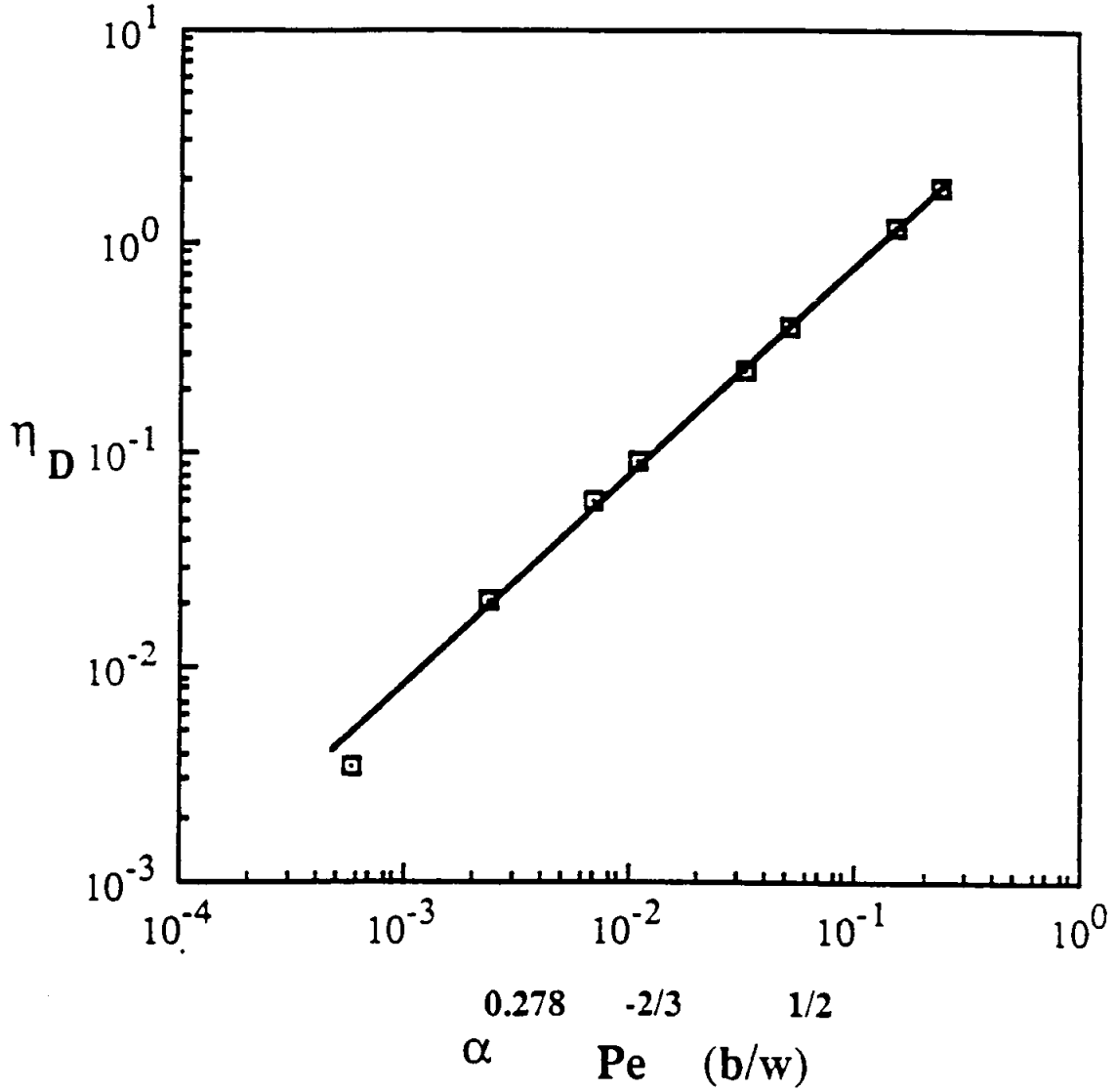

Figure 5.9 Best-fit line through calculated values of the true single fiber efficiency of rectangular fibers due to pure diffusion corresponding to b/w=1/1 and σ=0.08

the fiber aspect ratio. This equation, as shown in Figure 5.10, tends to give a very good correlation to the numerically obtained values of η_D for a wide range of the parameters considered.

Next, the calculation results of the interception single fiber efficiency will be presented and discussed.

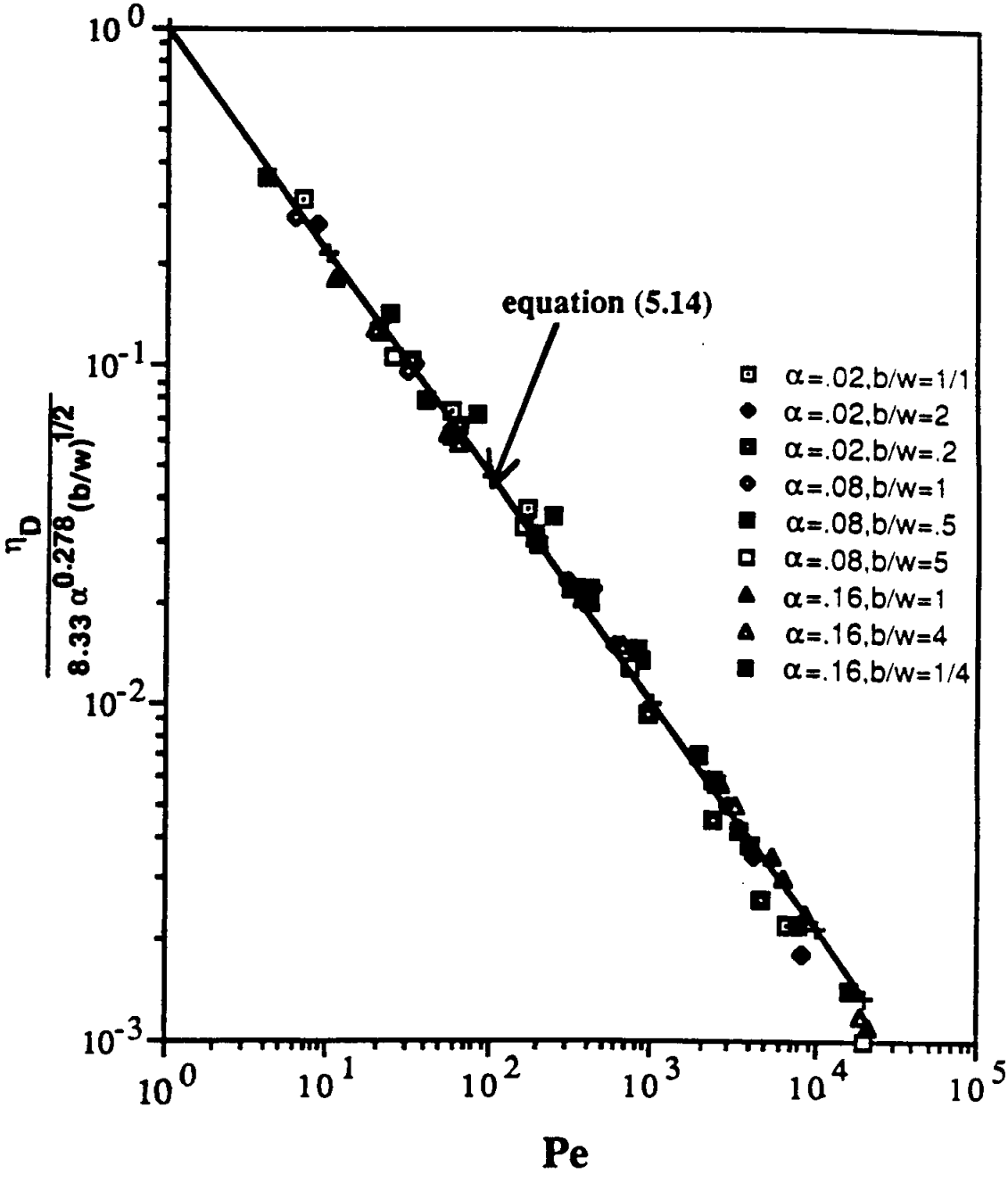

Figure 5.10 Fit performance of equation (5.14) to the calculated values of the single fiber capture efficiency due to pure diffusion for a wide range of parameters involved

5.3 Single Electret Fiber Capture Efficiency Results Due to Interception

As mentioned, the interception capture mechanism becomes important when the size of particles is not negligible relative to the fiber size. The values of the single fiber efficiency due to pure interception for several values of the interception parameter, N_R , and fiber aspect ratio were determined from equation (4.87). The calculations were made considering $0.1 \leq N_R < 1$; $\alpha = 0.04, 0.08, 0.16$; and several values of b/w and the results have been listed in Tables 5.7-5.9 and shown in Figures 5.11-5.13 for each value of α, respectively.

Table 5.7 Calculated single fiber capture efficiency values of rectangular fibers due to the interception mechanism for b/w=.5, 1, 2 and α=0.04

N_R	η_R (b/w=1/1)	η_R (b/w=2/1)	η_R (b/w=1/2)
0.2	0.0560	0.0420	0.0800
0.3	0.1060	0.0790	0.1490
0.4	0.1630	0.1230	0.2320
0.5	0.2300	0.1750	0.3260

Table 5.8 Calculated single fiber capture efficiency values of rectangular fibers due to the interception mechanism for several values of b/w and α=0.08

N_R	η_R (b/w=1/1)	η_R (b/w=2/1)	η_R (b/w=3/1)	η_R (b/w=5/1)	η_R (b/w=7/1)	η_R (b/w=10/1)	η_R (b/w=1/2)	η_R (b/w=1/4)	η_R (b/w=1/5)
0.1		0 0194					0 0430	0.0815	0 1125
0.2	0.0810	0.0590	0.0505	0.0445	0.0420	0.0440	0.1240	0.24	0.33
0.3	0.1525	0.1120	0.0960	0.0860		0.0860		0.45	0.61
0.4	0.2350	0.1750	0.1525	0.1375	0.1350	0.14		0.70	0.93
0.5	0.3300	0.2450	0.2175	0.1960	0.1950	0.20			
0.6	0.4300								
0.7		0.4150	0.3650	0.3330	0.3330				
0.8									
0.9		0.6050		0.4950	0.4950				

Table 5.9 Calculated single fiber capture efficiency values of rectangular fibers due to the interception mechanism for b/w=1, 2 and α=0.16

N_R	η_R (b/w=1/1)	η_R (b/w=2/1)
0.	0.0450	
0.2	0.1330	0.0980
0.3		0.1850
0.4		0.2875

As seen from the figures, for each b/w value, the logarithmic values of η_R and N_R appear to have a linear relationship with a slope which is found to be independent of b/w and α. In other words, the lines through the data symbols corresponding to different b/w and α values are found to be parallel with a slope of approximately 1.55. Moreover, as shown in Figure 5.11, the degree of dependency of η_R on b/w decreases as the value of b/w increases in such a way that for b/w $\geq$ 5 , the corresponding values of η_R for a given value of N_R were found to be virtually the same. Based on the relationship between η_R and N_R , as illustrated in the above figures, one can write the following

$$\eta_R = G(\alpha, b/w)\ N_R^{1.55} \qquad (5.15)$$

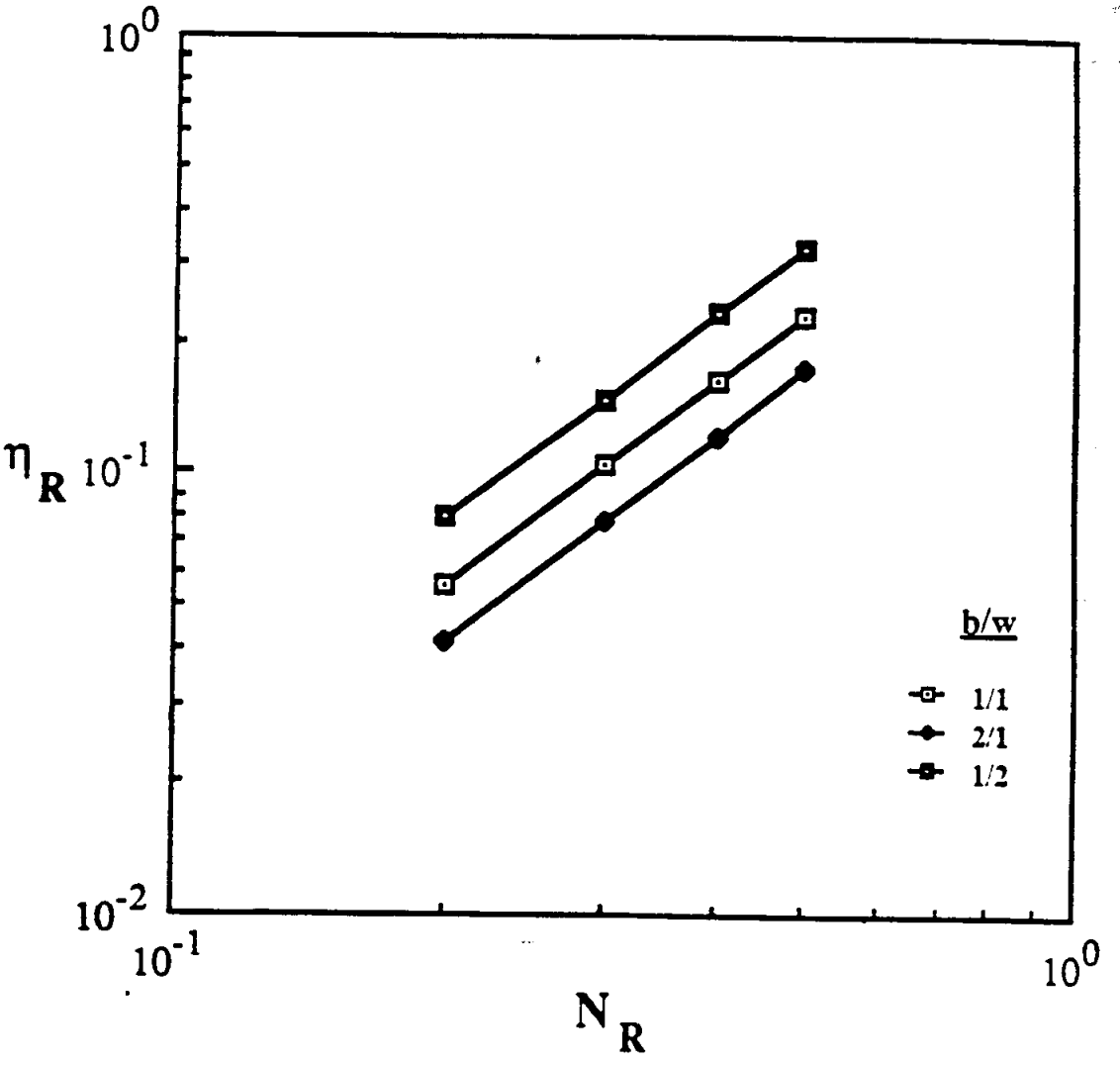

Figure 5.11 Effect of the interception parameter on the single fiber efficiency values for α=0.04

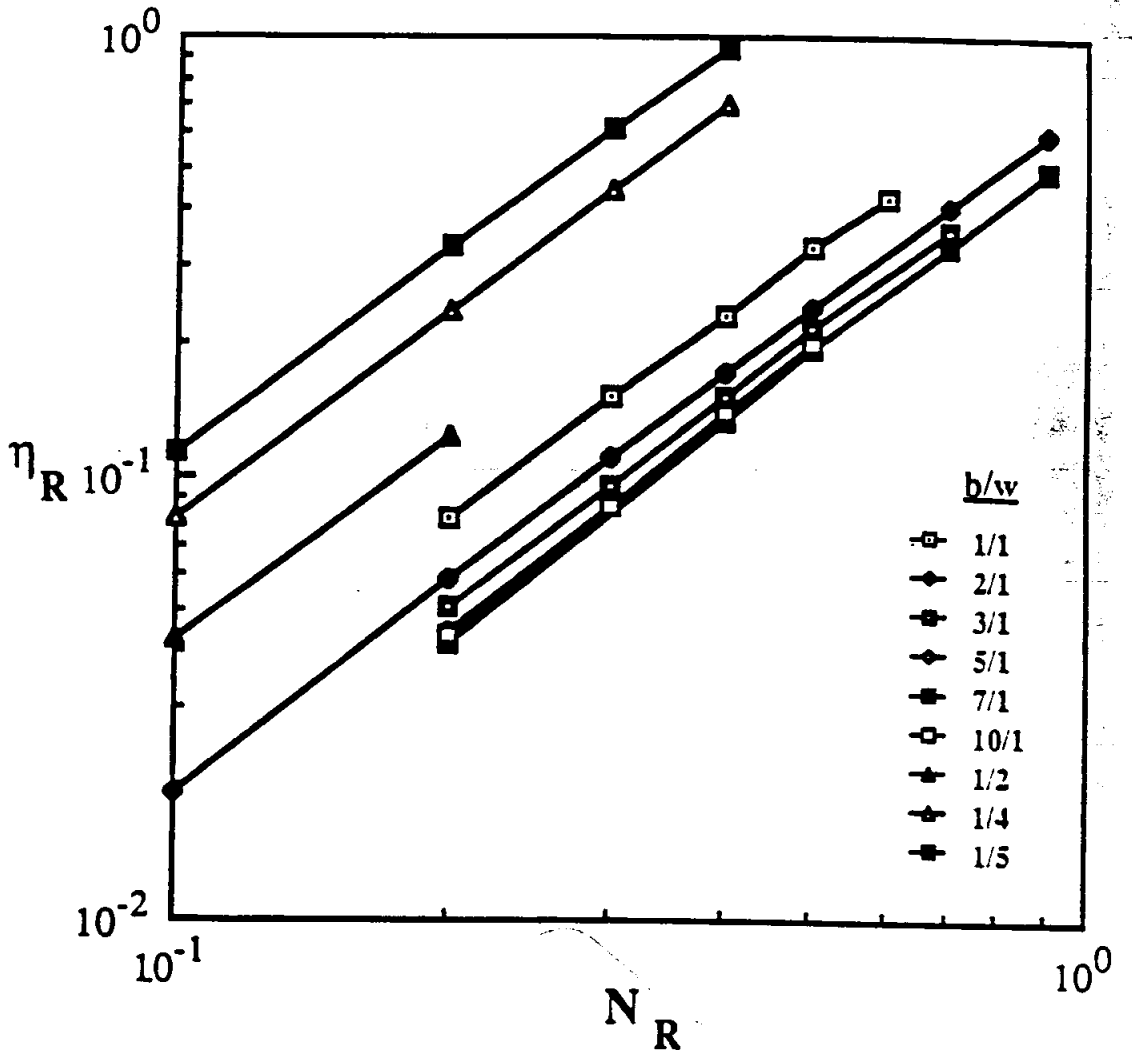

Figure 5.12 Effect of the interception parameter on the single fiber efficiency values for different fiber aspect ratios and α=0.08

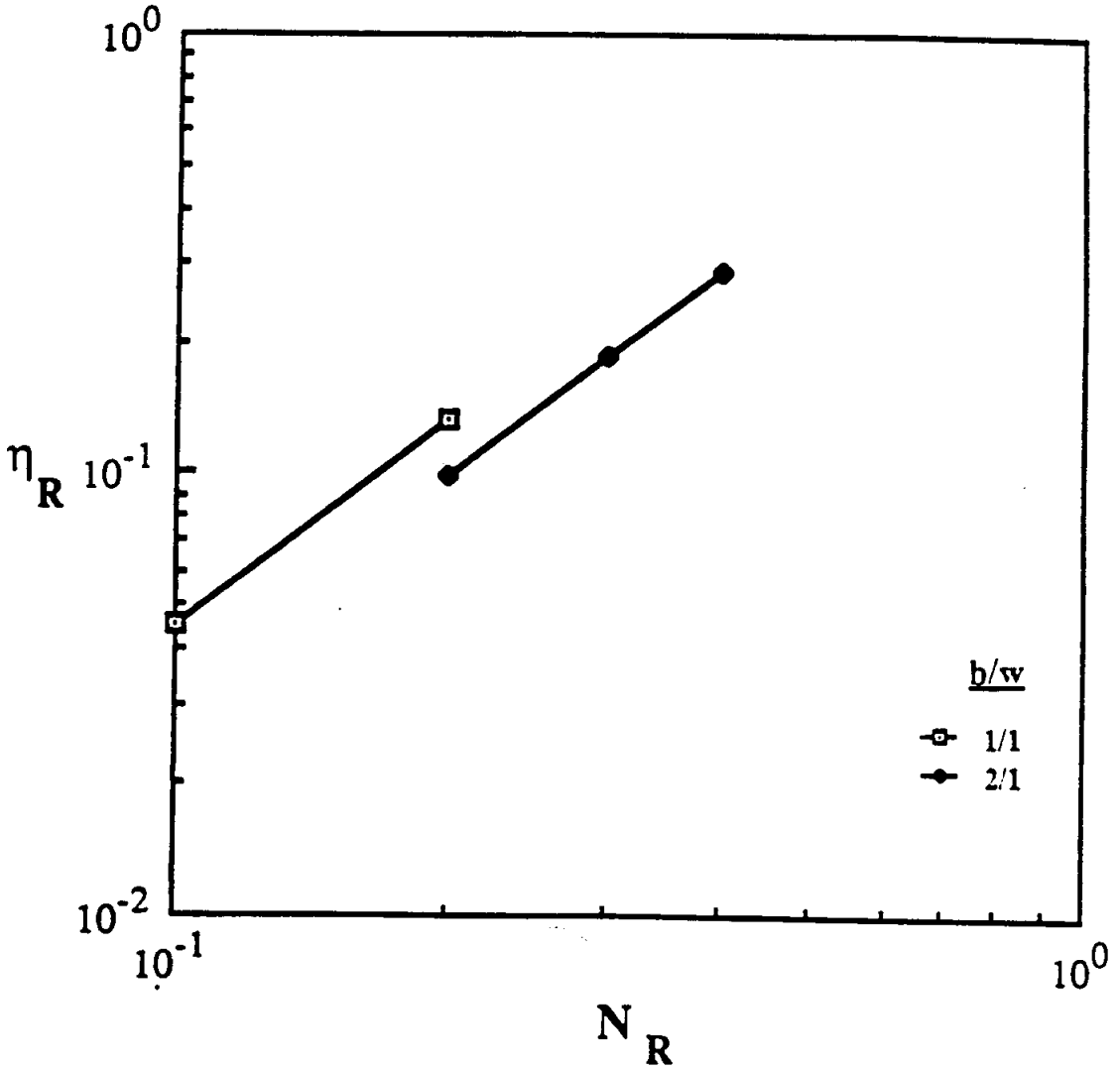

Figure 5.13 Effect of the interception parameter on the single fiber efficiency values for a=0.16

where G is a function of α and b/w . In order to determine this function, one should investigate the individual effect of each of the two parameters on the single fiber efficiency. To begin, let's consider the variation of η_R with α for given values of b/w and N_R. The values of η_R were calculated for several values of α for each of the following cases : b/w = 1/1 , N_R = 0.2; b/w = 1/2 , N_R = 0.2; and b/w = 2/1 , N_R = 0.8 . The results have been tabulated in Table 5.10 and plotted in Figure 5.14.

Table 5.10 Calculated single fiber capture efficiency values of rectangular fibers due to the interception mechanism as a function of the filter solid-volume fraction for different values of the interception parameter and b/w

α	η_R (b/w=1/2,N_R =0.2)	η_R (b/w=1/1,N_R =0.2)	η_R (b/w=2/1,N_R =0.8)
0.040	0.0800	0.0560	0.3580
0.050	0.0905	0.0635	
0.060		0.0695	
0.065	0.1050		
0.080	0.1240	0.0810	0.5080
0.100		0.0925	
0.120		0.1060	
0.160		0.1330	0.8400

As shown, the logarithmic values of η_R and α are found to be linearly related for each case with the slope being nearly

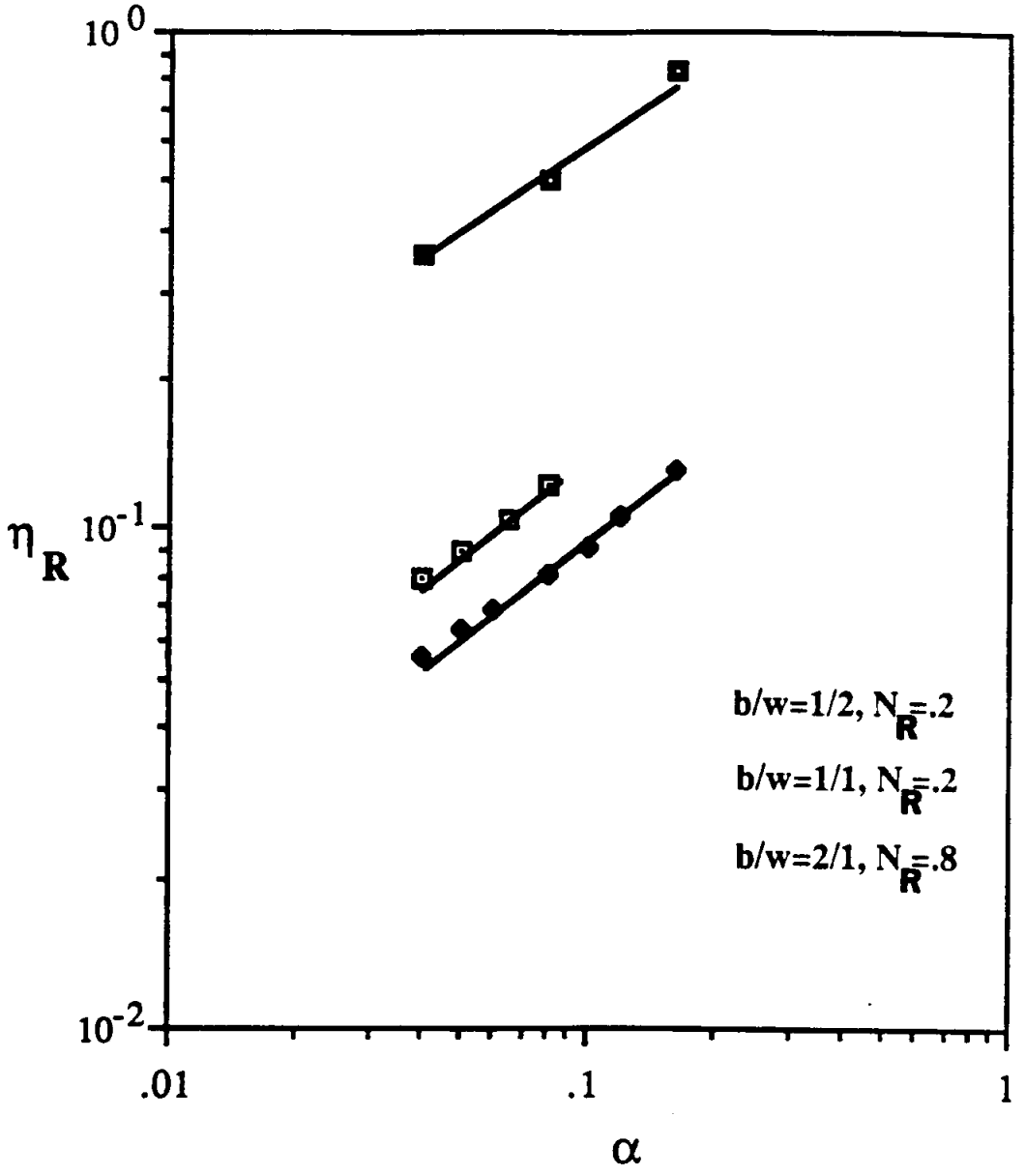

Figure 5.14 Effect of the solid-volume fraction on the interception single fiber efficiency of rectangular fibers

the same and equal to approximately 0.54. Thus, the following relationship between η_R and a can be written

$$\eta_R = H(b/w, N_R)\ a^{0.54} \qquad (5.16)$$

where H is a function of b/w and N_R. But the dependency of η_R on N_R is already known from equation (5.15). Therefore, it remains to find the relationship between η_R and b/w. By combining equations (5.15) and (5.16), one obtains the following

$$\eta_R = \lambda(b/w)\ a^{0.54}\ N_R^{1.55} \qquad (5.17)$$

where λ is a function of b/w only. Similarly, in order to determine the effect of b/w on η_R ,the values of η_R were calculated for different values of b/w considering a = 0.08 and N_R = 0.2. The results have been listed in Table 5.11 and shown in Figure 5.15.

Table 5.11 Values of coefficient of equation (5.17) as a function of b/w

b/w	λ
0.20	15.50
0.25	11.35
0.50	5.90
1.00	3.85
3.00	2.40
5.00	2.10
10.00	2.10

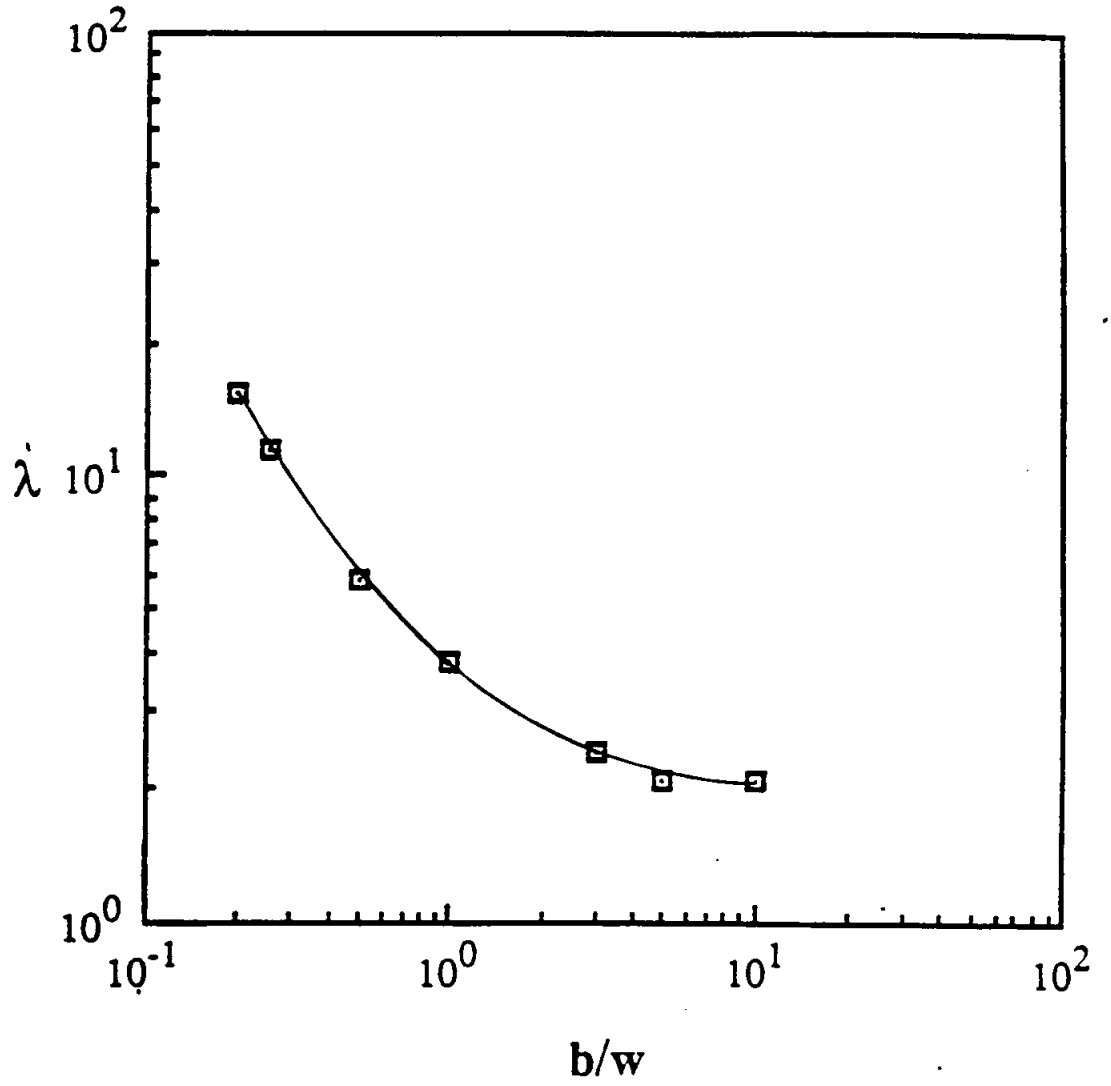

Figure 5.15 Variation of the coefficient of equation (5.17) with the fiber aspect ratio considering N_R=0.2 and ϕ=0.08

Notice that the relationship between η_R and b/w is not mathematically so simple as that found between η_R and N_R or a. Of course, one can try to fit a curve to the results and obtain an expression for the function λ but this was not attempted in the present study. Instead, taking advantage of the monotonic behavior of the curve λ vs. a as shown in Figure 5.15, it was decided to obtain the value of λ corresponding to a given value of b/w from this graph and use equation (5.17) to determine the single fiber efficiency due to pure interception.

To examine the accuracy of the above procedure, the values of η_R were determined for different values of N_R considering b/w = 1/1 and a = 0.06 and a = 0.10. The results as depicted by the data symbols are shown in Figure 5.16 in comparison with those obtained using equation (5.17) and Figure 5.15. The value of λ corresponding to b/w = 1/1 is approximately 3.85. As shown, the two sets of results are in excellent agreement verifying that the use of the combination of equation (5.17) and Figure 5.15 gives a very good prediction of the numerical results of the interception single fiber efficiency.

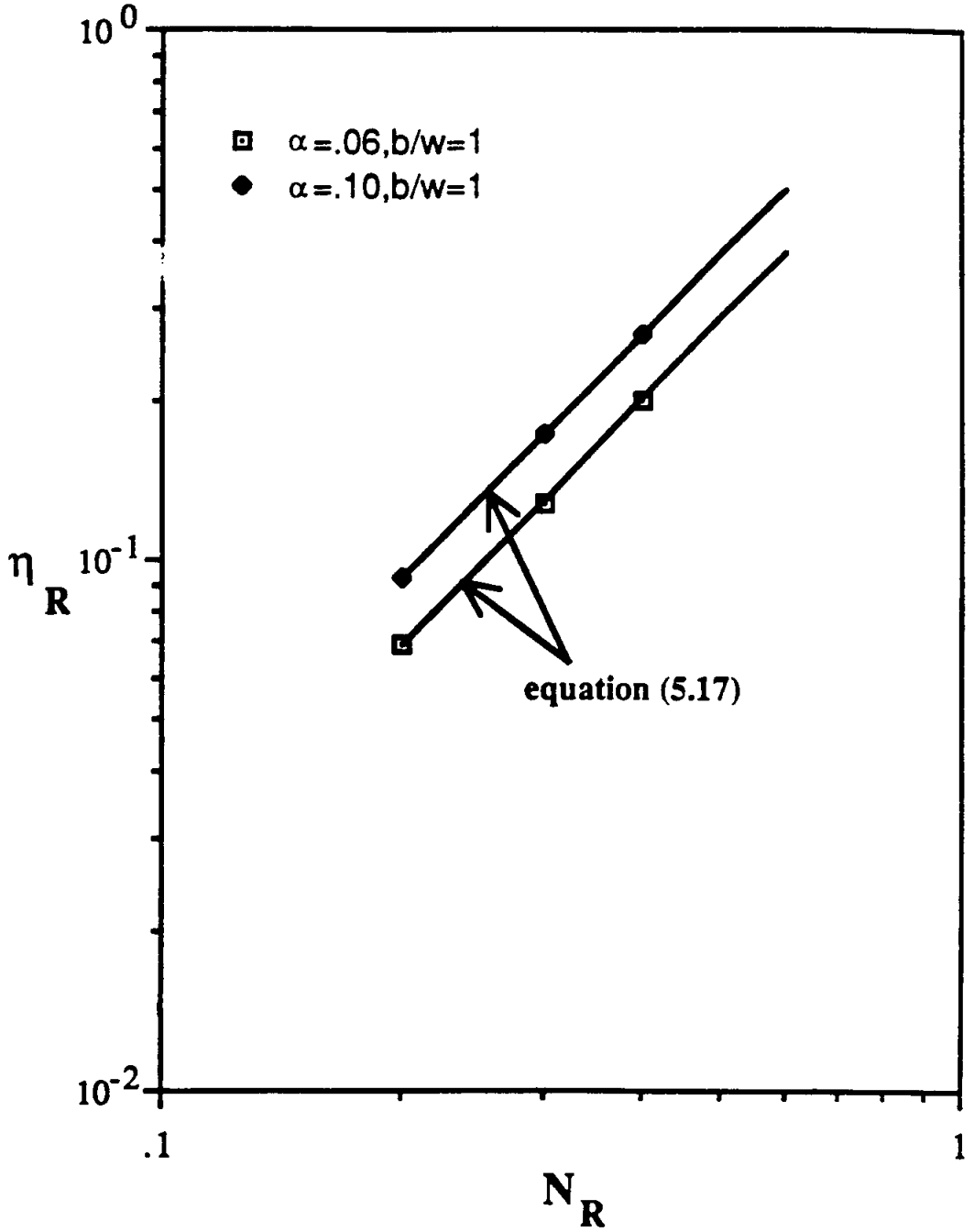

Figure 5.16 Fit performance of combination of equation (5.17) and Figure 5.15 to the calculated values of the interception single fiber efficiency for b/w=1/1, α=0.06 and α=0.10

5.4 Single Electret Fiber Capture Efficiency Results Due to Electrostatics

The electrostatic single fiber efficiency values of an electret fiber whose surrounding electric field intensity was approximated by that of several line charges of both polarities assumed on the fiber were obtained as a function of dimensionless force parameters N_C and N_I. The calculations were performed for several values of α to investigate the influence of fiber interference on the single fiber efficiency. It should be mentioned, however, that in the present work the influence of neighboring fibers was accounted for only in the flow field calculations and was not considered in the approximation of the electric field intensity around a single fiber. The values of the single fiber efficiency were determined for a rectangluar fiber with an aspect ratio equal to 1/4 which is a common value for the manufactured electret fibers (Van Turnhout (1976)). However, several efficiency values corresponding to b/w equal to 4/1 were also obtained to determine the effect of fiber orientation on the single fiber efficiency.

All the calculations were carried out assuming $2n_c = 100$ positive and negative line charges on the fiber or $n_c = 50$ line charges on half the fiber which

was considered in the calculations due to symmetry. Emi et al. (in press) who initiated the theoretical work on rectangular electret fibers remark that the error in the calculated electric field is less than 1% for $n_c = 30$.

The calculation results of each electrostatic interaction considered in this work, namely, Coulombic and induced, are presented and discussed next.

5.4.1 Coulombic Interaction

This type of electrostatic interaction between an electret fiber and a particle is important when the particle is charged. The Coulombic force is attractive when the polarity of particle is opposite to the fiber and repulsive when the polarities are the same.

The calculated values of the single fiber efficiency due to the Coulombic forces, η_E^C , were plotted and tabulated as a function of N_C as shown in Figures 5.17 through 5.20 and Table 5.12 for values of α equal to 0.005, 0.02, 0.08, and 0.16, respectively, and b/w = 1/4. The Reynolds number values of the calculated flow fields were kept below or in the vicinity of 0.2, a value below which the flow field was found to be independent of the Reynolds number, as explained previously. On a logarithmic scale, η_E^C and N_C appear to be linearly related in the range of N_C values considered for

Table 5.12 Calculated single fiber capture efficiency values of charged rectangular fibers with b/w=1/4 due to the Coulombic forces for various values of the dimensionless force parameter and solid-volume fraction

α	0·005		0·02		0·08		0·16	
	N_C	η_E^C	N_C	η_E^C	N_C	η_E^C	N_C	η_E^C
	0.099	0.0516	0.050	0.0281	0.099	0 0583	0.010	0.0577
	0.248	0.1188	0.099	0.0549	0.149	0.0872	0.050	0.0734
	0.495	0.2152	0.297	0.1521	0.198	0.1162	0.099	0.0933
	0.990	0.3765	0 495	0.2399	0.297	0.1736	0.248	0.1583
	1.980	0.6600	0.990	0.4341	0.495	0.2754	0.495	0.2887
	2.970	0.8888	2.475	0.8780	0 742	0.3918	0.990	0.5531
					0.990	0.5065	1.485	0.8088
					1.485	0.7233		
					1.980	0.9064		

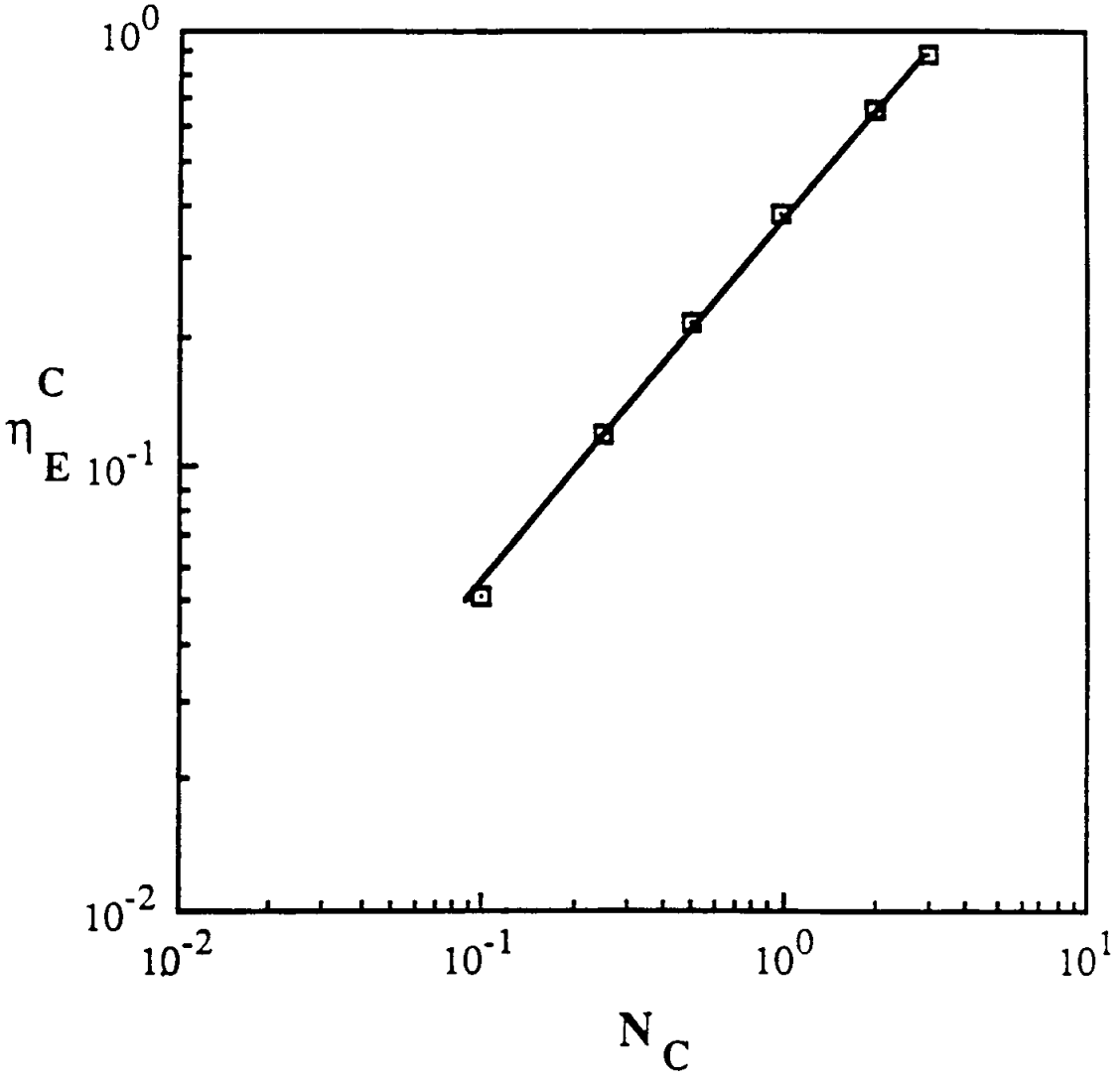

Figure 5.17 Effect of the Coulombic force parameter on the electrostatic single fiber capture efficiency of elecret fibers for b/w=1/4 and α=0.005

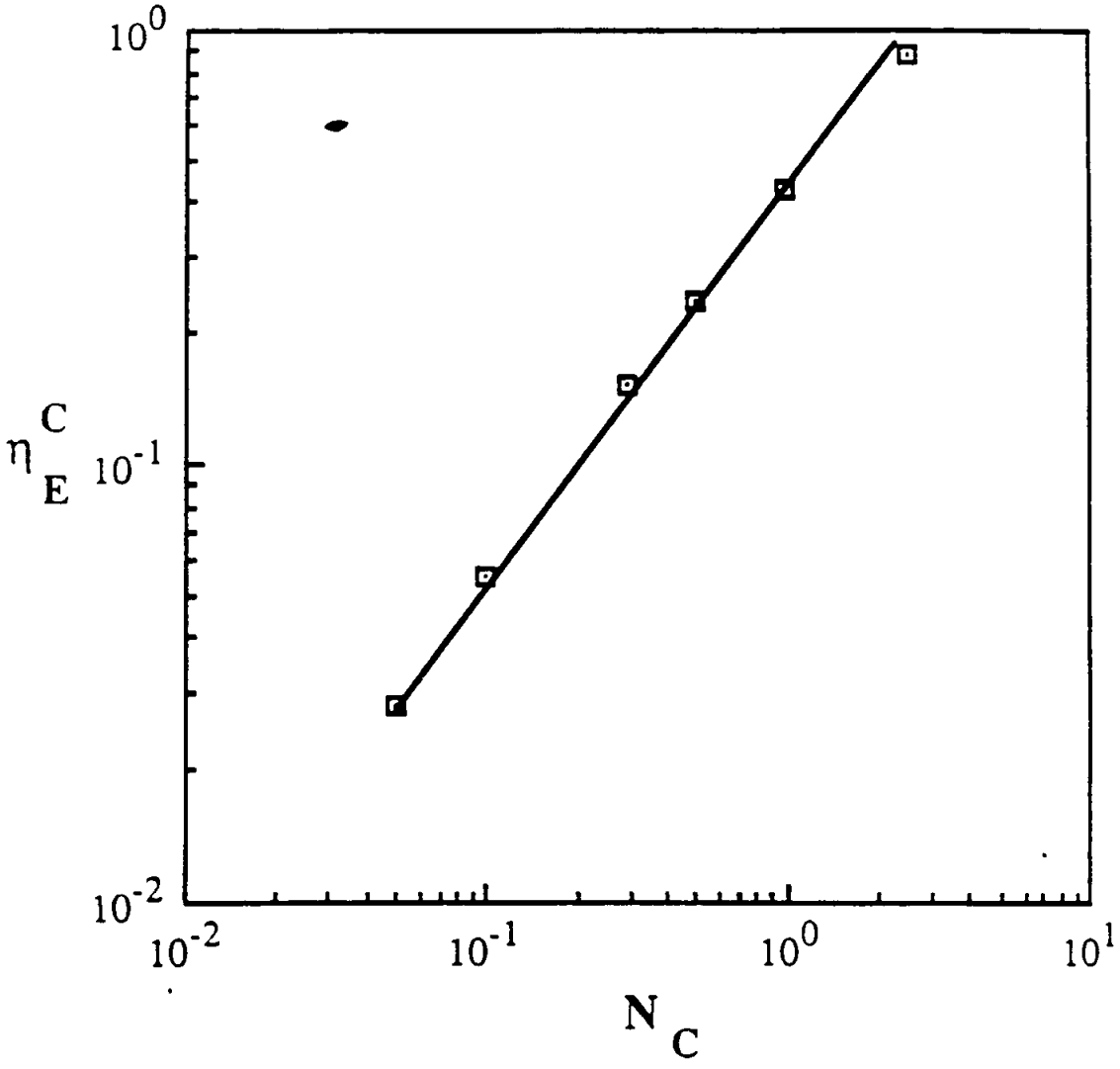

Figure 5.18 Effect of the Coulombic force parameter on the electrostatic single fiber capture efficiency of elecret fibers for b/w=1/4 and α=0.02

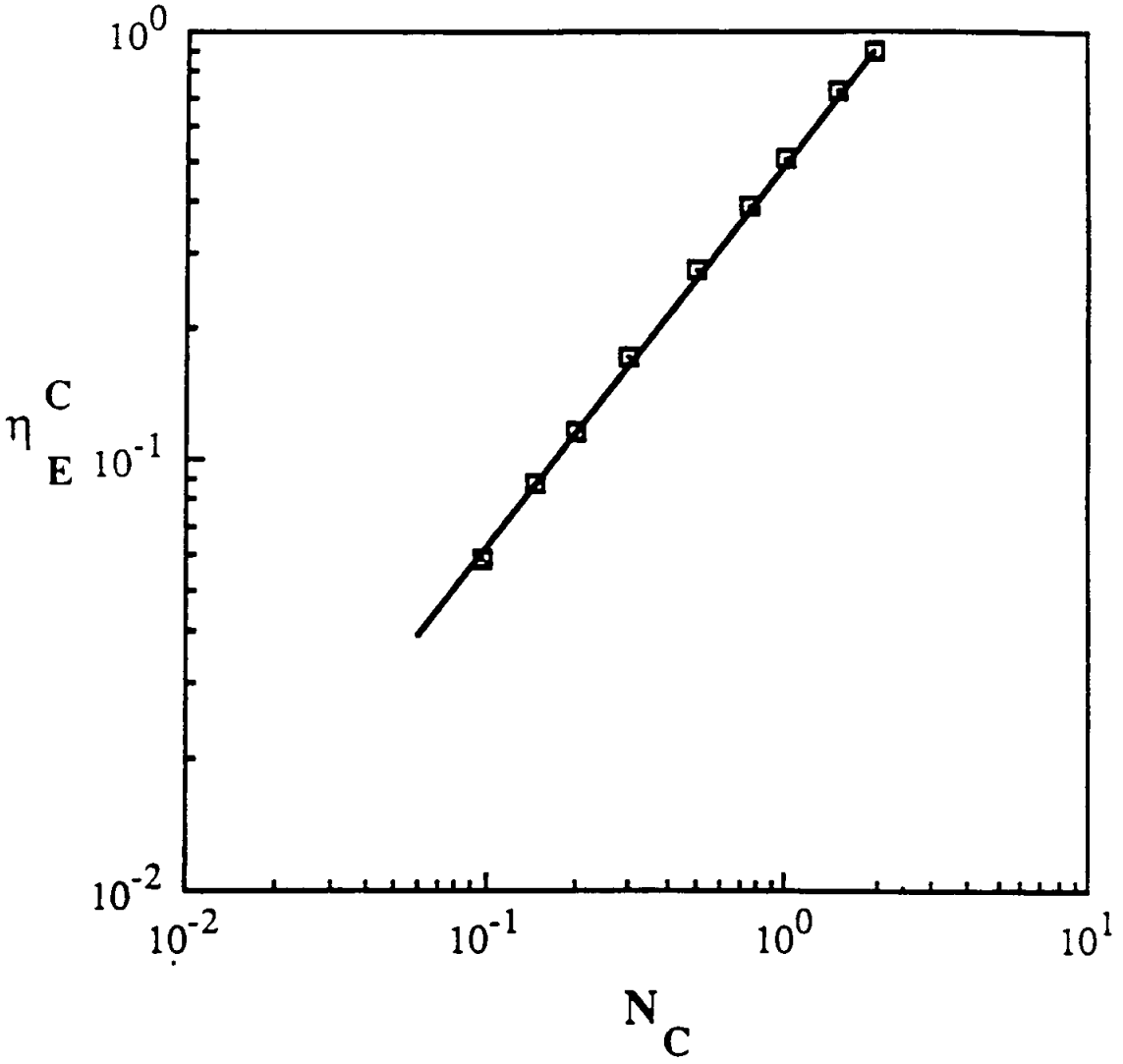

Figure 5.19 Effect of the Coulombic force parameter on the electrostatic single fiber capture efficiency of elecret fibers for b/w=1/4 and α=0.08

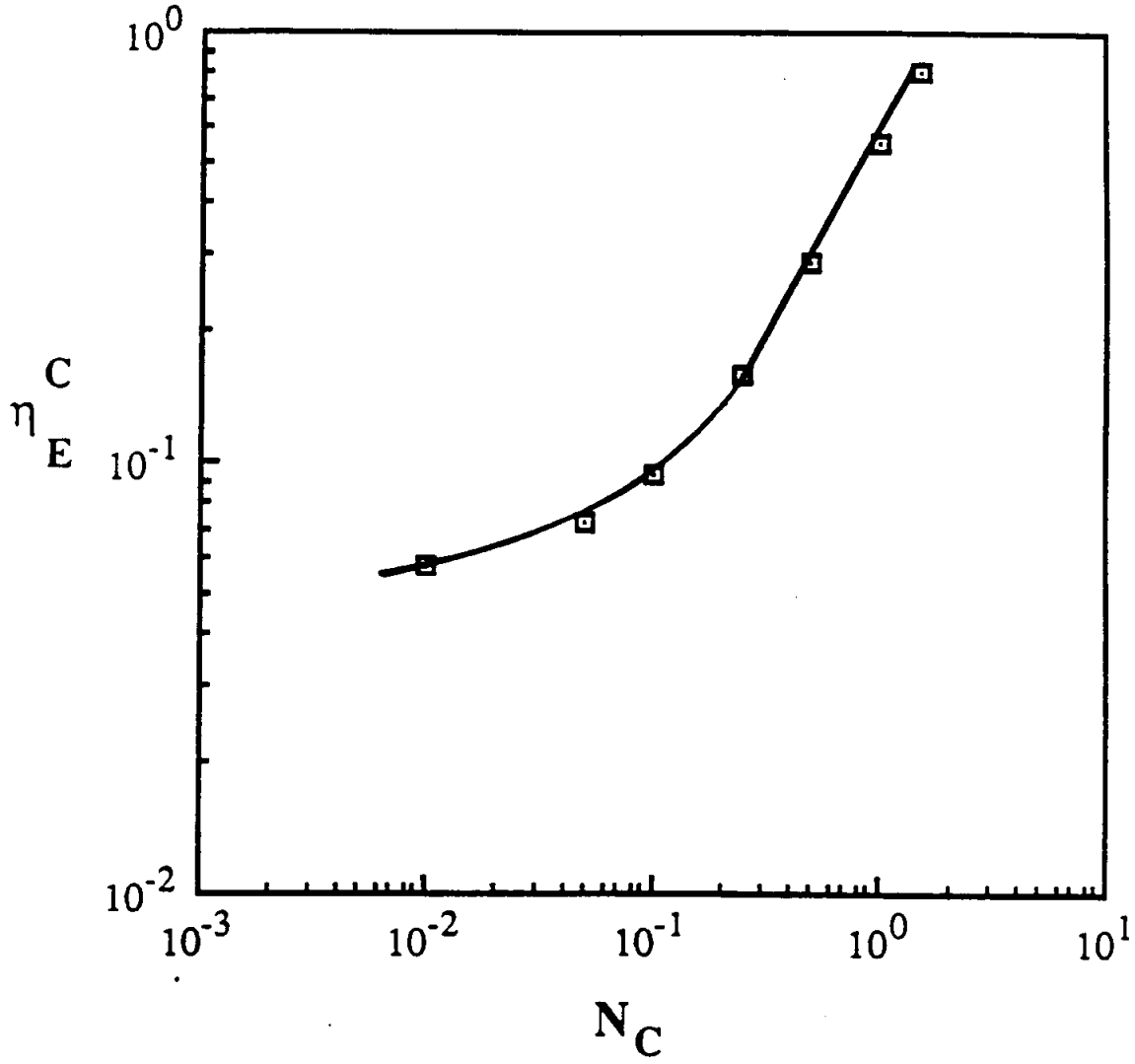

Figure 5.20 Effect of the Coulombic force parameter on the electrostatic single fiber capture efficiency of elecret fibers for b/w=1/4 and α=0.16

the cases of α equal to 0.005, 0.02, and 0.08 while, for the case of α equal to 0.16, the linear relationship between η_E^C and N_C is preceded by a non-linear region for values of N_C below approximately 0.2. The cause of such transition is not known but it is suspected to exist also for the other values of α except that it occurs at N_C values below those considered in Figures 5.17 through 5.19. In any event, the slope of the linear region varies from 0.81 for α = 0.005 to approximately 0.92 for other three values of α, an increase of nearly 10% as α is increased by a factor of 30. This difference could be attributed to the calculation error in the flow field, electric field intensity and particles critical trajectories. Thus, the electrostatic single fiber efficiency due to the Coulombic forces can be expressed, in general, as

$$\eta_E^C = \Omega(\alpha, b/w)\ N_C^{0.92} \tag{5.18}$$

where Ω is a function of α and b/w. In comparison to the above equation, Emi et al. (in press) found their results to be correlated well by the following expression

$$\eta_E^C = \Phi\ N_C^{0.75} \tag{5.19}$$

for their isolated fiber with Φ being a proportionality coefficient.

In order to investigate the interference effect of neighboring fibers on the flow field and in turn, on the calculated single fiber efficiency, the values of η_E^C corresponding to $N_C = 1$ and $b/w = 1/4$ were plotted as a function of α as shown in Figure 5.21. As seen, the results tend to be well correlated by

$$\eta_E^C = \chi(N_C, b/w)\ \alpha^{0.15} \tag{5.20}$$

with χ being a function of N_C and b/w. Combining equations (5.18) and (5.20) gives

$$\eta_E^C = \mathfrak{R}(b/w)\ \alpha^{0.15}\ N_C^{0.92} \tag{5.21}$$

where $\mathfrak{R}$ is a function of the fiber aspect ratio.

Finally, based on the above results, the single fiber capture efficiency of charged particles by rectangular electret fibers with an aspect ratio, b/w, equal to 1/4 with w being the side normal to the flow direction, can be approximated by

$$\eta_E^C = 0.715\ \alpha^{0.15}\ N_C^{0.92} \tag{5.22}$$

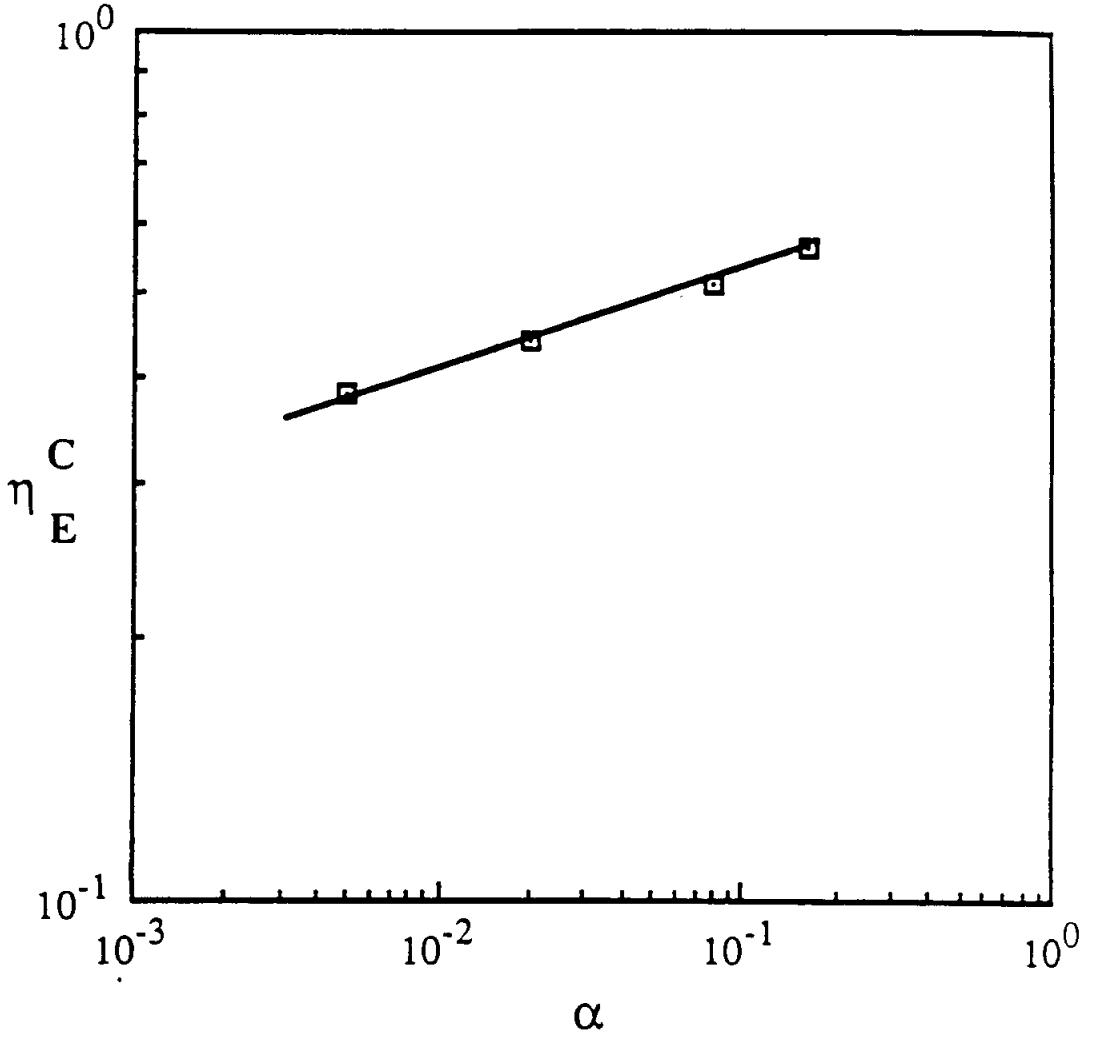

Figure 5.21 Effect of the solid-volume fraction on the electrostatic single fiber efficiency of electret fibers due to Coulombic forces for N_C=1.0 and b/w=1/4

with the multiplier being calculated from the tabulated results.

The effect of orientation of the fiber on the calculated efficiency values was also investigated by considering a fiber with an aspect ratio equal to 4/1 and $a = 0.08$. The results are shown in Figure 5.22. Although, the power-law relationship between η_E^C and N_C for b/w = 4/1 seems to be similar to that for b/w = 1/4 (the line in Figure 5.22 has a slope equal to approximately 0.96), the single fiber efficiency values are found to be higher when the fiber is oriented by 90^o.

5.4.2 Induced Interaction

Opposite to the Coulombic forces, the induction forces act on uncharged particles by inducing in them charges having a polarity opposite to that of the fiber. Therefore, the induction forces are always attractive in nature and enable the fiber to collect particles both on the front and rear surfaces. Hence, a particle which passes over the fiber may be drawn back toward the rear surface by the strong induced forces.

The flow field, number of charges on the fiber and values of a used in the calculation of induction single fiber efficiency were the same as those used in the case of

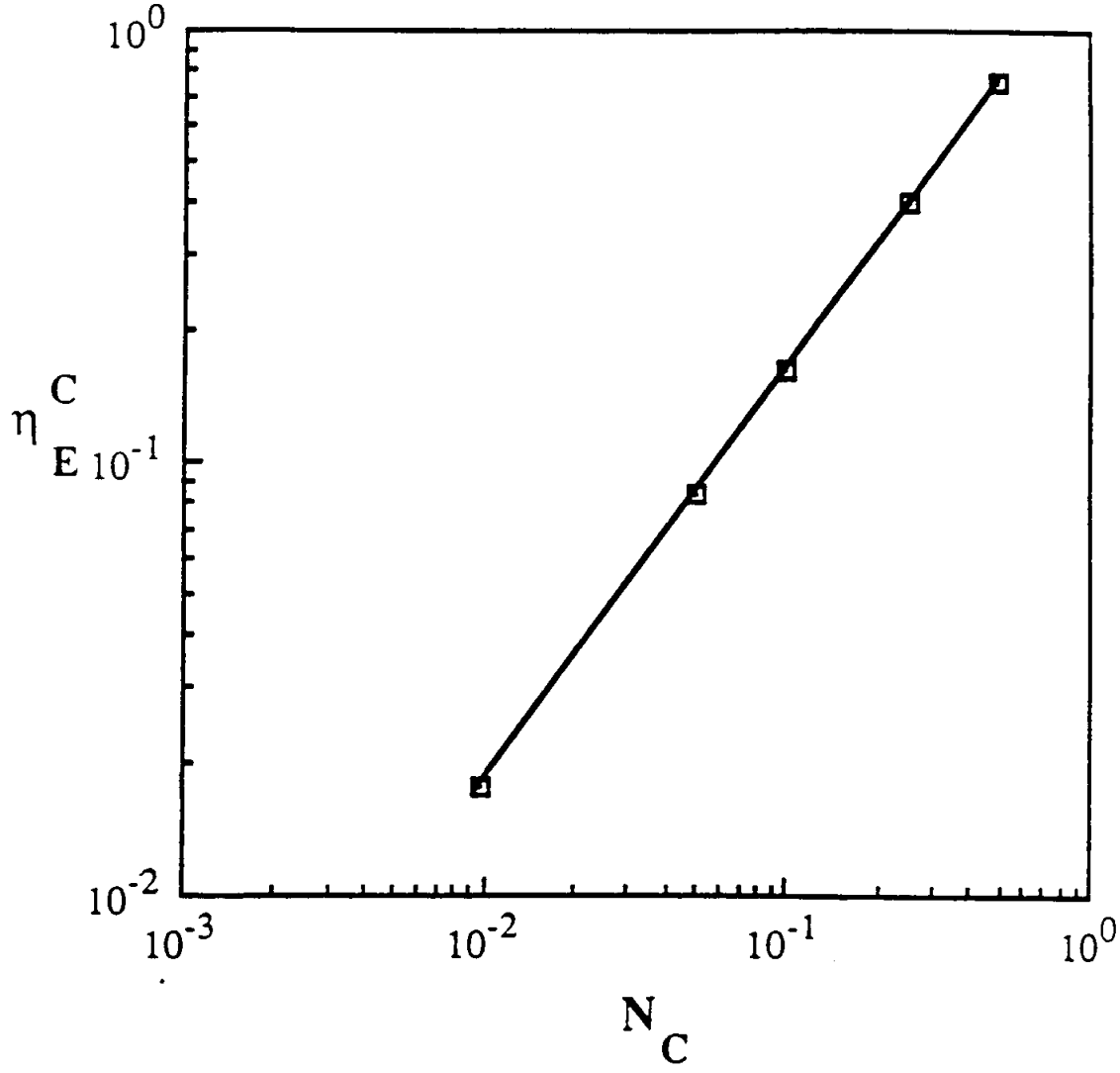

Figure 5.22 Effect of the fiber orientation by 90 degrees (b/w=4/1) on the calculated values of the electrostatic single fiber efficiency as a function of N_C for α=0.08

the Coulombic interaction. The results are plotted in Figures 5.23 through 5.26 and tabulated in Table 5.13 for various values of α and b/w = 1/4. As shown, the data symbols in each figure tend to lie on a straight line suggesting that a power-law relationship between η_E^I , the single fiber efficiency due to the induced forces, and N_I exists with the exponent being equal to the slope of the line. The slope varies from 0.419 for α = 0.020 to 0.540 for α = 0.16, while those corresponding to α = 0.005 and 0.08 are 0.445 and 0.465, respectively. Although there is about 30% diffrence between minimum and maximum values of the calculated slopes and knowing that there exist calculation errors as mentioned above, One may simply use the average of slope values in formulating the following expression for η_E^I,

$$\eta_E^I = G(\alpha, b/w)\ N_I^{0.47} \qquad (5.23)$$

where G is a function of α and b/w. Similar relationship was obtained also by Emi et al. (in press) with the exponent being equal to 0.4. Thus, the agreement between the present result and that of Japanese is fairly good for this type of electrostatic interaction. Considering only rectangular fibers with an aspect ratio of 1/4, equation (5.23) can be

Table 5.13 Calculated single fiber capture efficiency values of charged rectangular fibers with b/w=1/4 due to the induction forces for various values of the dimensionless force parameter and solid-volume fraction

α	0·005		0·02		0·08		0·16	
	N_I	η_E^I	N_I	η_E^I	N_I	η_E^I	N_I	η_E^I
	0.980	0.0760	0.490	0.0778	0.098	0.0607	0.098	0.0934
	4.901	0.1600	0.980	0.1087	0.196	0.0835	0.490	0.2106
	9.801	0.2200	4.901	0.2245	0.490	0.1292	0.980	0.3029
	49.005	0.4349	9.801	0.3038	0.980	0.1801	2.450	0.4977
	98.010	0.5687	49.005	0.5948	1.960	0.2490	4.901	0.7291
	294.030	0.8693	98.010	0.7868	4.901	0.3827		
					9.801	0.5249		
					19.602	0.7180		
					29.403	0.8580		

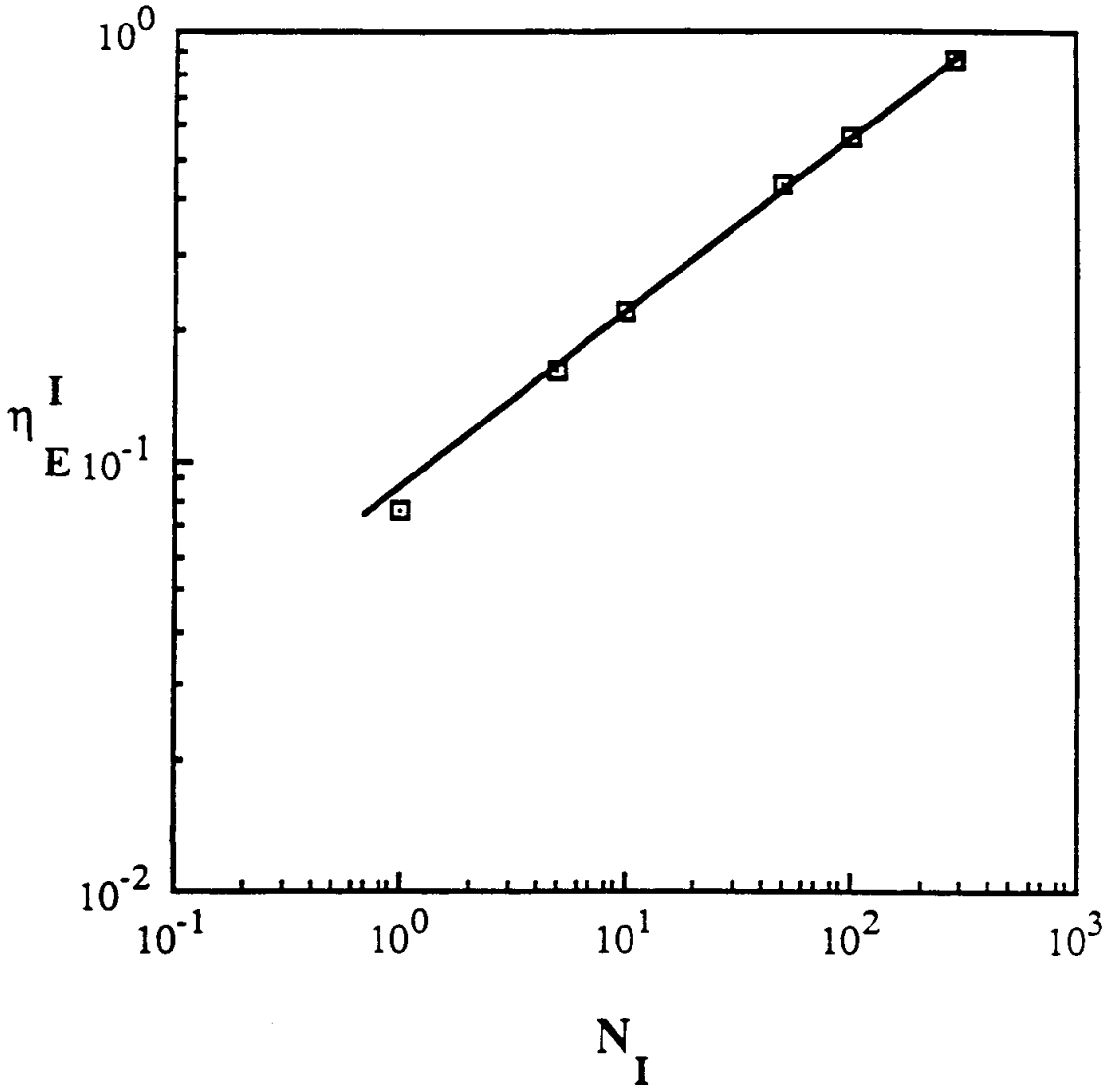

Figure 5.23 Effect of the induction force parameter on the electrostatic single fiber efficiency of electret fibers for b/w=1/4 and α=0.005

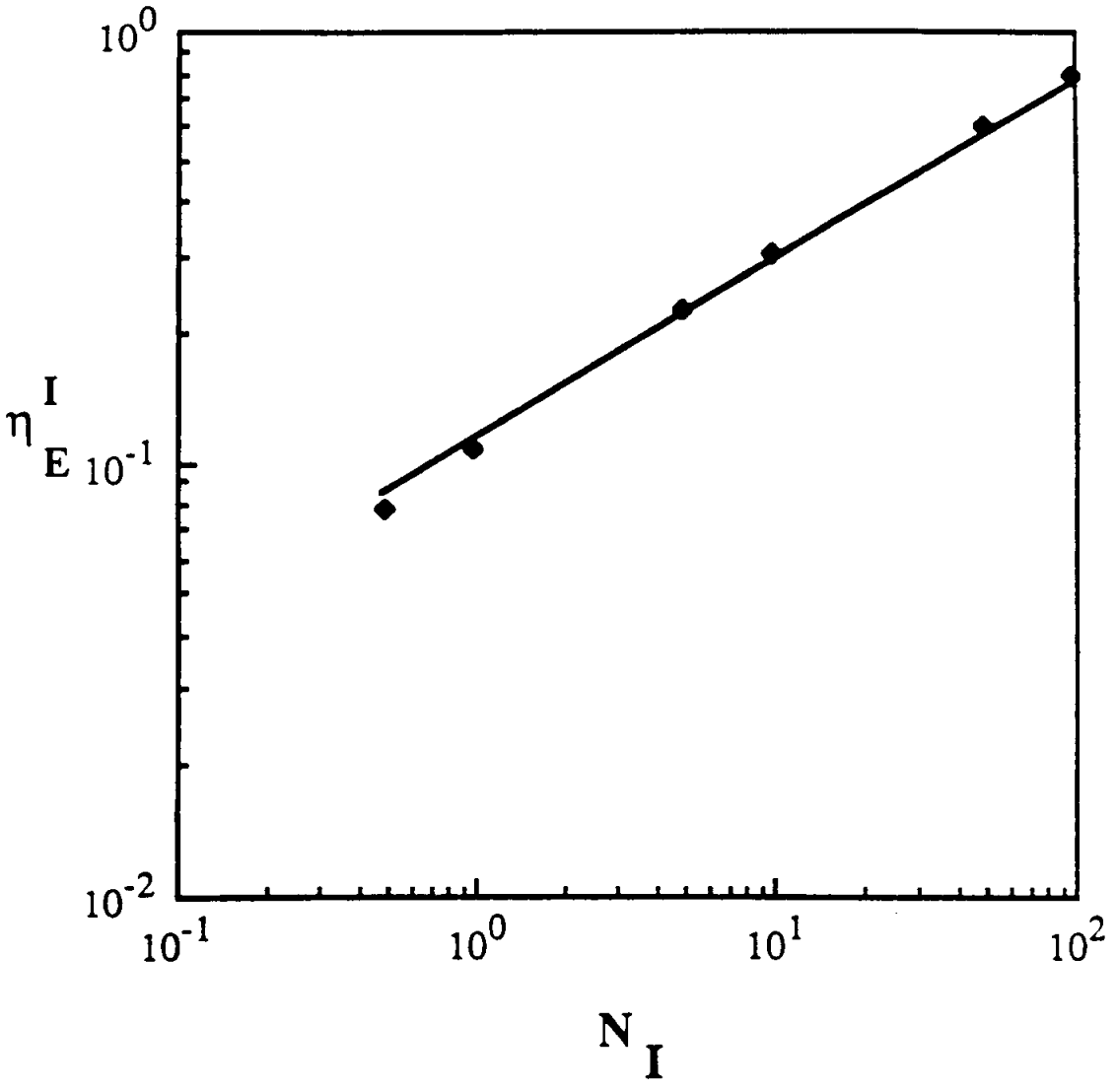

Figure 5.24 Effect of the induction force parameter on the electrostatic single fiber efficiency of electret fibers for b/w=1/4 and α=0.02

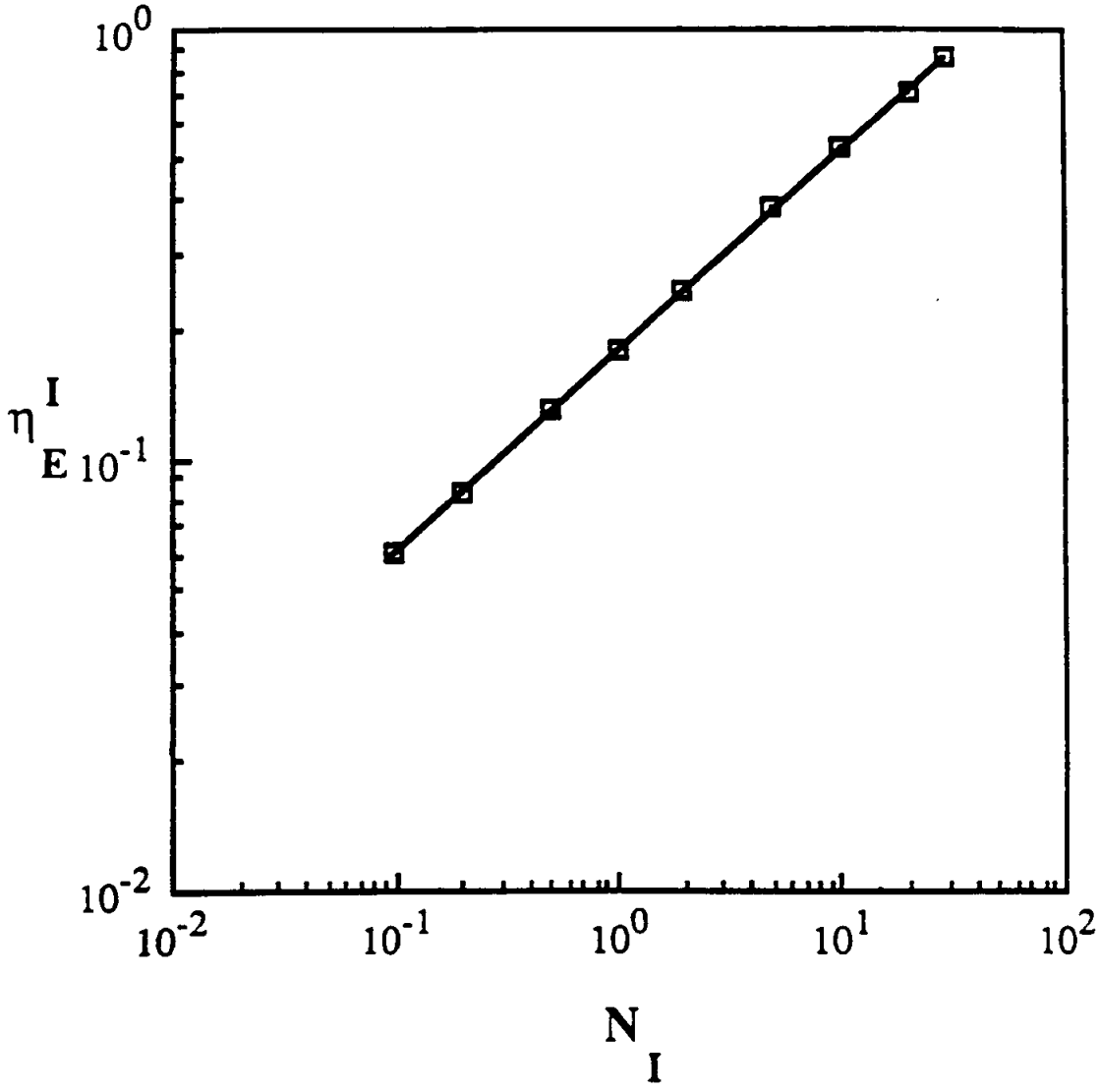

Figure 5.25 Effect of the induction force parameter on the electrostatic single fiber efficiency of electret fibers for b/w=1/4 and α=0.08

rewritten as

$$\eta_E^I = \aleph(\alpha)\ N_I^{0.47} \tag{5.24}$$

where $\aleph$ is a function of α only. In order to determine the nature of this function, discrete values of $\aleph$ corresponding to different values of α considered here were obtained from the calculated values of η_E^I and N_I. The results are plotted in Figure 5.27. Note that the linear logarithmic relationship which was found for the case of the Coulombic forces is not present for the case of the induction forces. However, one can approximate the electrostatic single fiber capture efficiency of uncharged particles by rectangular electret fibers having an aspect ratio, b/w, equal to 1/4, with w being the side normal to the flow direction, using equation (5.24) and Figure 5.27 for desired values of α and N_I.

In addition, the calculation results for b/w = 4/1 and α = 0.08 were also obtained and plotted as shown in Figure 5.28. The power-law relationship still holds with the exponent equal to 0.48 or nearly equal to that of equation (5.22). But notice that the single fiber efficiency values corresponding to b/w = 4/1 are smaller than those corresponding to b/w = 1/4, a finding which is opposite to that for the case of the Coulombic forces.

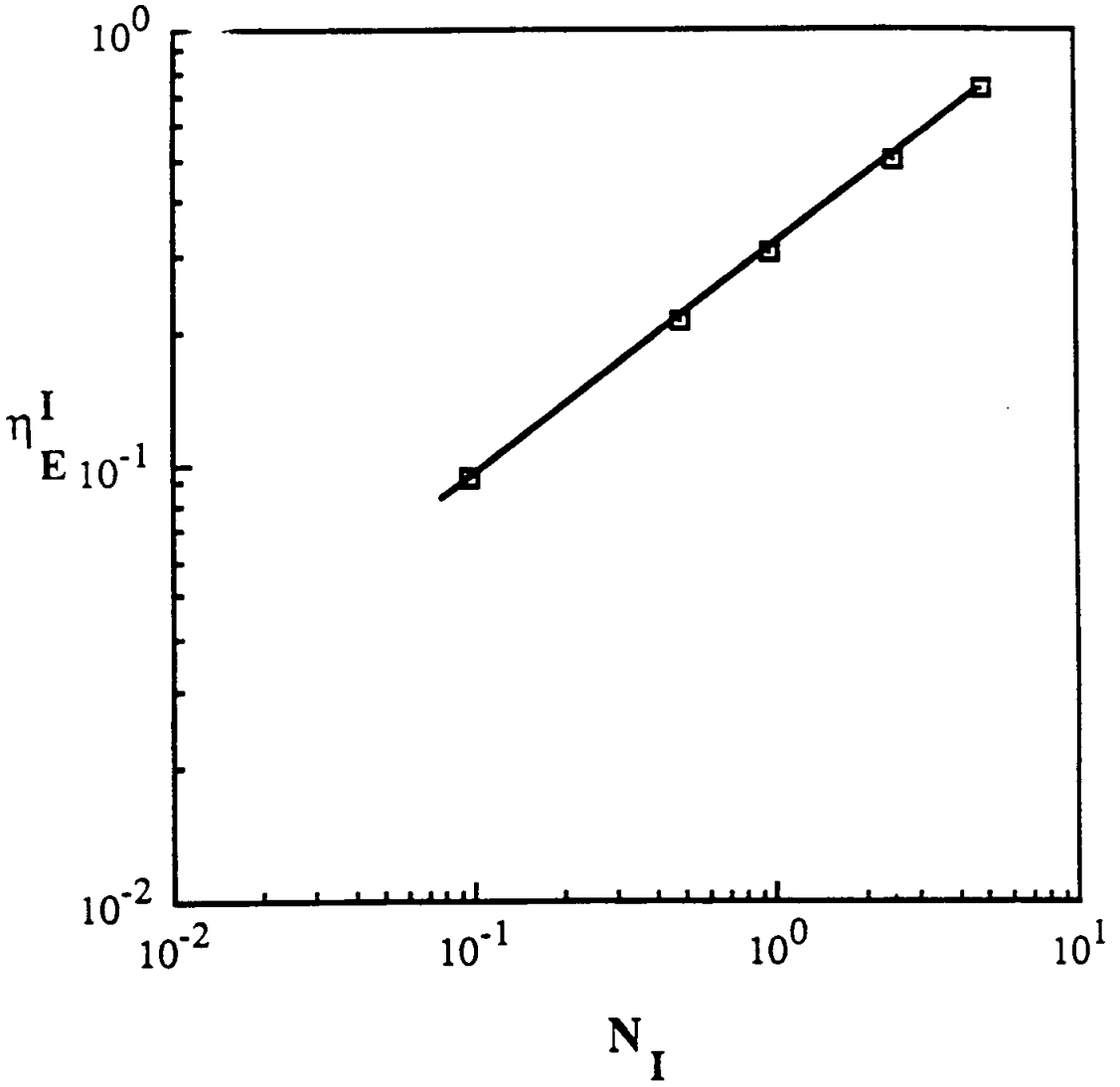

Figure 5.26 Effect of the induction force parameter on the electrostatic single fiber efficiency of electret fibers for b/w=1/4 and α=0.16

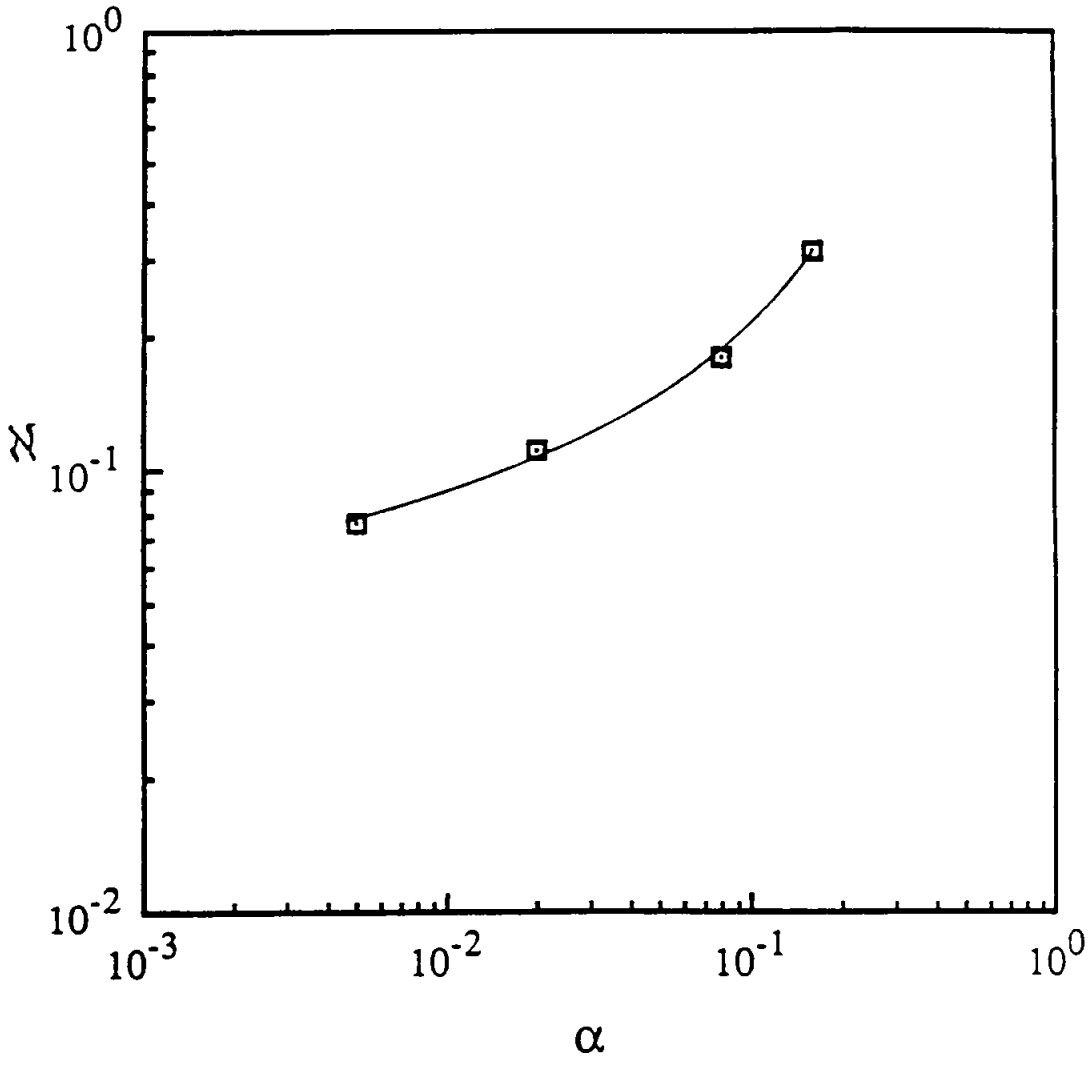

Figure 5.27 Effect of the solid-volume fraction on the electrostatic single fiber efficiency of electret fibers due to the induction forces for N_I=1.0 and b/w=1/4

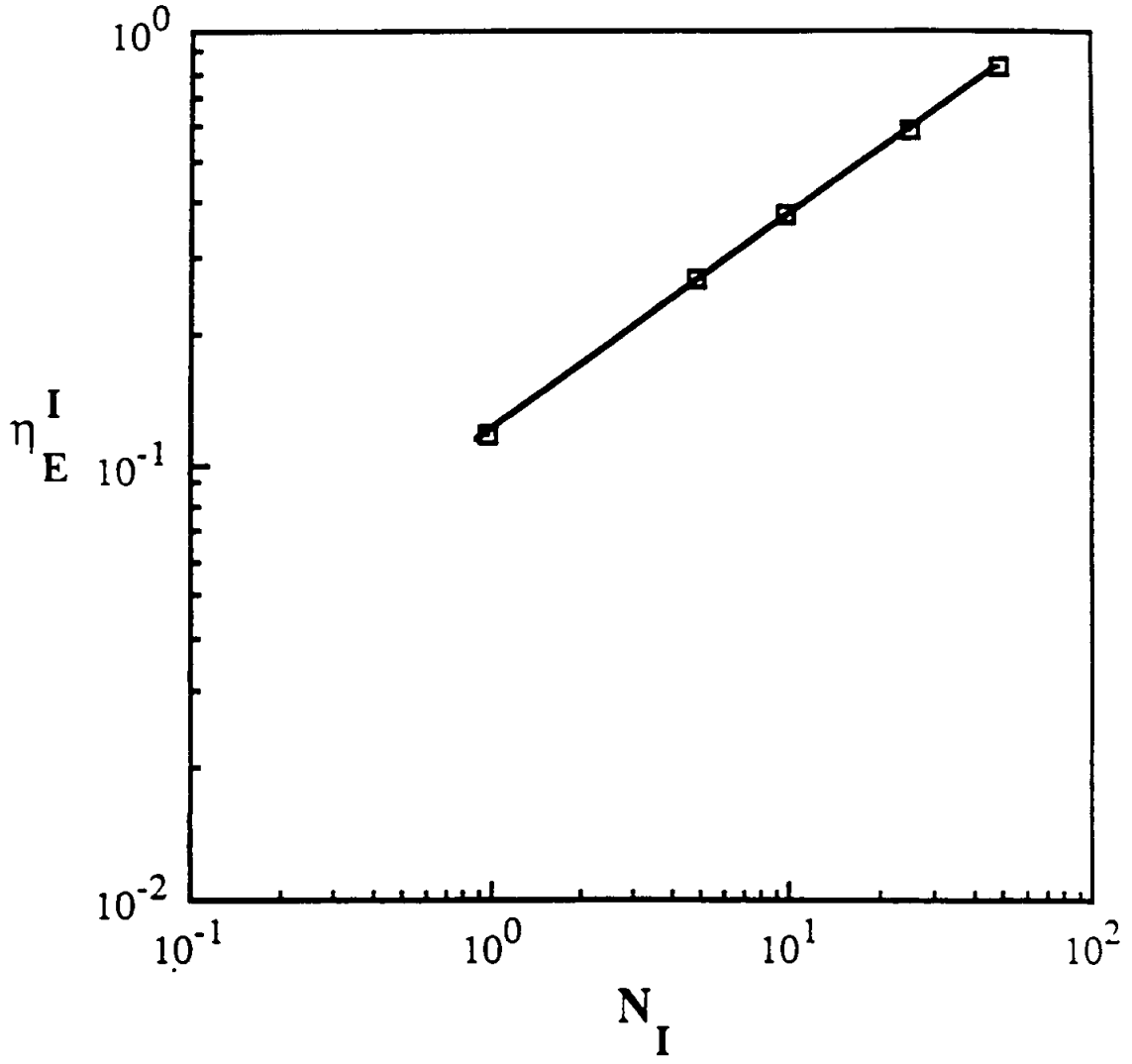

Figure 5.28 Effect of the fiber orientation by 90 degrees (b/w=4/1) on the calculated values of the electrostatic single fiber efficiency as a function of N_I

for α=0.08

Chapter 6

EXPERIMENTAL RESULTS

6.1 Results of Penetration and Pressure Drop Measurements

The principal experimental results are shown in the sequence of figures and tables presented below. The results are discussed in more detail along with the sequence of figures presented. A total of six filters were tested, each at three flow rates leading to a total of eighteen data sets.

Figures 6.1, 6.2, and 6.3 along with Tables 6.1 and 6.2 show the measured aerosol penetration through a dust and mist filter (D/M) manufactured by manufacturer A at the flow rates of 16, 28, and 48 liters per minute. Notice that Figures 6.1 and 6.2 contain the penetration measurements of both DOP and NaCl particles while, Figure 6.3 shows the penetration of DOP particles only. The curves are all similar in shape, showing first a rising aerosol penetration with increasing particle size for small particles and then a decreasing penetration with increasing particle size for larger particles. In each case, there is a distinct particle size for which the aerosol penetration through the filter is a maximum and the corresponding filter efficiency, a

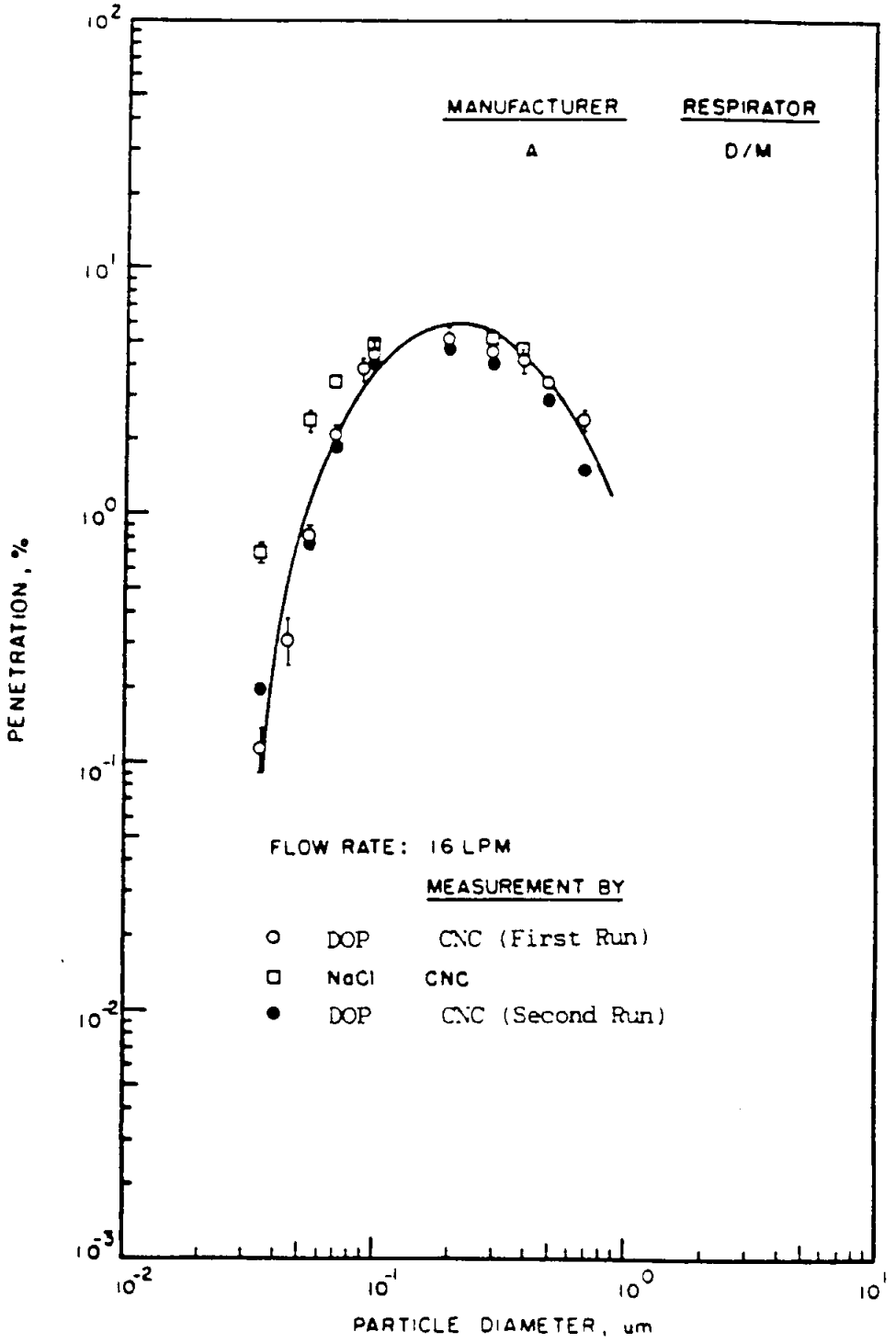

Figure 6.1 Aerosol penetration through respirator at 16 liters per minute for dust/mist respirator of manufacturer A

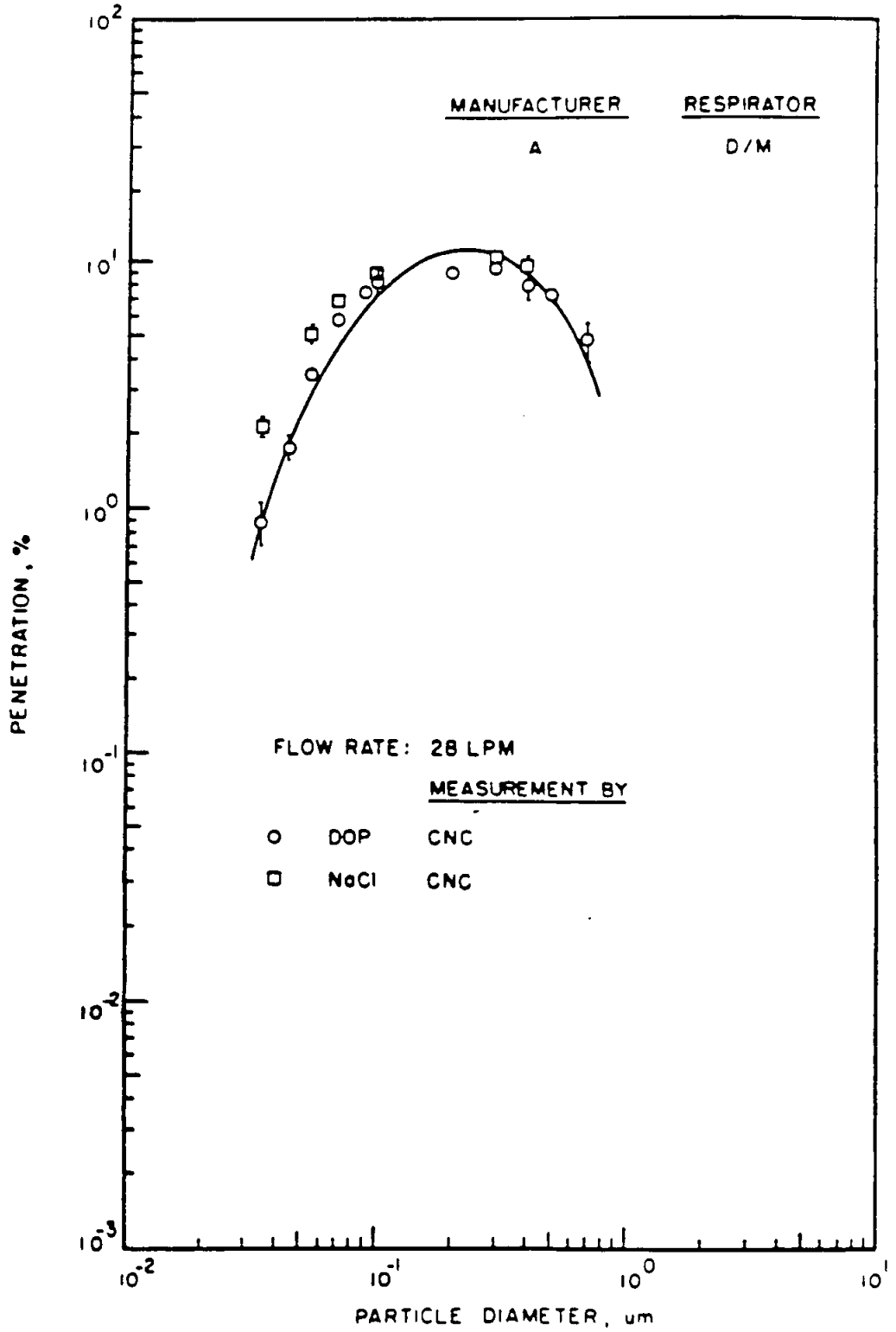

Figure 6.2 Aerosol penetration through respirator at 28 liters per minute for dust/mist respirator of manufacturer A

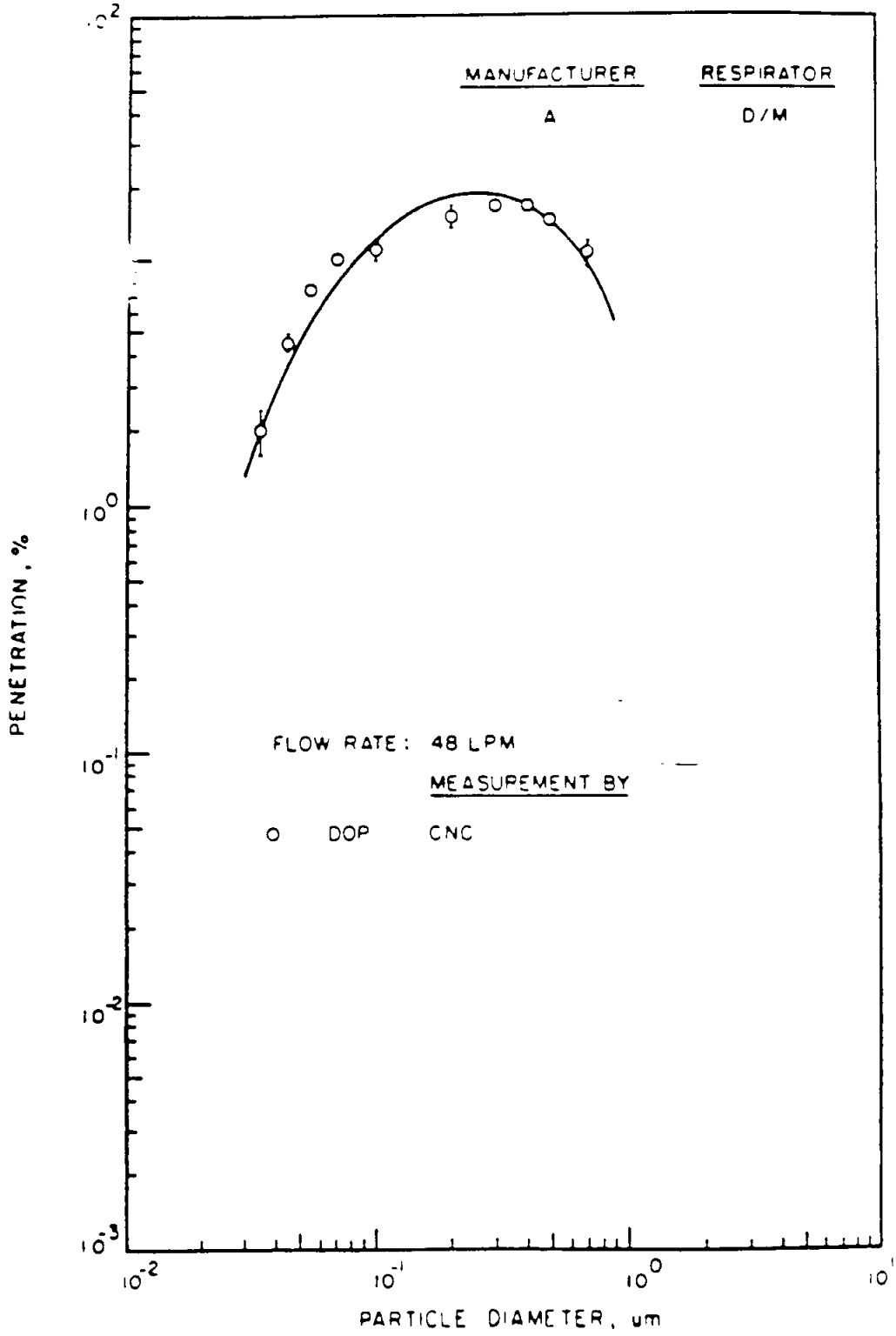

Figure 6.3 Aerosol penetration through respirator at 48 liters per minute for dust/mist respirator of manufacturer A

Table 6.1 CNC penetration measurements of monodisperse DOP aerosol through dust/mist respirator of manufacturer A at 16, 28, and 48 Lpm

Dp, μ	Penetration (16Lpm)	Penetration (28Lpm)	Penetration (48Lpm)
0.035	0.0012±0.0002	0.0090±0.0018	0.0202±0.0041
0.045	0.0031±0.0006	0.0177±0.0018	0.0461±0.0029
0.055	0.0082±0.0008	0.0344±0.0018	0.0746±0.0038
0.070	0.0212±0.0022	0.0576±0.0019	0.1022±0.0054
0.090	0.0389±0.0041	0.0751±0.0064	
0.100	0.0449±0.0070	0.0825±0.0091	0.1111±0.0134
0.200	0.0524±0.0056	0.0900±0.0085	0.1545±0.0180
0.300	0.0456±0.0039	0.0947±0.0081	0.1691±0.0108
0.400	0.0426±0.0046	0.0795±0.0093	0.1689±0.0113
0.500	0.0347±0.0029	0.0743±0.0048	0.1486±0.0074
0.700	0.0245±0.0025	0.0482±0.0082	0.1079±0.0121

Table 6.2 CNC penetration measurements of monodisperse NaCl aerosol through dust/mist respirator of manufacturer A at 16 and 28 Lpm

Dp, μ	Penetration (16Lpm)	Penetration (28Lpm)
0.035	0.0070±0.0006	0.0214±0.0018
0.055	0.0240±0.0020	0.0508±0.0037
0.070	0.0345±0.0020	0.0694±0.0037
0.100	0.0480±0.0039	0.0870±0.0073
0.300	0.0522±0.0033	0.1040±0.0047
0.400	0.0470±0.0040	0.0972±0.0102

minimum. The most penetrating particle size is in the vicinity of 0.2 μm. The peak penetration at the most penetrating particle size varies from approximately 6% at a flow rate of 16 liters per minute, to 10% at 28 liters per minute and 20% at the flow rate of 48 liters per minute.

As mentioned above, this respirator as well as others were challenged with several monodisperse, NaCl aerosols at the same flow rates as the DOP aerosols to compare the penetration characteristics of solid and liquid particles. It should be mentioned that a clean respirator was used for each complete test which involved measuring penetration of a sequence of DOP or NaCl particles of desired size. As illustrated by the figures, the peak penetration and most penetrating particle size for the NaCl aerosol seem to coincide with those for the DOP aerosol. However, the NaCl particles smaller than the most penetrating particle size have slightly higher penetration than the corresponding DOP particles of equal size, while for particles larger than the most penetrating size, the penetration of two aerosols is similar. This type of behavior was observed for all the respirator filters tested. However, the apparent disagreement between the penetration characteristics of solid and liquid particles below the most penetrating particle size is believed to be the result of the experimental errors in the particle concentration

measurements and the size determination of NaCl particles due to the assumption that they are spherical. But a photograph of NaCl particles taken by Berglund and Liu (1973) shows that the NaCl particles are rather cubical than spherical. Therefore, by diameter of a NaCl particle in the present penetration-vs.-particle diameter curves, one means the diameter of a spherical particle having the same electrical mobility as the NaCl particle, which, in turn, may be different from the diameter of a true spherical DOP particle with the same mobility. It should be noted also that the difference in penetration values of solid and liquid particles is not due to the possible bouncing of solid particles off the fibers since the disagreement seems to be more significant at the lower flow rate of 16 liters per minute than at the other two higher flow rates of 28 and 48 liters per minute, a trend which is in contradiction with the particle-bounce phenomenon.

Another case of interest was the repeatibility of the penetration measurements, which was examined three months later by repeating the experiments using clean respirators. The results are depicted in Figures 6.1 and 6.2 by the solid circles. As shown, the agreement between the old and new penetration measurements (open and solid circles, respectively) is quite good thus, verifying the repeatibility of the measurements. The solid circles in all

the subsequent figures designate the repeated measurements.

The pressure drop versus flow characteristics of the respirator are shown in Figure 6.4. The pressure drop is seen to increase linearly from zero to approximately 0.2 inch of water over the flow rate range of zero to 50 liters per minute.

Figures 6.5, 6.6, and 6.7 show the results for the flat-sheet filter media of the type used in the respirator air filters produced by manufacturer L. The measurements are listed also in Tables 6.3 and 6.4. Again, there is a distinct particle size for which the aerosol penetration is a maximum. The most penetrating particle size varies from approximately 0.15 at a flow rate of 16 liters per minute (for a filter area of 41.88 cm^2) to approximately 0.10 μm at a flow rate of 28 liters per minute and approximately 0.11 μm at 48 liters per minute. The peak penetration varies from approximately 10% at the flow rate of 16 liters per minute to approximately 15% and 17% at the flow rates of 28 and 48 liters per minute, respectively. Again, the repeatibility of data is excellent as shown by the agreement between open and solid circles. Note also the comparison between the penetration measurements made by CNC and the other two aerosol instruments, namely, APS (Aerodynamic Particle Sizer), and OPC (Optical Particle Counter) which were to be evaluated in the present study for their capability to

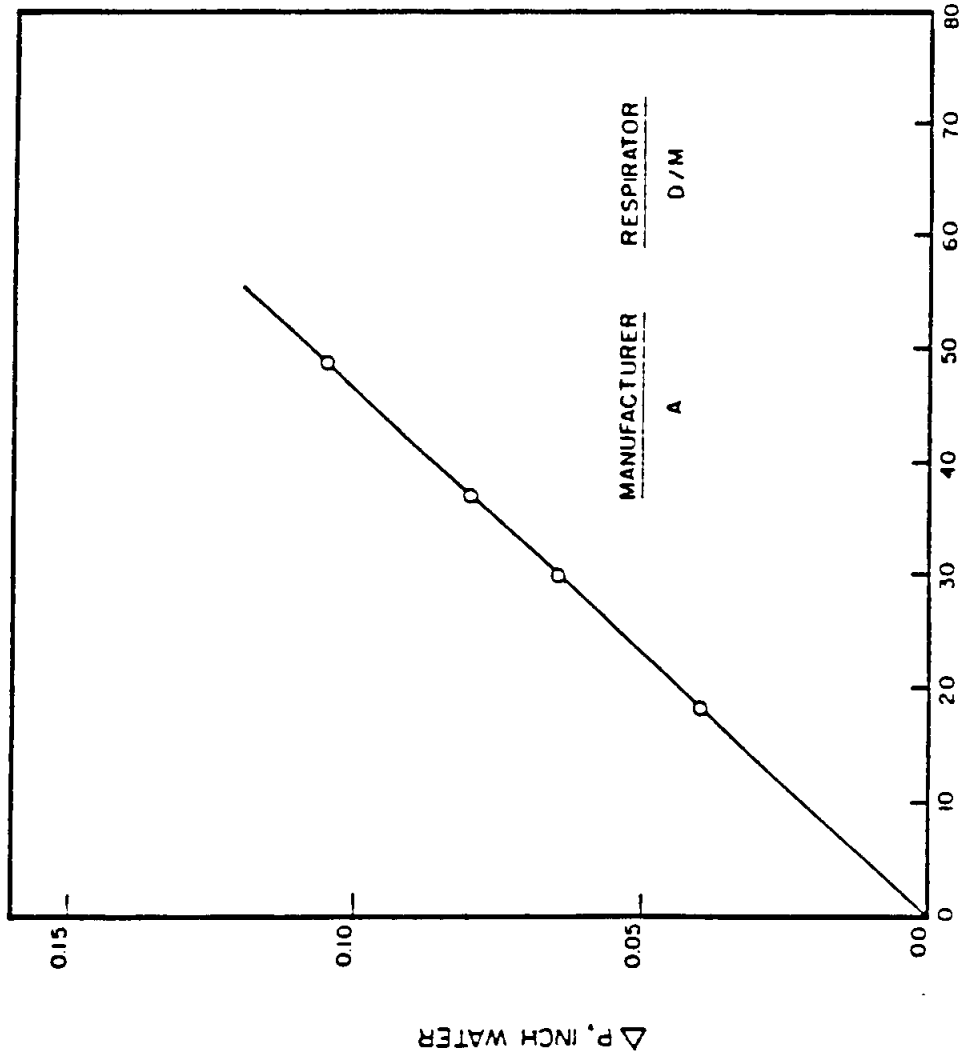

Figure 6.4 Pressure drop as a function of flow rate for dust/mist respirator of manufacturer A

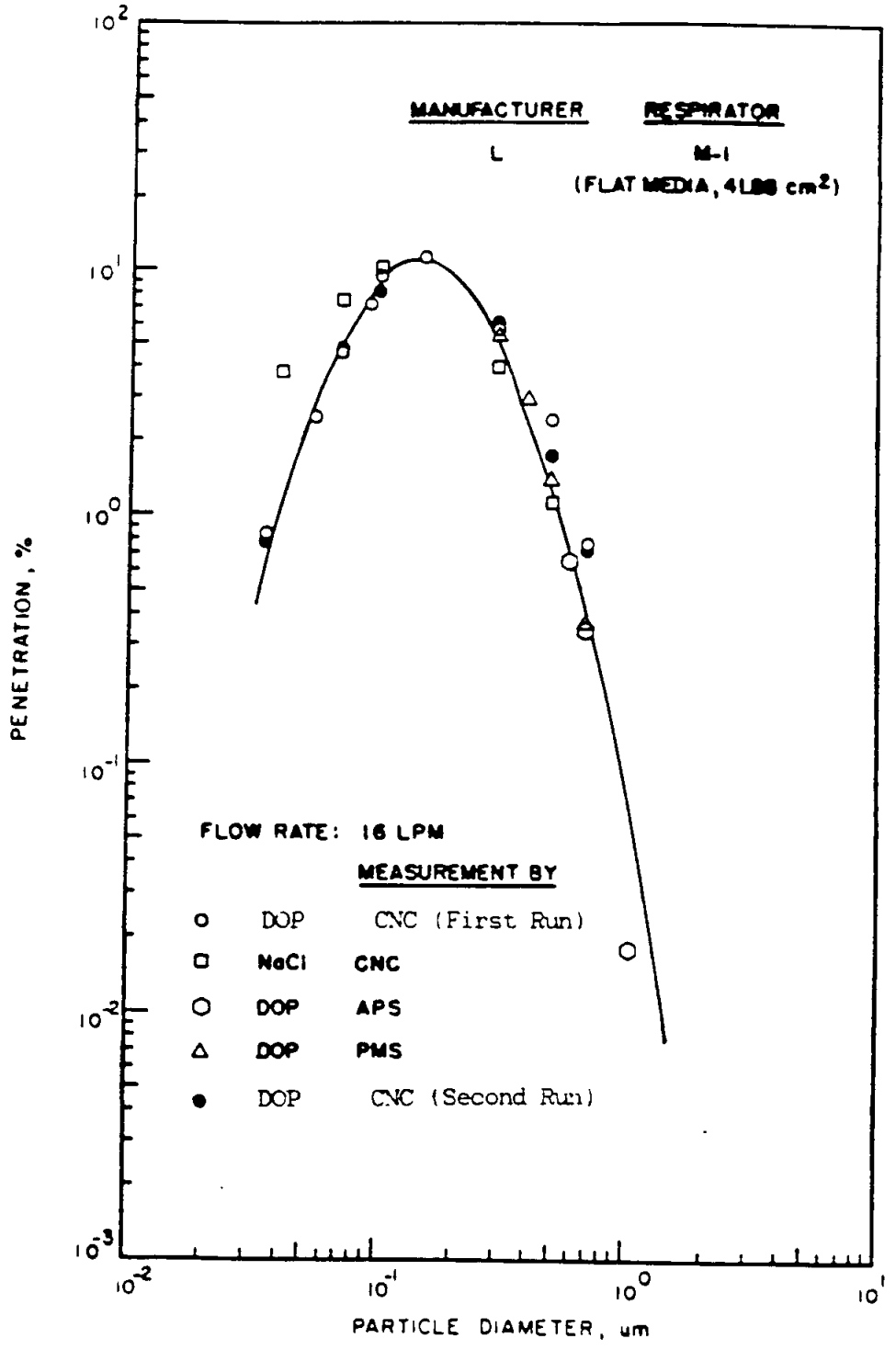

Figure 6.5 Aerosol penetration through respirator at 16 liters per minute for flat-sheet filter media of manufacturer L

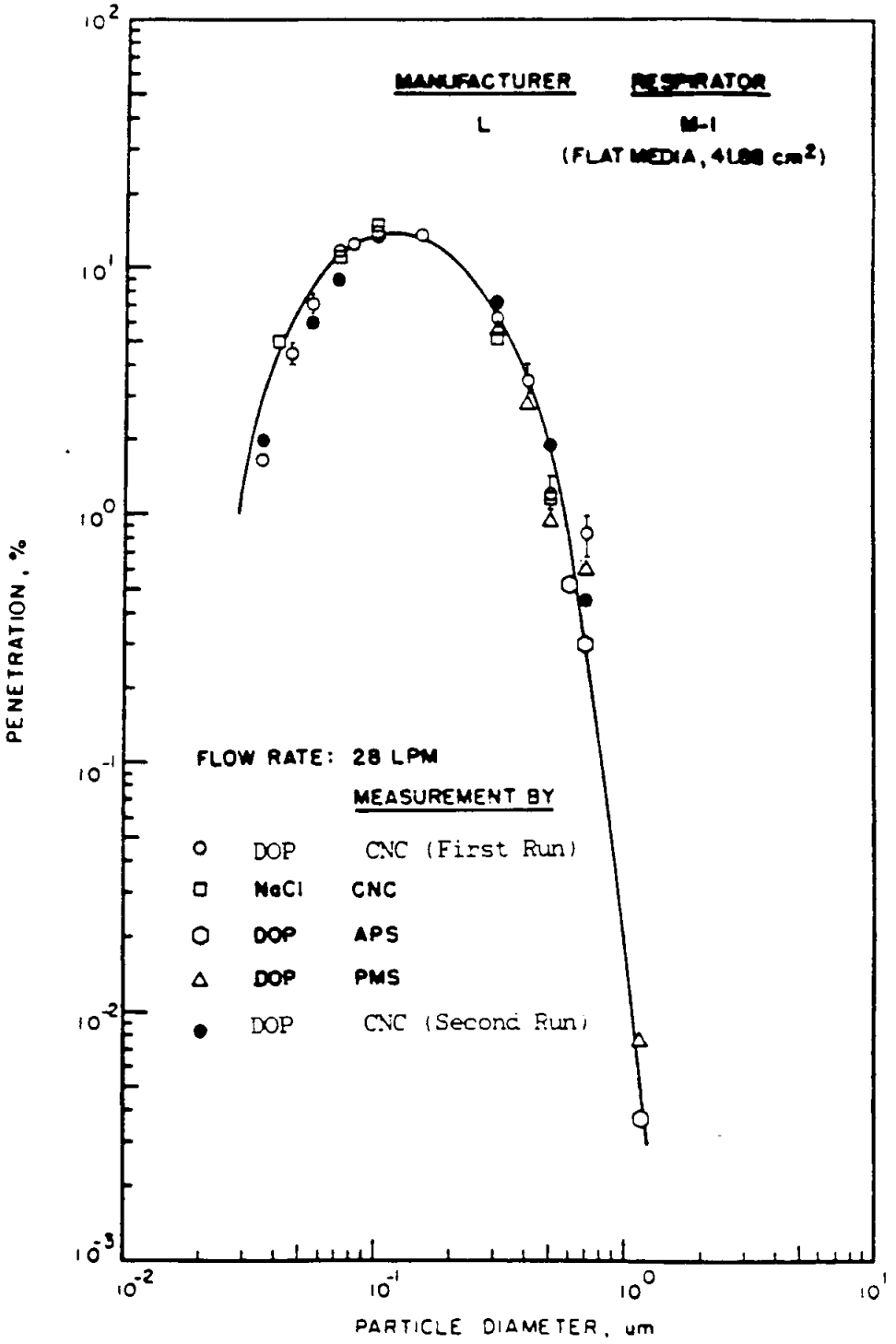

Figure 6.6 Aerosol penetration through respirator at 28 liters per minute for flat-sheet filter media of manufacturer L

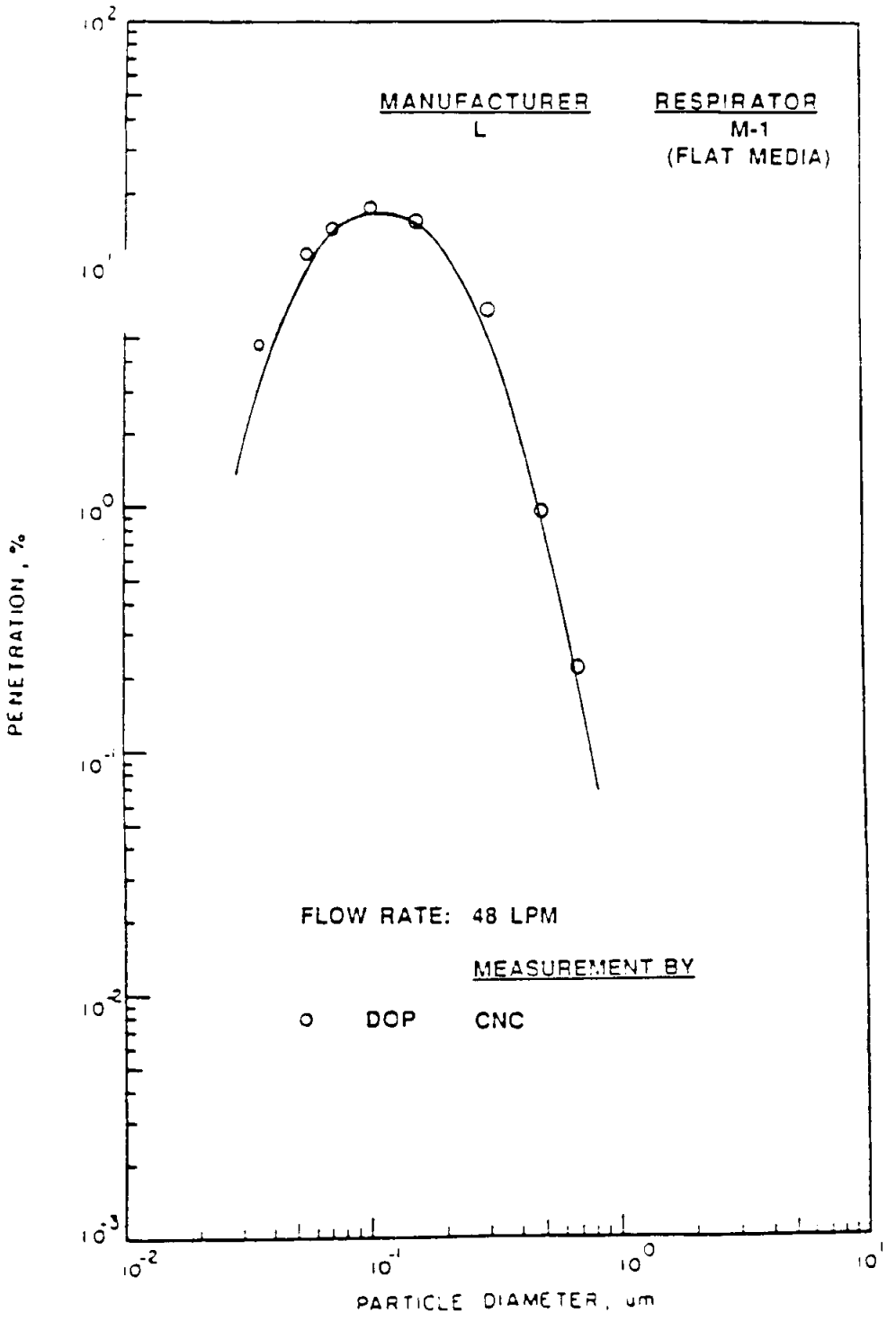

Figure 6.7 Aerosol penetration through respirator at 48 liters per minute for flat-sheet filter media of manufacturer L

Table 6.3 CNC penetration measurements of monodisperse DOP aerosol through flat-sheet filter media of manufacturer L at 16, 28, and 48 Lpm

Dp, μ	Penetration (16Lpm)	Penetration (28Lpm)	Penetration (48Lpm)
0.035	0.0084±0.0009	0.0167±0.0027	0.0482±0.0052
0.045		0.0446±0.0046	
0.055	0.0252±0.0026	0.0711±0.0052	0.1135±0.0073
0.070	0.0473±0.0049	0.1183±0.0124	0.1449±0.0130
0.080		0.1250±0.0084	
0.090	0.0735±0.0110	0.1383±0.0075	
0.100	0.0950±0.0055	0.1392±0.0075	0.1717±0.0100
0.150	0.1131±0.0126	0.1366±0.0147	0.1541±0.0052
0.300	0.0581±0.0063	0.0643±0.0058	0.0671±0.0030
0.400		0.0353±0.0055	
0.500	0.0247±0.0026	0.0127±0.0019	0.0109±0.0017
0.700	0.0079±0.0010	0.0086±0.0021	0.0023±0.0005

Table 6.4 CNC penetration measurements of monodisperse NaCl aerosol through flat-sheet filter media of manufacturer L at 16 and 28 Lpm

Dp,μ	Penetration (16Lpm)	Penetration (28Lpm)
0.04	0.0379±0.0039	0.0500±0.0063
0.07	0.0754±0.0079	0.1124±0.0100
0.10	0.1007±0.0113	0.1460±0.0157
0.30	0.0404±0.0064	0.0517±0.0054
0.50	0.0115±0.0023	0.0117±0.0024

measure the filtration efficiency of filters. A detailed discussion of the comparison between penetration measurements of the three instruments is given below. Meanwhile, as shown in Figure 6.8, the pressure drop across the filter medium of the respirator L increases linearly and rapidly with the flow rate at the rate of 0.03 inch of water per liter per minute of the flow.

In the case of the dust/mist respirator manufactured by manufacturer M, which also recommendes the respirator for use for lead and asbestos protection, the results are shown in Figures 6.9, 6.10, and 6.11 and listed in Tables 6.5 and 6.6 for aerosol penetration and in Figure 6.12 for filter pressure drop. The peak aerosol penetration varies from 30 to 50% at a size of approximately 0.4 μm. Such large most-penetrating particle size and high filter penetration are suggestive of the use of relatively coarse fibers in the respirator. Also, as gathered from a private communication with the respirator manufacturer, the respirator filter is composed of uncharged fibers which have lower collection efficiency than comparable charged fibers used in the high efficiency respirators. Furthermore, as shown in Figure 6.12, the pressure drop across the respirator filter and the air flow rate through the filter are linearly related with the slope being equal to approximately 0.0045 inch water per liter per minute of the flow.

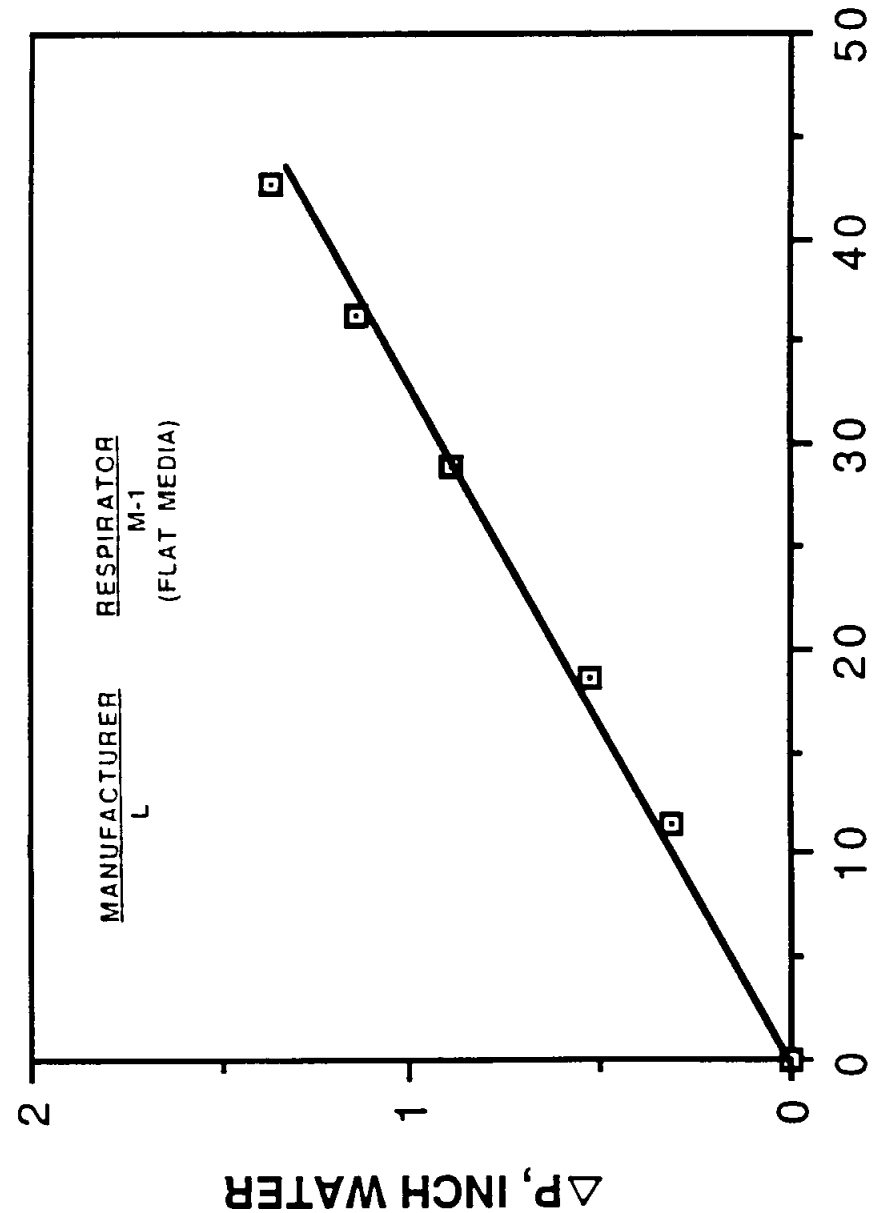

Figure 6.8 Pressure drop as a function of flow rate for flat-sheet filter media of manufacturer L

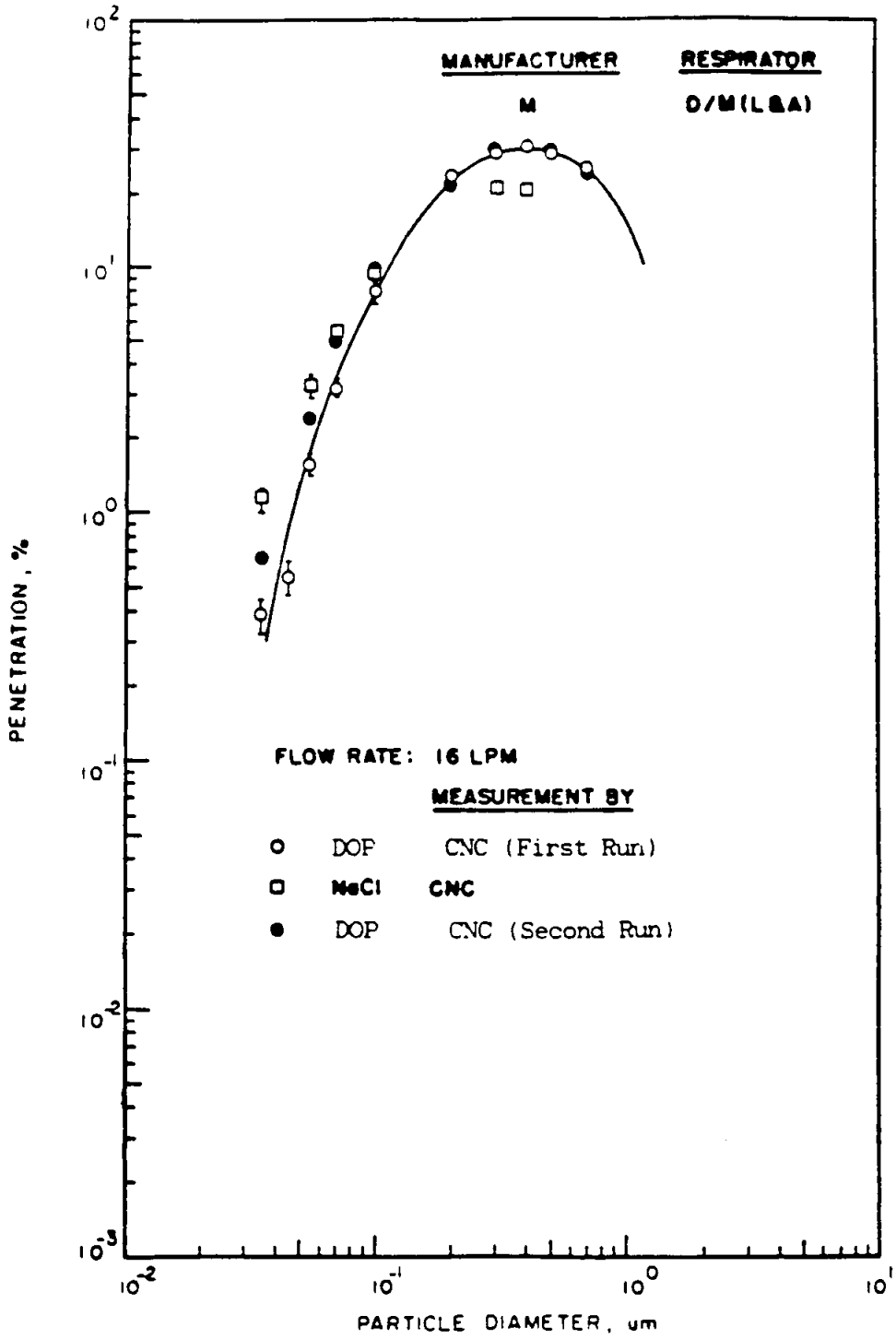

Figure 6.9 Aerosol penetration through respirator at 16 liters per minute for dust/mist respirator of manufacturer M

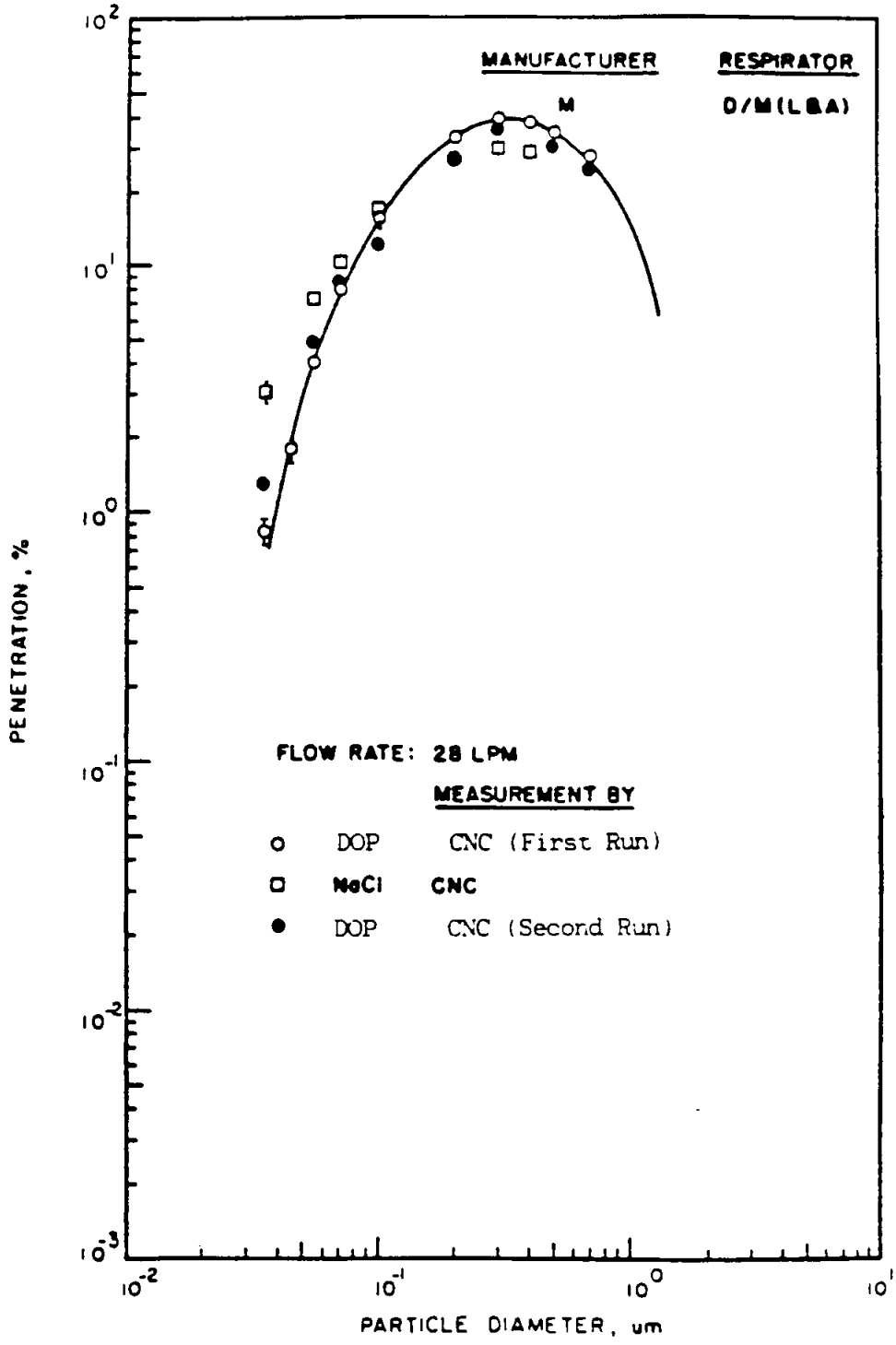

Figure 6.10 Aerosol penetration through respirator at 28 liters per minute for dust/mist respirator of manufacturer M

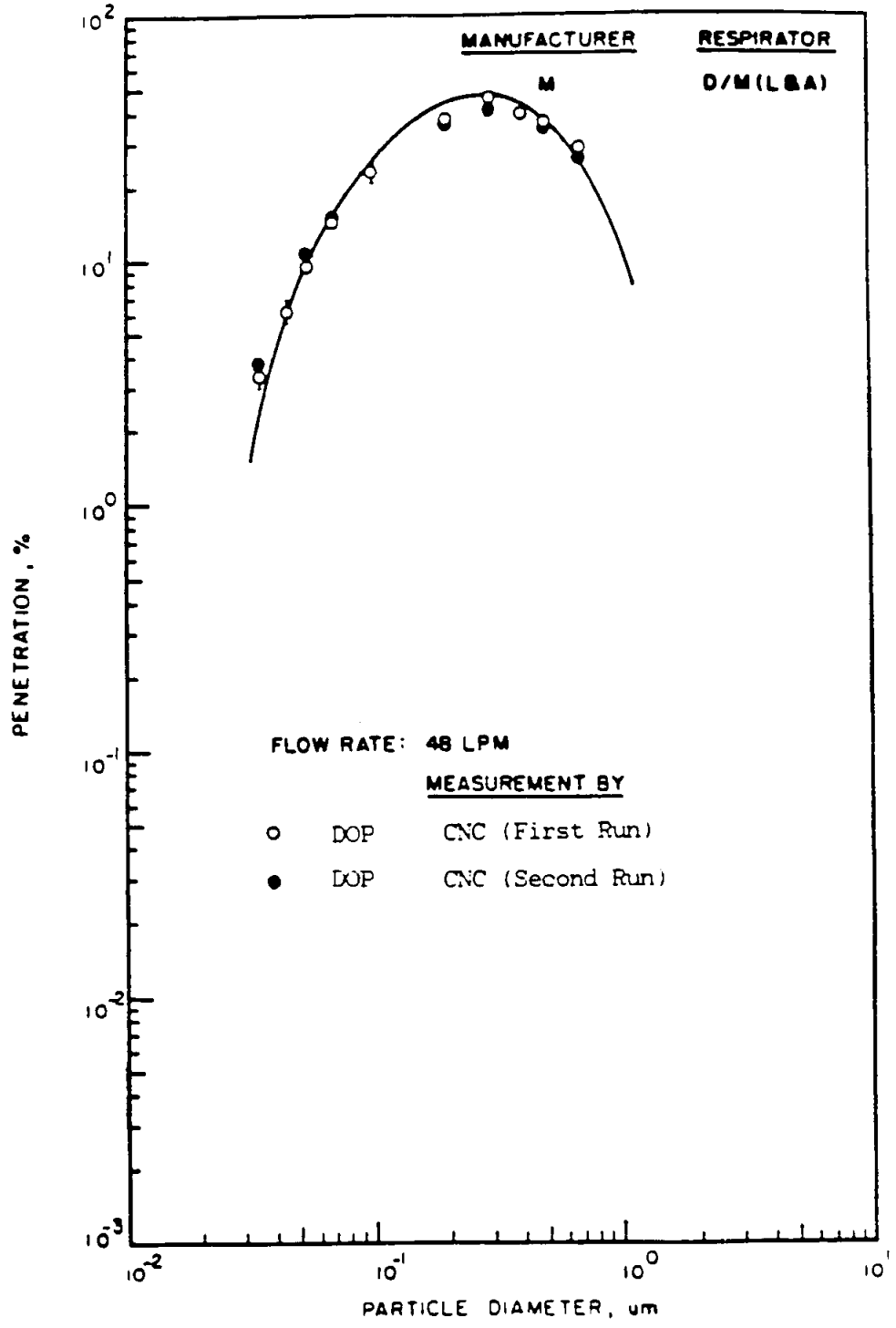

Figure 6.11 Aerosol penetration through respirator at 48 liters per minute for dust/mist respirator of manufacturer M

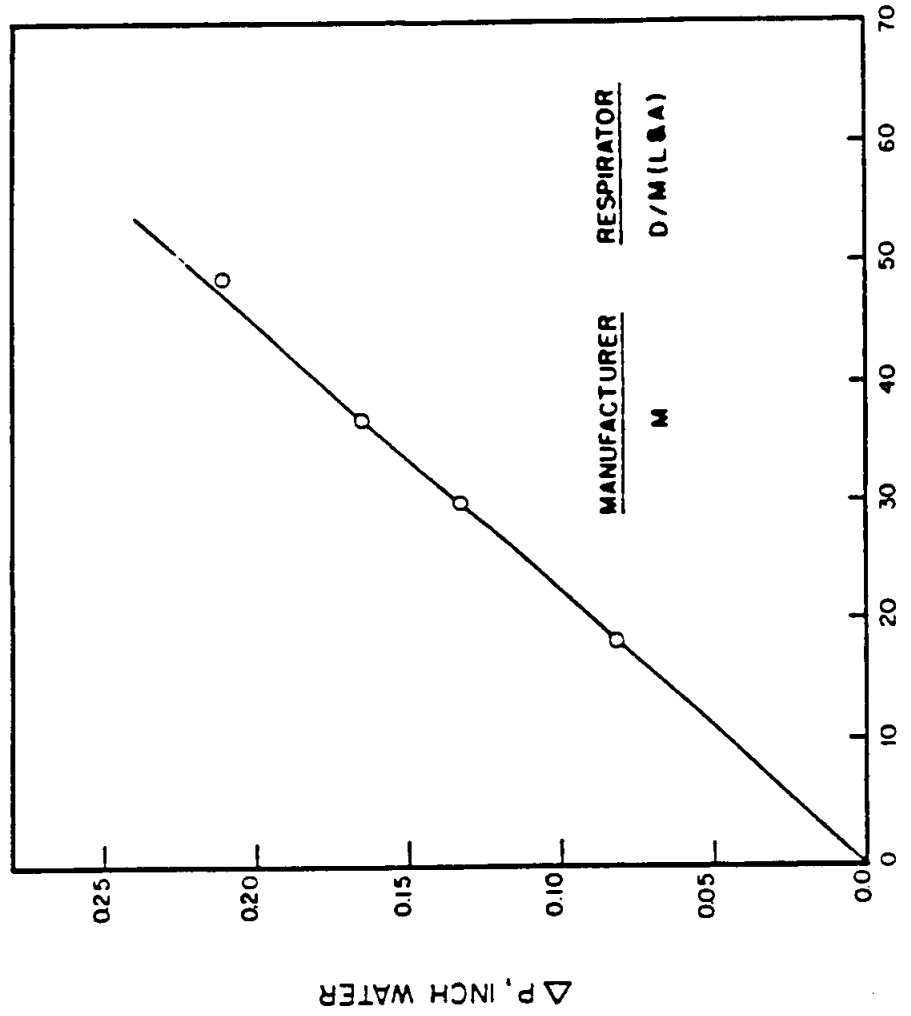

Figure 6.12 Pressure drop as a function of flow rate for dust/mist respirator of manufacturer M

Table 6.5 CNC penetration measurements of monodisperse DOP aerosol through dust/mist respirator of manufacturer M at 16, 28, and 48 Lpm

Dp,μ	Penetration (16Lpm)	Penetration (28Lpm)	Penetration (48Lpm)
0.035	0.0039±0.0006	0.0085±0.0009	0.0337±0.0036
0.045	0.0056±0.0008	0.0183±0.0022	0.0627±0.0065
0.055	0.0158±0.0017	0.0413±0.0022	0.0097±0.0035
0.070	0.0322±0.0025	0.0820±0.0052	0.1440±0.0064
0.100	0.0791±0.0079	0.1610±0.0152	0.2330±0.0220
0.200	0.2330±0.0098	0.3350±0.0071	0.3774±0.0136
0.300	0.2870±0.0167	0.3960±0.0127	0.4660±0.0198
0.400	0.3125±0.0288	0.3770±0.0266	0.4000±0.0170
0.500	0.2850±0.0103	0.3506±0.0126	0.3704±0.0160
0.700	0.2510±0.0091	0.2789±0.0118	0.2860±0.0143

Table 6.6 CNC penetration measurements of monodisperse NaCl aerosol through dust/mist respirator of manufacturer M at 16 and 28 Lpm

Dp, μ	Penetration (16Lpm)	Penetration (28Lpm)
0.035	0.0116±0.0010	0.0311±0.0026
0.055	0.0326±0.0033	0.0750±0.0040
0.070	0.0540±0.0040	0.1044±0.0047
0.100	0.0940±0.0101	0.1700±0.0092
0.300	0.2070±0.0081	0.2960±0.0148
0.400	0.2080±0.0176	0.2860±0.0270

The remaining figures show the experimental results for the three respirators manufactured by manufacturer T. Figures 6.13-6.16 and Tables 6.7 and 6.8 show the results for dust/mist respirator 1 (D/M-1), Figures 6.17-6.20 and Tables 6.9 and 6.10 for dust/mist respirator 2 (D/M-2), while Figures 6.21-6.24 and Tables 6.11 and 6.12 for a dust/mist/fume respirator (D/M/F). For D/M-1 respirator, the peak aerosol penetration varies from approximately 8% at a flow rate of 16 liters per minute to approximately 20% at 48 liters per minute. The shape of the penetration-versus-particle size curves is also different from that for the other respirators reported earlier. The curves are flatter in shape, suggestive of a more constant and uniform performance for particles in the most penetrating size range. Like for other respirators, the pressure drop across the D/M-1 respirator is strictly proportional to the flow rate with the proportionality constant being approximately equal to 0.002 inch water per liter per minute, a value which is nearly half that for the respirator M whose filtration efficiency is also considerably lower. In the case of respirator D/M-2, the penetration-versus-particle size curves are more like those of other respirators reported earlier for other manufacturers, but the penetration is considerably lower, varying from approximately 2.5% at a flow rate of 16 liters

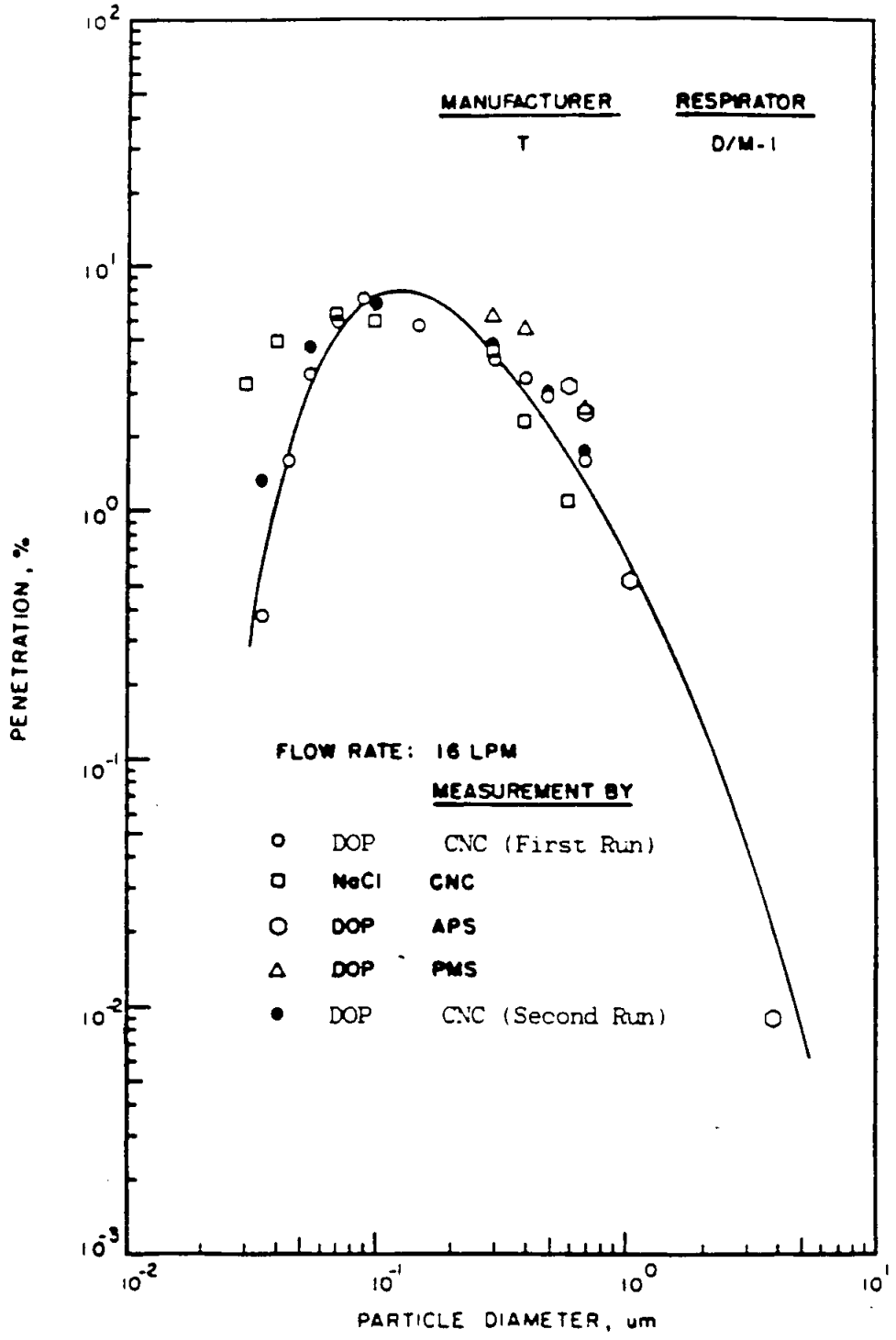

Figure 6.13 Aerosol penetration through respirator at 16 liters per minute for dust/mist respirator 1 of manufacturer T

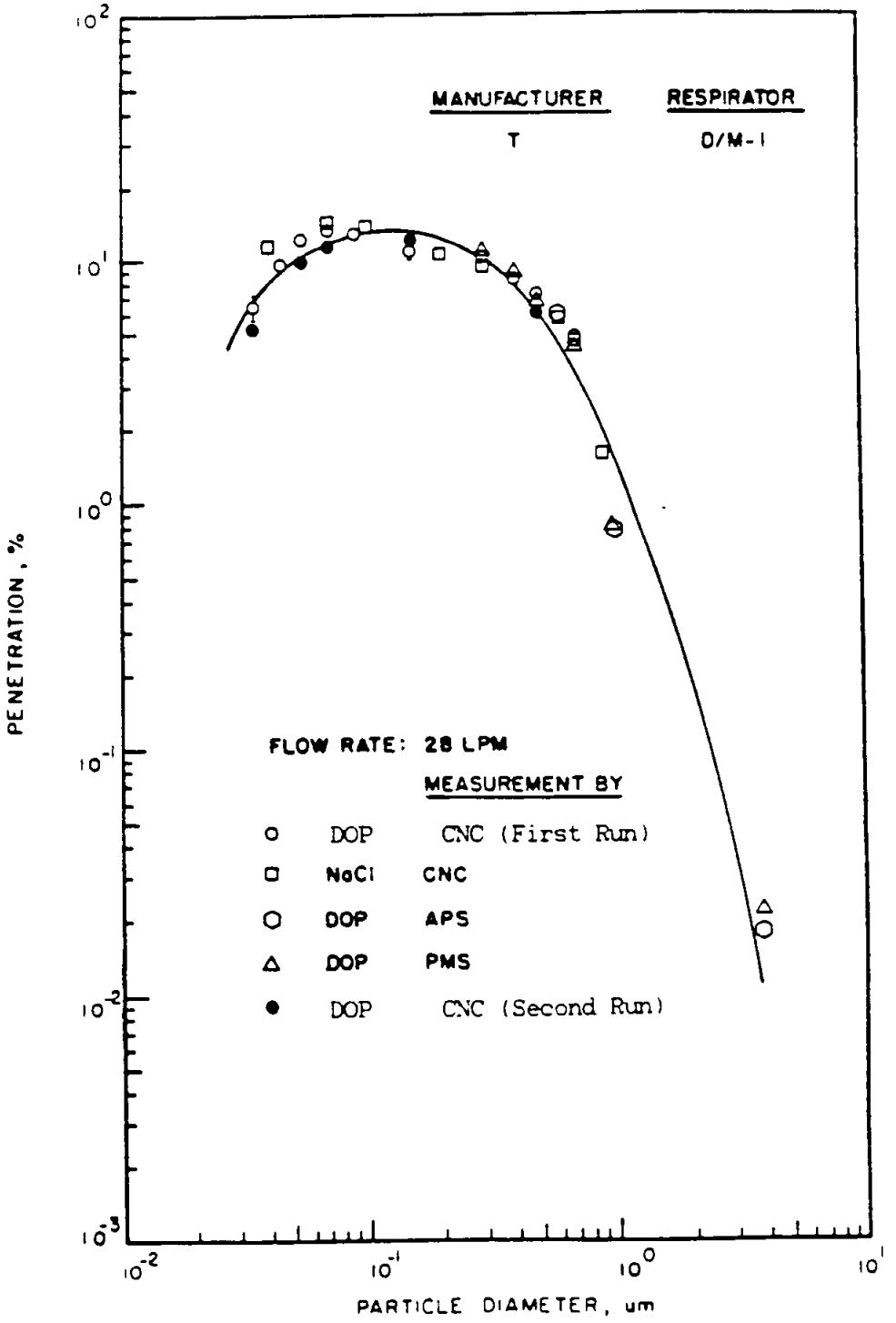

Figure 6.14 Aerosol penetration through respirator at 28 liters per minute for dust/mist respirator 1 of manufacturer T

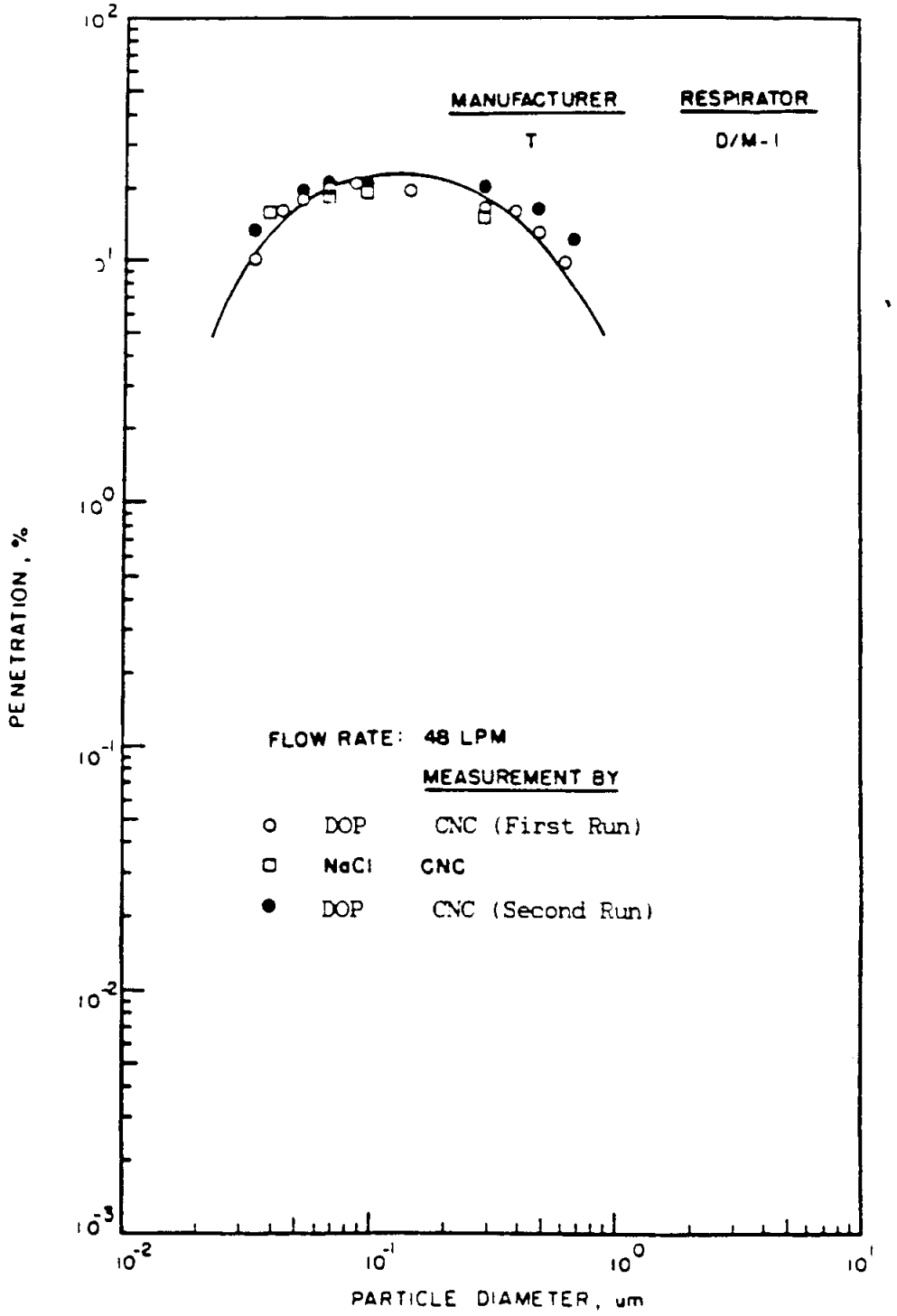

Figure 6.15 Aerosol penetration through respirator at 48 liters per minute for dust/mist respirator 1 of manufacturer T

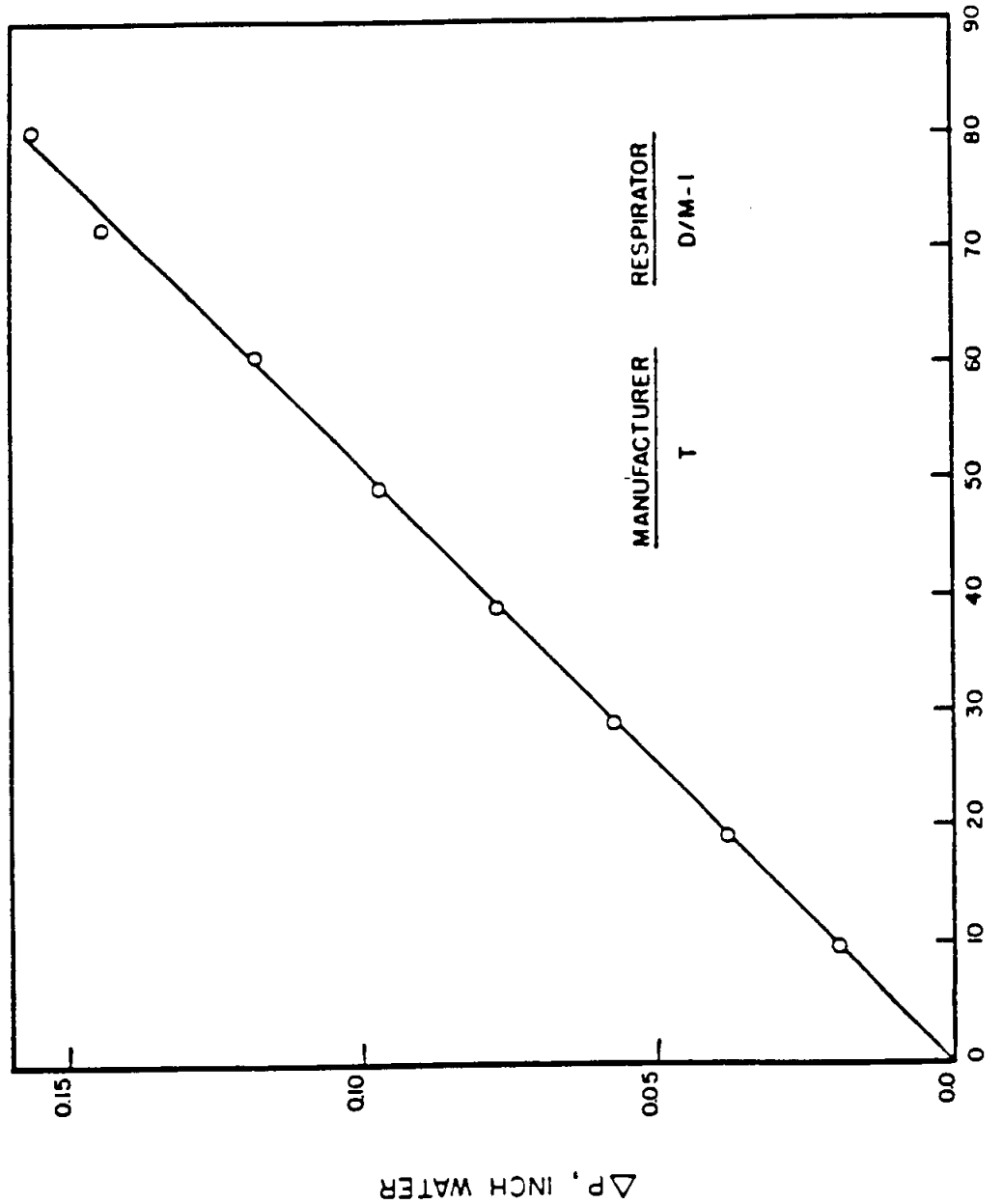

Figure 6.16 Pressure drop as a function of flow rate for dust/mist respirator 1 of manufacturer T

Table 6.7 CNC penetration measurements of monodisperse DOP aerosol through dust/mist respirator 1 of manufacturer T at 16, 28, and 48 Lpm

Dp, μ	Penetration (16Lpm)	Penetration (28Lpm)	Penetration (48Lpm)
0.035	0.0038±0.0008	0.0652±0.0073	0.1020±0.0091
0.045	0.0165±0.0017	0.0978±0.0057	0.1600±0.0122
0.055	0.0358±0.0029	0.1219±0.0071	0.1746±0.0102
0.070	0.0604±0.0062	0.1320±0.0138	0.1970±0.0115
0.080		0.1371±0.0074	
0.090	0.0731±0.0039	0.1296±0.0135	0.2082±0.0121
0.100		0.1288±0.0134	
0.150	0.0568±0.0059	0.1114±0.0065	0.1955±0.0175
0.300	0.0423±0.0035	0.1069±0.0054	0.1671±0.0149
0.400	0.0350±0.0036	0.0852±0.0036	0.1642±0.0184
0.500	0.0291±0.0062	0.0727±0.0042	0.1323±0.0107
0.650			
0.700	0.0163±0.0017	0.0488±0.0076	0.0970±0.0080

Table 6.8 CNC penetration measurements of monodisperse NaCl aerosol through dust/mist respirator 1 of manufacturer T at 16, 28, and 48 Lpm

Dp, μ	Penetration (16Lpm)	Penetration (28Lpm)	Penetration (48Lpm)
0.03	0.0334±0.0068		
0.04	0.0487±0.0026	0.1165±0.0068	0.1540±0.0083
0.07	0.0626±0.0034	0.1428±0.0083	0.1848±0.0083
0.10	0.0595±0.0062	0.1381±0.0154	0.1875±0.0106
0.20		0.1061±0.0057	
0.30	0.0426±0.0057	0.0950±0.0124	0.1523±0.0110
0.40	0.0227±0.0029	0.0842±0.0133	
0.60	0.0113±0.0014	0.0577±0.0182	

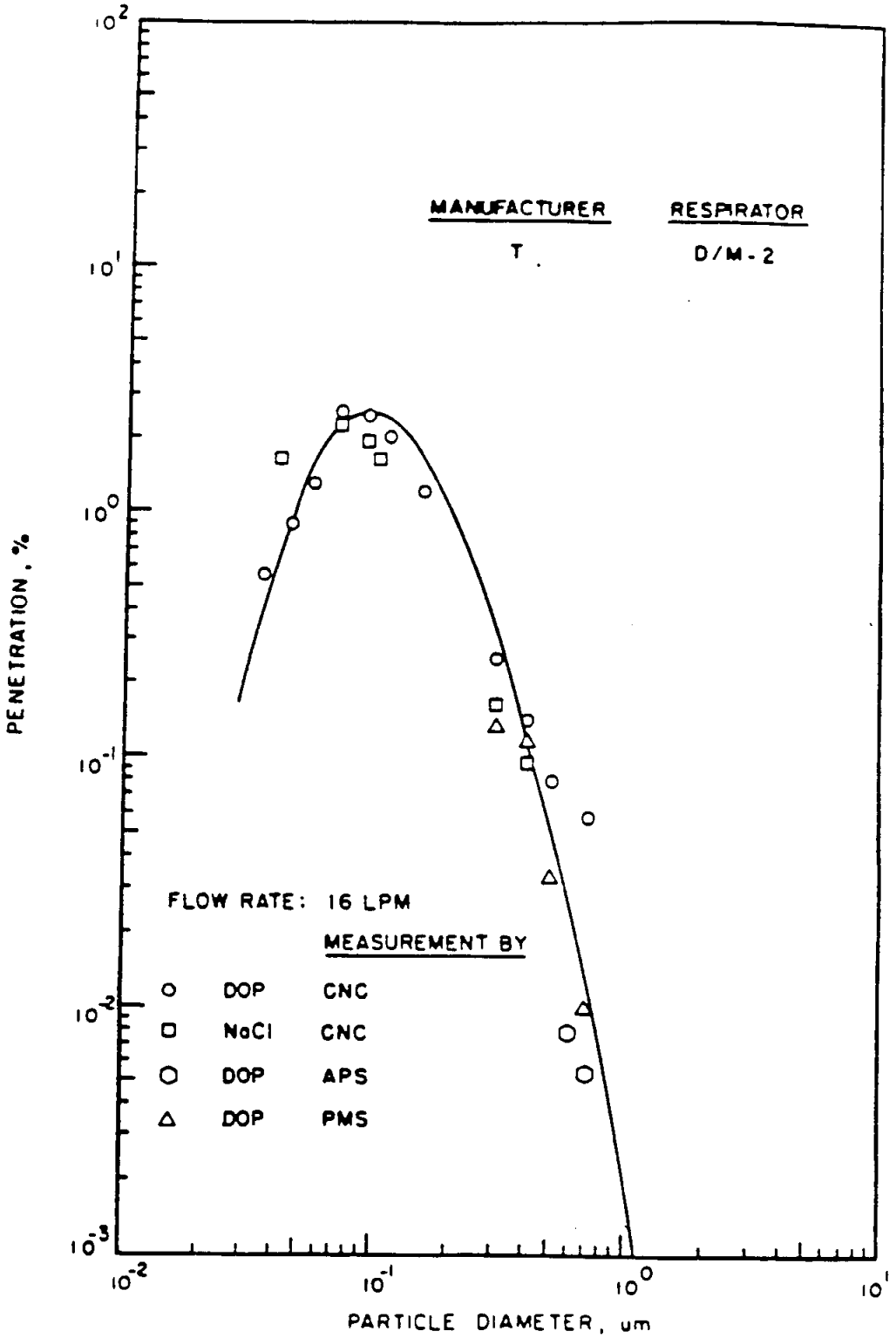

Figure 6.17 Aerosol penetration through respirator at 16 liters per minute for dust/mist respirator 2 of manufacturer T

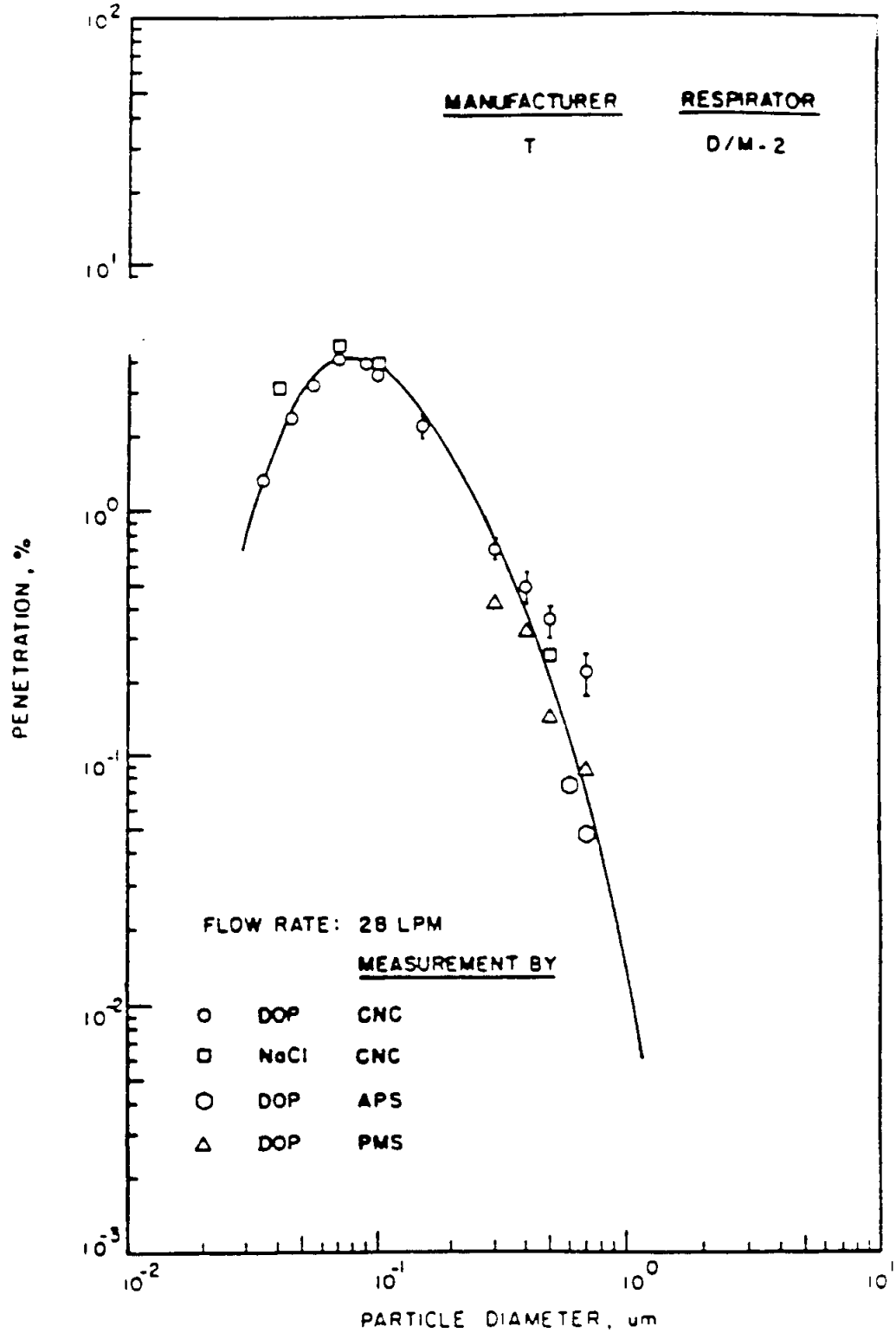

Figure 6.18 Aerosol penetration through respirator at 28 liters per minute for dust/mist respirator 2 of manufacturer T

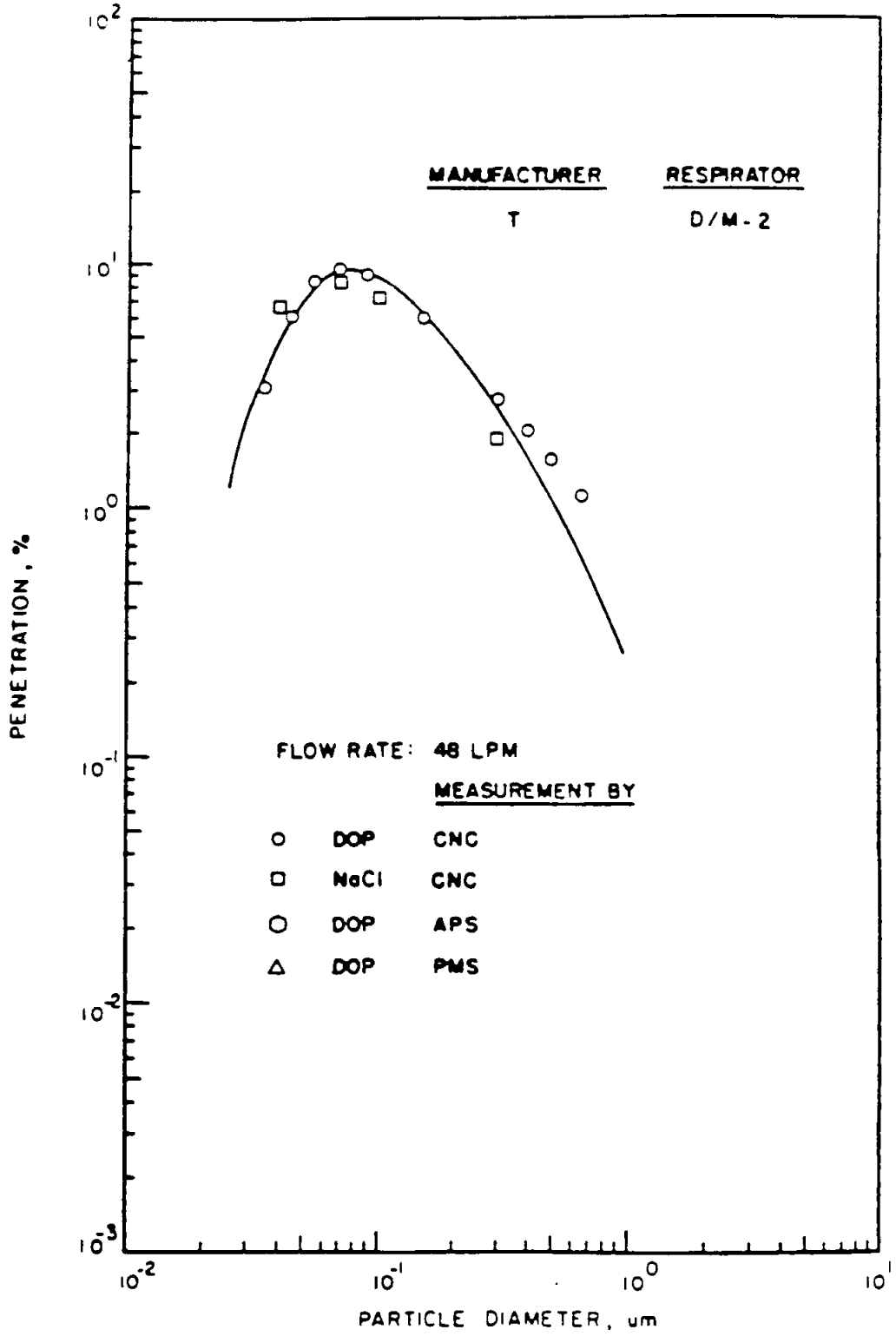

Figure 6.19 Aerosol penetration through respirator at 48 liters per minute for dust/mist respirator 2 of manufacturer T

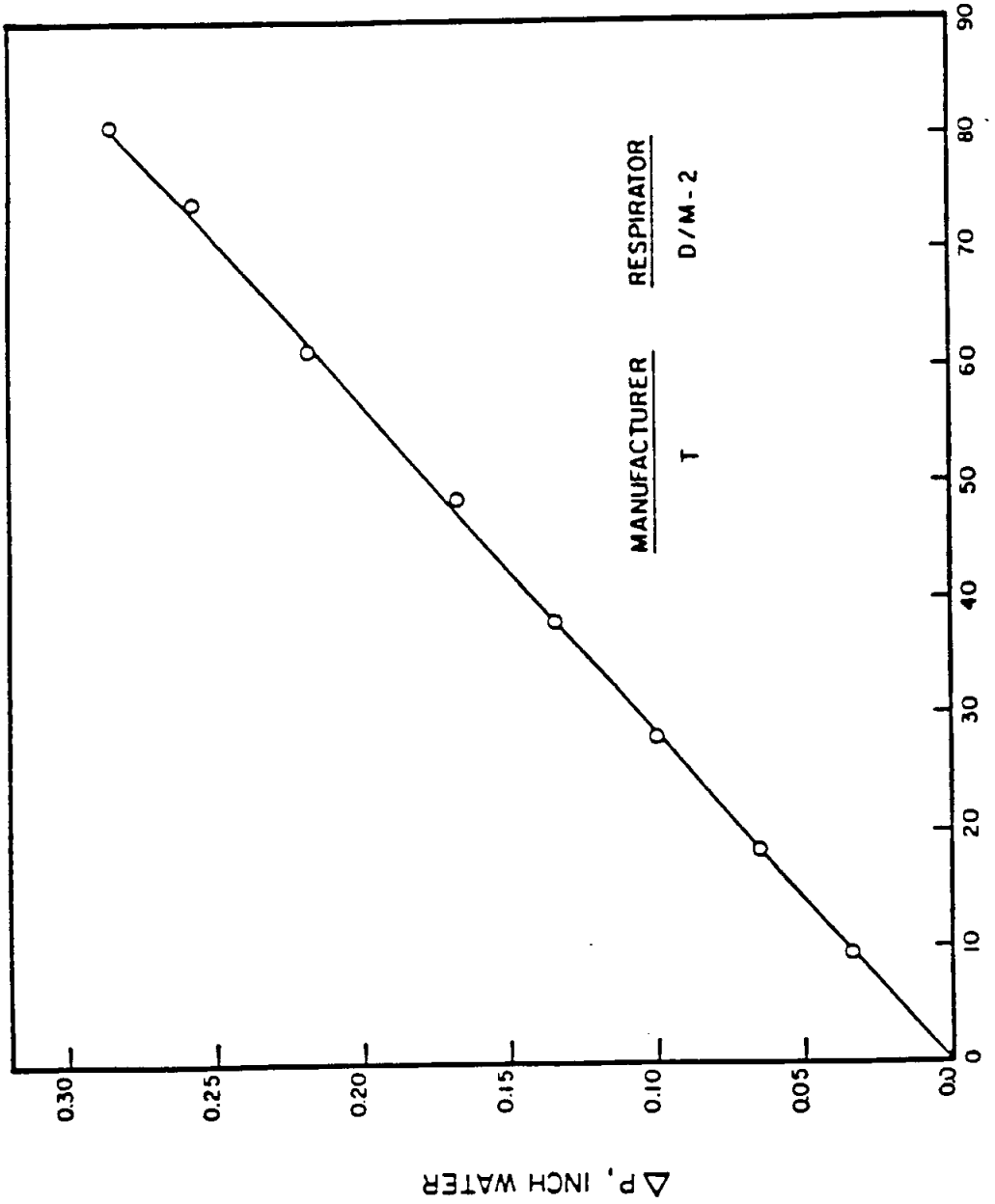

Figure 6.20 Pressure drop as a function of flow rate for dust/mist respirator 2 of manufacturer T

Table 6.9 CNC penetration measurements of monodisperse DOP aerosol through dust/mist respirator 2 of manufacturer T at 16, 28,and 48 Lpm

Dp, μ	Penetration (16Lpm)	Penetration (28Lpm)	Penetration (48Lpm)
0.035	0.0055±0.0011	0.0133±0.0014	0.0313±0.0033
0.045	0.0088±0.0013	0.0238±0.0015	0.0600±0.0062
0.055	0.0131±0.0020	0.0323±0.0030	0.0833±0.0056
0.070	0.0254±0.0026	0.0412±0.0034	0.0953±0.0056
0.090	0.0239±0.0013	0.0388±0.0021	0.0887±0.0076
0.100		0.0350±0.0019	
0.150	0.0124±0.0019	0.0222±0.0024	0.0602±0.0067
0.300	0.0025±0.0003	0.0071±0.0007	0.0284±0.0043
0.400	0.0014±0.0003	0.0049±0.0007	0.0218±0.0014
0.500	0.0008±0.0002	0.0036±0.0005	0.0157±0.0009
0.650			0.0117±0.0013
0.700	0.0006±0.0002	0.0022±0.0004	

Table 6.10 CNC penetration measurements of monodisperse NaCl aerosol through dust/mist respirator 2 of manufacturer T at 16, 28, and 48 Lpm

Dp,μ	Penetration (16Lpm)	Penetration (28Lpm)	Penetration (48Lpm)
0.04	0.0164±0.0017	0.0314±0.0017	0.0665±0.0051
0.07	0.0219±0.0018	0.0472±0.0048	0.0832±0.0056
0.10	0.0167±0.0017	0.0380±0.0040	0.0720±0.0077
0.30	0.0016±0.0003	0.0069±0.0011	0.0192±0.0020
0.40	0.0009±0.0002		
0.50	0.0025±0.0008		

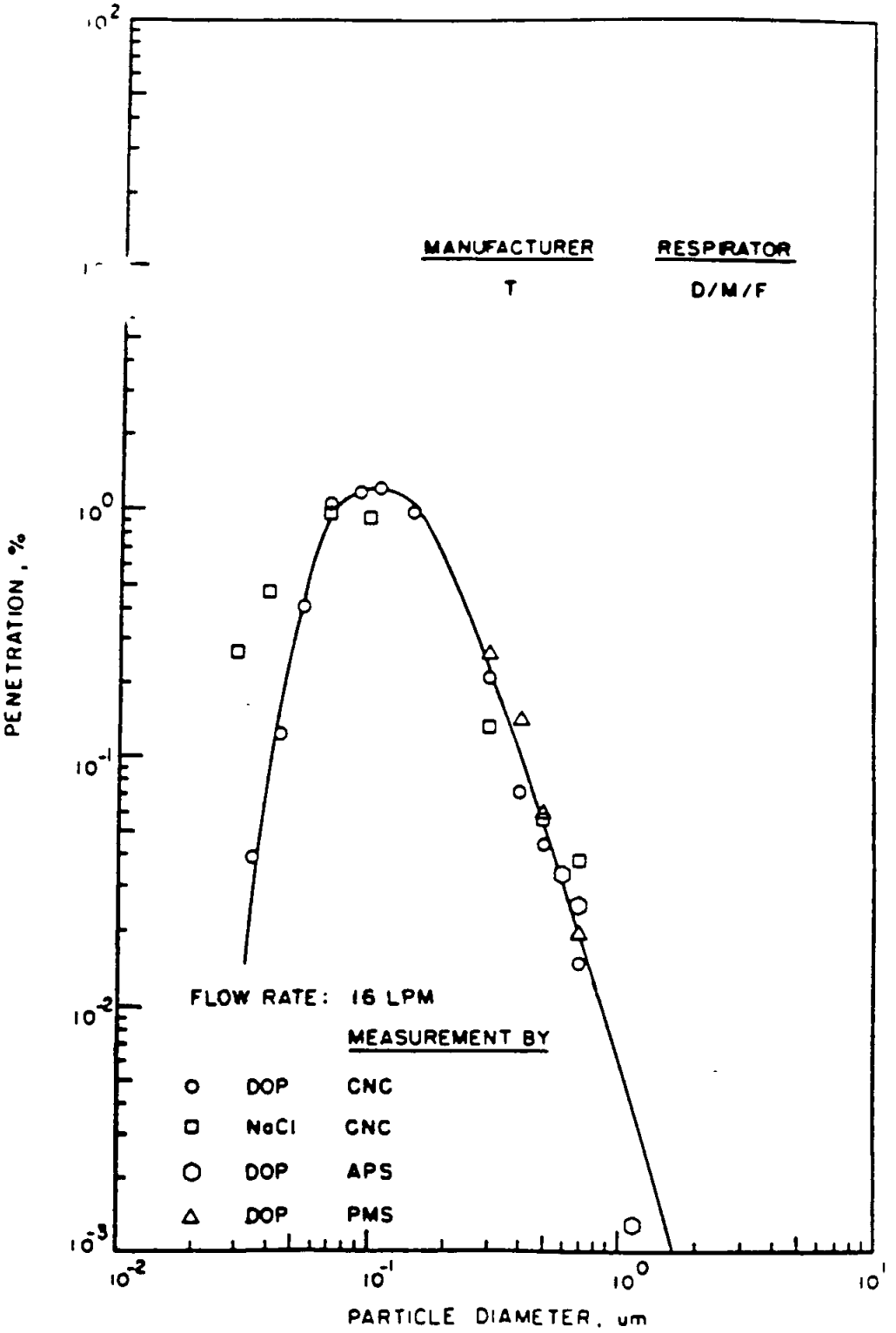

Figure 6.21 Aerosol penetration through respirator at 16 liters per minute for dust/mist/fume respirator of manufacturer T

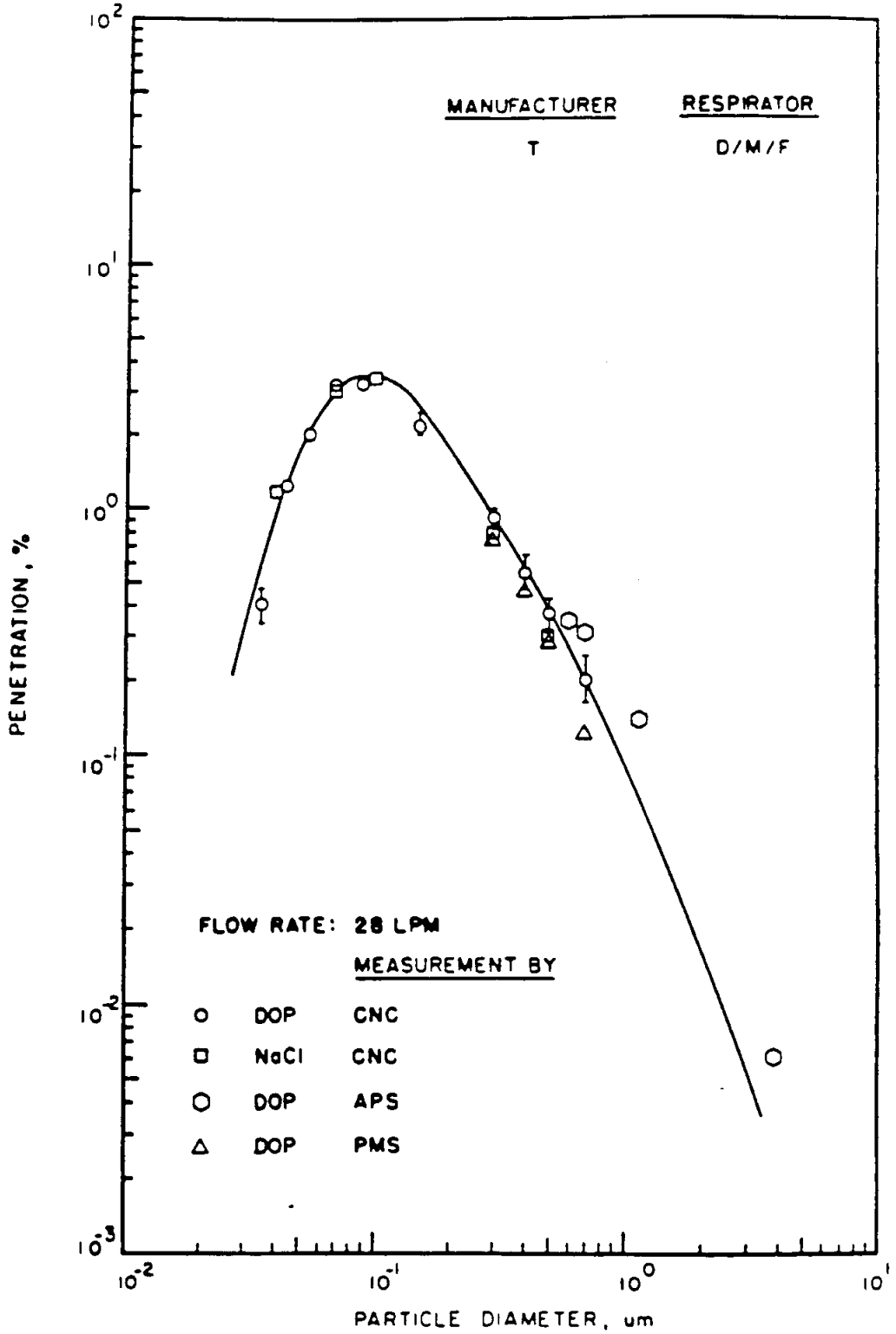

Figure 6.22 Aerosol penetration through respirator at 28 liters per minute for dust/mist/fume respirator of manufacturer T

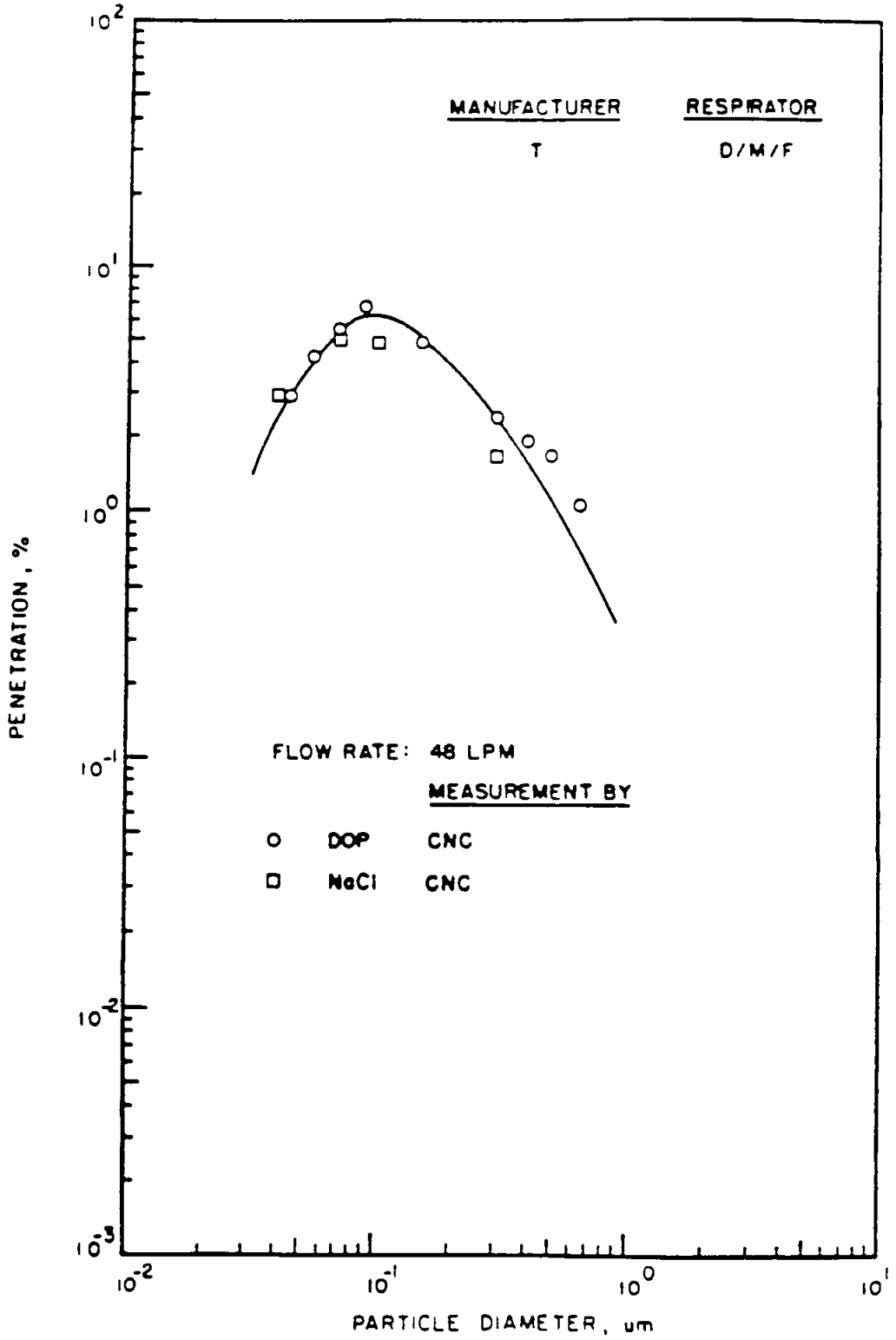

Figure 6.23 Aerosol penetration through respirator at 48 liters per minute for dust/mist/fume respirator of manufacturer T

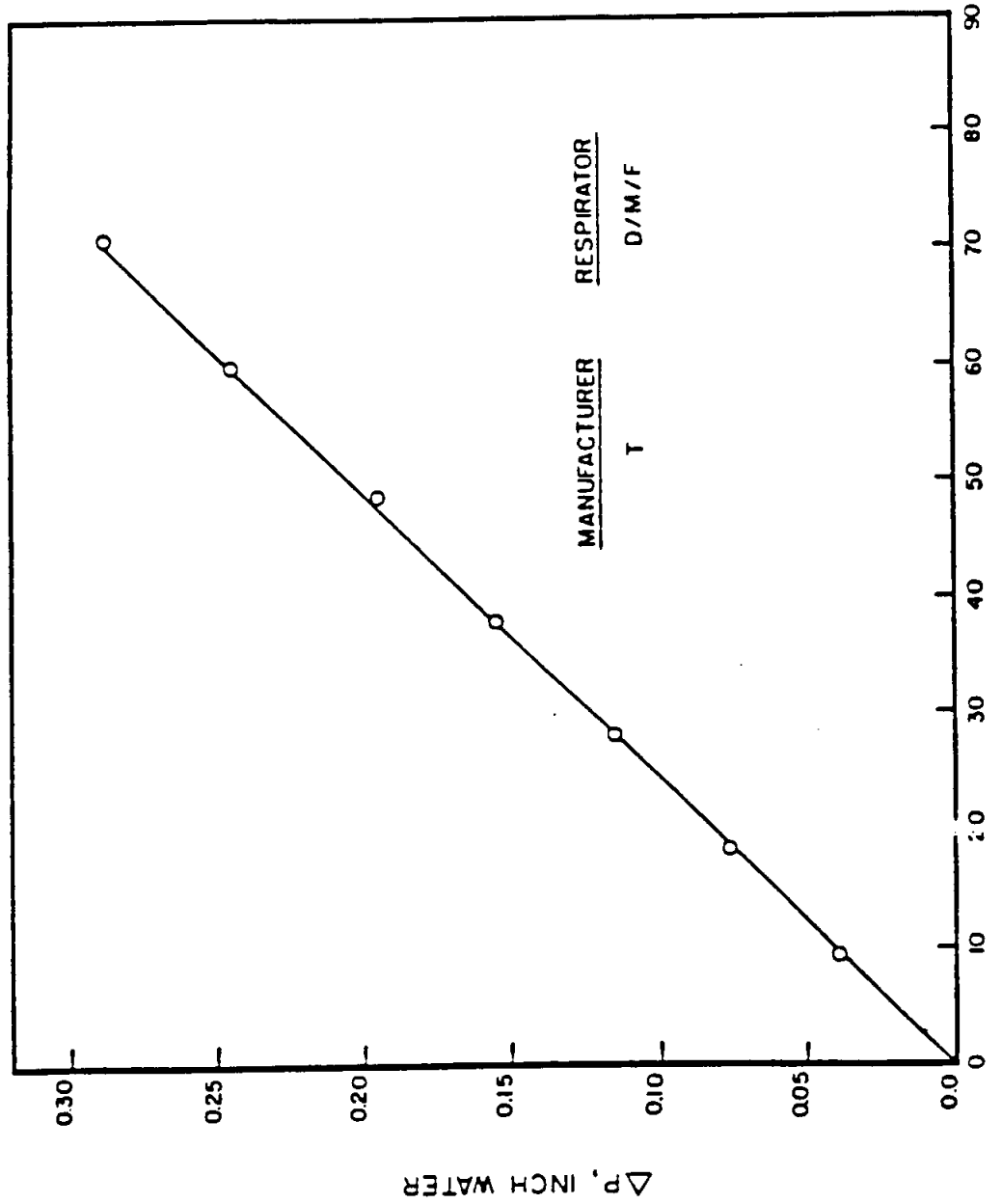

Figure 6.24 Pressure drop as a function of flow rate for dust/mist/fume respirator of manufacturer T

Table 6.11 CNC penetration measurements of monodisperse DOP aerosol through dust/mist/fume respirator of manufacturer T at 16, 28, and 48 Lpm

Dp,μ	Penetration (16Lpm)	Penetration (28Lpm)	Penetration (48Lpm)
0.035	0.0004±0.0001	0.0040±0.0006	0.0138±0.0022
0.045	0.0012±0.0002	0.0125±0.0011	0.0291±0.0021
0.055	0.0042±0.0004	0.0202±0.0017	0.0421±0.0036
0.070	0.0104±0.0011	0.0325±0.0034	0.0551±0.0058
0.090	0.0145±0.0022	0.0325±0.0018	0.0682±0.0071
0.110	0.0121±0.0012		
0.150	0.0085±0.0013	0.0223±0.0024	0.0487±0.0050
0.300	0.0021±0.0004	0.0093±0.0010	0.0239±0.0024
0.400	0.0007±0.0001	0.0056±0.0009	0.0194±0.0024
0.500	0.0004±0.0001	0.0037±0.0006	0.0168±0.0018
0.650			0.0107±0.0011
0.700	0.0002±0.00005	0.0021±0.0004	

Table 6.12 CNC penetration measurements of monodisperse NaCl aerosol through dust/mist/fume respirator of manufacturer T at 16, 28, and 48 Lpm

Dp, μ	Penetration (16Lpm)	Penetration (28Lpm)	Penetration (48Lpm)
0.04	0.0047±0.0005	0.0117±0.0012	0.0291±0.0030
0.07	0.0095±0.0010	0.0300±0.0031	0.0501±0.0050
0.10	0.0091±0.0012	0.0345±0.0056	0.0479±0.0030
0.30	0.0013±0.0003	0.0079±0.0085	0.0167±0.0015
0.50	0.0006±0.0001	0.0030±0.0009	

per minute, to 4% at 28 liters per minute and 10% at 48 liters per minute. The most penetrating particle size for this respirator varies in the vicinity of 0.08 μm for the three flow rates considered. The slope of the linear relationship between the pressure drop and flow rate as shown in Figure 6.20 is about 0.0036 inch of water per liter per minute of the flow. For D/M/F respirator which had an exhaust valve, the aerosol penetration is still lower than that for all the respirators considered, so far. The peak penetration ranges from about 1.2% at 16 liters per minute to 3.5% and 6% at flow rates of 28 and 48 liters per minute, respectively. The most penetrating particle size is in the vicinity of 0.1 μm. Also, as shown in Figure 6.24, the pressure drop across the respirator increases linearly at the rate of approximately 0.0041 inch of water per liter per minute over the range of the flow rate shown.

It should be noted that the test results for various respirators described above apply only to the case of a clean respirator without substantial particle loading on the filter. The tests were conducted purely for the purpose of understanding the fractional aerosol penetration characteristic of clean, unloaded filters. With heavy particle loading on the filter, such as that encountered in the traditional NIOSH certification tests, the filtration characteristics would vary. In the present work, the loading

characteristics of the flat-sheet filter medium were investigated briefly and the results are presented and discussed later in the chapter.

6.2 Figure of Merit

The filtration performance of any filter should not be based upon the total collection efficiency or resistance to air flow alone, but rather, upon a combination of both. Therefore, several investigators including Cadle and Thuman (1960) and Pich (1966) have suggested using a filter quality parameter or figure of merit, f_m, defined as

$$f_m = - \frac{\log P_f}{\Delta p} \qquad (6.1)$$

or a slight variation thereof. In this equation, P_f is the penetration value through the filter for a given particle size and Δp is the pressure drop across the filter at a known flow rate. The figure of merit increases with increasing efficiency or decreasing pressure drop. Thus, it can be used for quantitative filter comparisons. This parameter is especially useful for comparing the performance of respirator filters whose efficiency and resistance to air flow are both very important in their acceptance for use.

Therefore, the figure of merit values were determined

for each respirator filter tested in the present study using the DOP penetration values corresponding to 0.1 μm particle diameter and the pressure drop corresponding to each of the flow rates considered. Notice that the above particle diameter is equal to or near the most penetrating particle diameter as shown in the penetration figures presented earlier. Thus, the calculated values of the figure of merit correspond to nearly the worst-case condition. The results are presented in tabular form in Table 6.13.

Table 6.13 Values of Figure of Merit of respirator filters corresponding to penetration values at 0.1 um particle diameter at 16, 28, and 48 Lpm

Respirator	f_m (16 Lpm)	f_m (28 Lpm)	f_m (48 Lpm)
A	40.58	16.87	8.85
L	2.23	1.02	0.53
M	15.45	6.59	2.81
T, D/M-1	36.27	15.52	7.21
T, D/M-2	28.11	14.20	6.19
T, D/M/F	29.10	12.66	6.13

As seen, the figure of merit for respirator A is highest at each of the flow rates followd by slightly lower values of

D/M-1 respirator of manufacturer T. Respirators D/M-2 and D/M/F of manufacturer T also show relatively high values of f_m while, the respirator M shows significantly lower values. The lowest values in the table correspond to the flat-sheet media of manufacturer L, which are 10 to 20 times lower than those for respirator A.

It should be noted that the calculated values of the figure of merit provide a means for comparing the filtration performance of the respirator filters only and by no means represent the overall performance of the respirators which includes also the amount of leakage through the face seal and inhalation and exhalation valves if they exist, as well as general wearing comfort.

6.3 Loading Test and Results

The penetration characteristics of respirator filters when loaded with liquid and/or solid aerosol particles are of interest since most of such filters are electrostatically charged and their capture efficiency may decrease as a result of neutralization of fiber charges by those on particles or shielding of electric field around a fiber by the deposited particles, in particular the liquid particles which may coalesce and form a liquid film around the fiber. Of course, the degradation of the electrostatic efficiency will be eventually compensated for by the increase in the mechanical efficiency which is also accompanied by an increasing pressure drop as a result of particle loading.

But the particle loading test in the present work was conducted on the flat-sheet filter media L which is composed of uncharged fibers according to its manufacturer. The filter mat was placed in the test chamber as described previously and was then exposed to 28 liters per minute of polydisperse NaCl aerosol which was generated from a 0.1 gram of NaCl per cm^3 of distilled water solution by a collison atomizer. The aerosol was used for the purpose of loading the filter only and had a geometric mean diameter of approximately 0.07 μm and a geometric standard deviation of about 2. The loading was continued until the pressure drop

across the filter was increased to twice the value corresponding to the clean filter at the same flow rate. At that time, the loading was terminated and the penetration measurements of monodisperse DOP particles were performed as for the case of clean filters. The filter was further loaded to 3 and 4 times the clean filter pressure drop and the penetration of monodisperse DOP particles was measured at each loading step. The results are presented in Figure 6.25. As shown, the penetration-versus-particle size curves corresponding to different loading conditions are similar with the most penetrating particle size appearing to be independent of the amount of particle loading on the filter. But the peak penetration decreases from 14% for a clean filter to 2.7% , 0.64% and 0.4% for loading steps corresponding to 2, 3 and 4 times the pressure drop of the clean filter at 28 liters per minute, respectively. Meanwhile, the pressure drop across the filter for each loading step was measured as a function of the flow rate and the results are shown in Figure 6.26. The linear relationship between the pressure drop and the flow rate appear to be unaffected over the amount of particle loading considered in the present work.

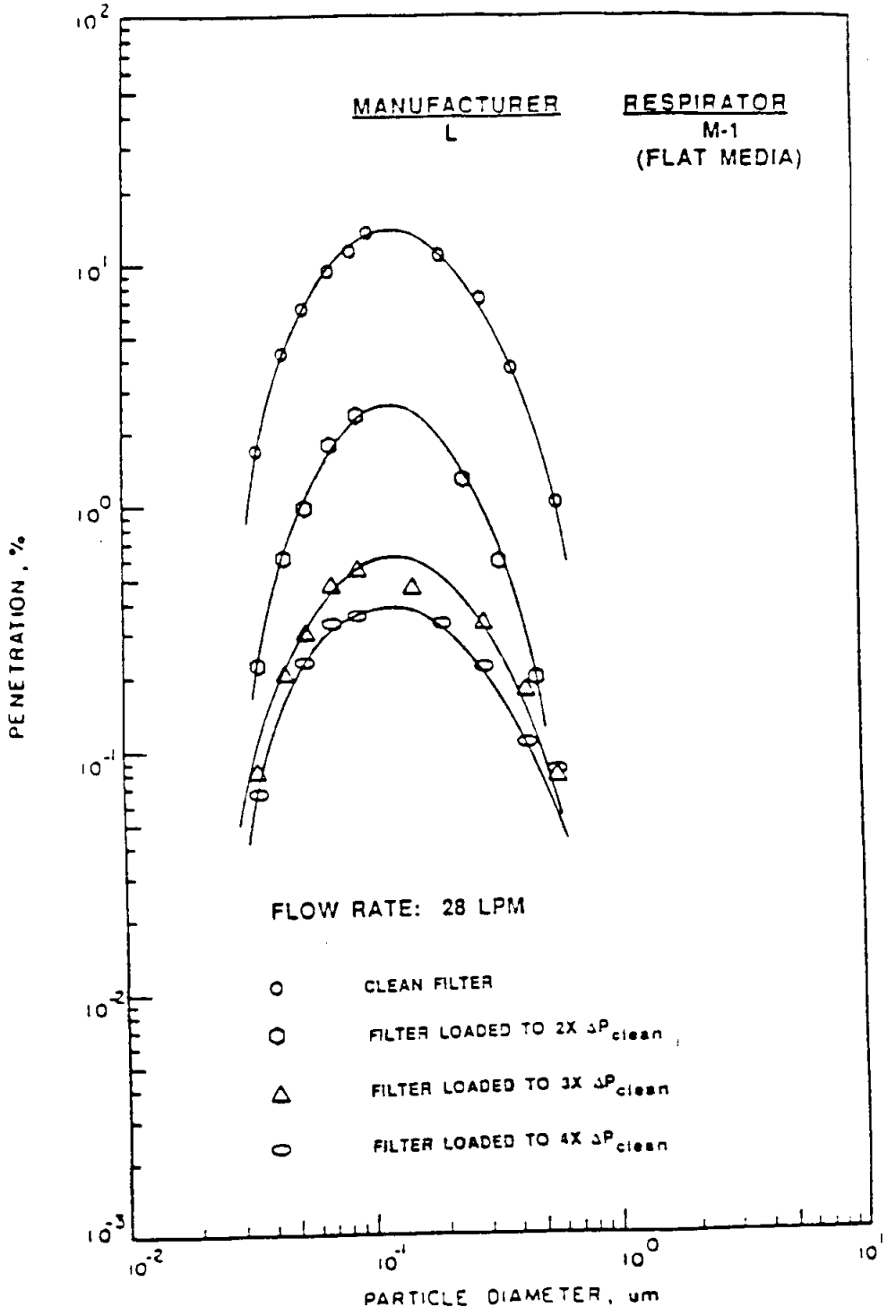

Figure 6.25 Aerosol penetration through respirator L loaded with NaCl particles to two, three, and four times the pressure drop corresponding to clean respirator at 28 liters per minute

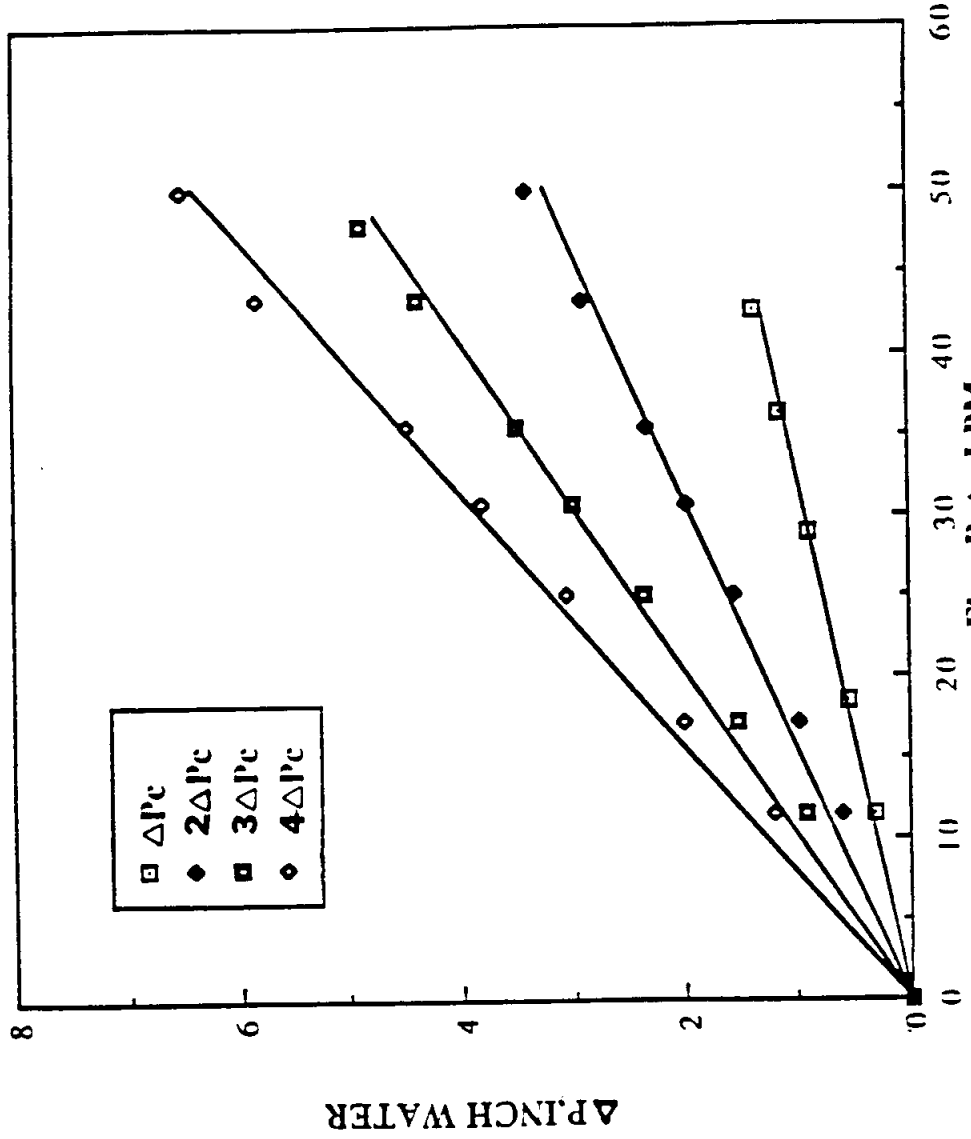

Figure 6.26 Pressure drop as function of flow rate for flat-sheet filter media of manufacturer L at each loading step

6.4 Comparison of Penetration Measurements Made by Different Instruments

The use of optical particle counters in the filtration studies has recently received great attention mainly because of their capability of in-situ measurement of size distribution of particles in an aerosol and their particle size sensitivity of 0.1-0.3 μm which coincides with the range of most penetrating particle size of most fibrous filters.

In the present study, the ASAS-300x optical prticle counter was used to determine the penetration of monodisperse DOP particles of known size through some of the respirator filters considered at the flow rates of 16 and 28 liters per minute. In addition, the aerodynamic particle sizer was used also for comparison. This instrument is not commonly used in the filtration studies because of its relatively large particle size sensitivity of approximately 0.5 μm which is beyond the range of most penetrating particle size range of moderate to high efficiency filters. A detail description of these instruments and their operation was given in Chapter 3.

Most of penetration measurements made by the above two instruments were for particles below 1 μm in diameter, while a few measurements for particles equal or larger than 1μm in

diameter were also obtained.

Let's first investigate the response of these instruments to a highly monodisperse DOP aerosol produced by the electrostatic classifier as explained previously. The aerosol contained particles having a geometric mean diameter and standard deviation of 0.6 μm and 1.02, respectively, and was maintained at a flow rate of 28 liters per minute. Figure 6.27 shows the size distribution of the aerosol particles as measured by the Optical Particle Counter (OPC). Assuming log-normal size distribution, the geometric mean and standard deviation of the measured size distribution were determined as 0.53 μm and 1.07, respectively. Note that the monodispersity of the measured size distribution is less than that of the actual size distribution but such response is typical of laser particle counters since the intensity of the laser beam is not uniform and has a guassian distribution with the intensity being maximum at the center of the beam. Therefore, it is very unlikely for particles of even a monodisperse aerosol to be all counted in one channel since not all particles pass through the laser beam at the same spot.

Figure 6.28 illustrates the particle size distribution of the same aerosol as determined by the Aerodynamic Particle Sizer (APS). The mean and σ_g of this aerosol were calculated to be 0.55 μm and 1.04, respectively. Comparing

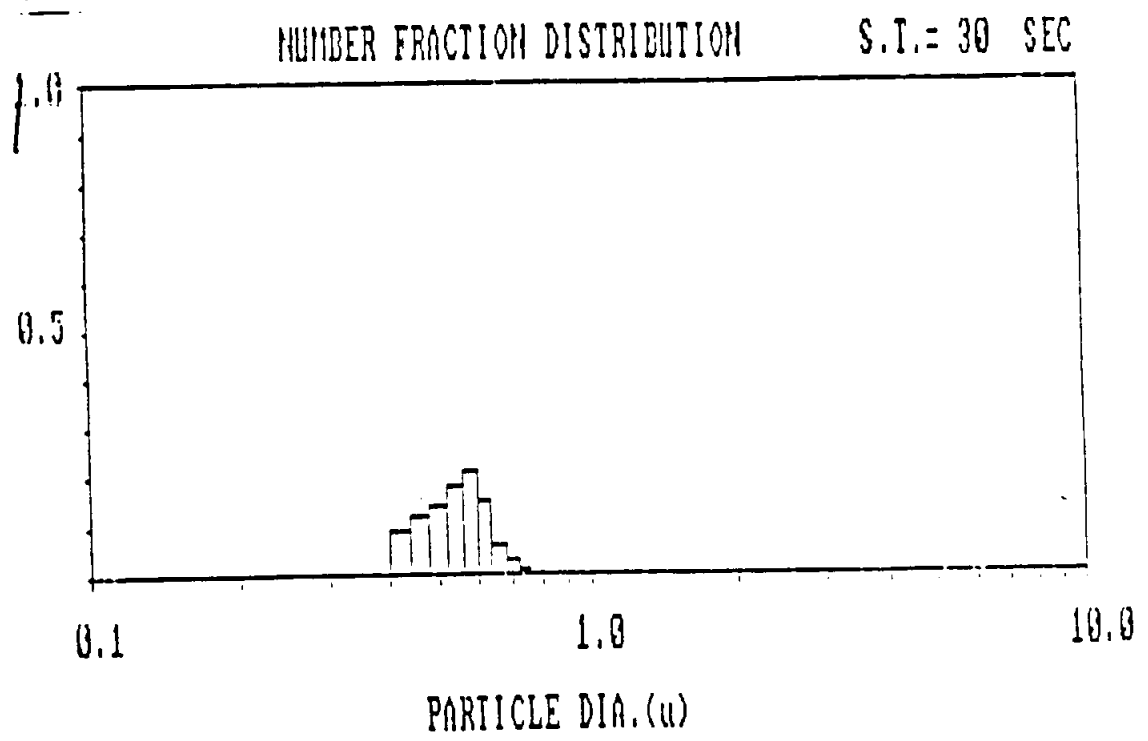

Figure 6.27 Size distribution of monodisperse 0.6μm DOP particles as measured by PMS ASAS-300X laser optical particle counter

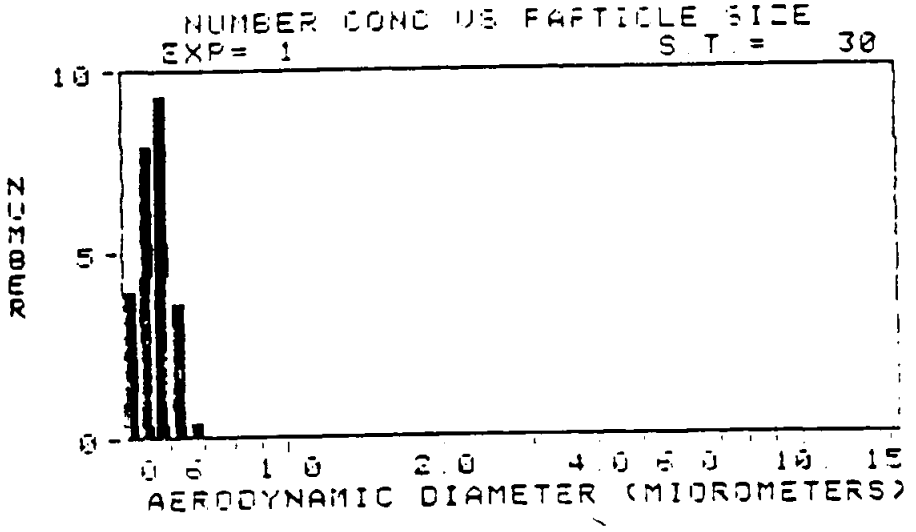

Figure 6.28 Size distribution of monodisperse 0.6μm DOP particles as measured by TSI aerodynamic particle sizer

the results obtained by the APS and OPC, one finds that the OPC gives a slightly wider size distribution than the APS for the same aerosol. In addition, the geometric mean diameter values determined from the APS and OPC measurements are found to be different from the nominal value by approximately 8% and 12%, respectively. But as mentioned before, the sizing capability of these instruments was not utilized in the present study and therefore, the above inaccuracies in the particle diameter measurements should have no effect on the present results.

In order to determine the amount of penetration of a monodisperse aerosol using the OPC or APS, the total upstream and downstream concentration values were obtained by adding the counts in two or three channels, as necessary, containing the most counts. Although, the absolute values of the particle concentration at the upstream and downstream of a given filter as measured by the APS and OPC were significantly different from each other, or even from the CNC measurements, but the penetration values obtained from the ratio of the concentration values were in considerably better agreement.

Reviewing among Figures 6.1 through 6.24 those showing the penetration measurements of all three instruments, one finds a reasonably good agreement between the results considering the great difference in the measurement

technique of these instruments, losses in the connecting tubes, difference in the sampling flow rates and etc. Unfortunately, since the most-penetrating particle diameter through most of the respirator filters tested was approximately 0.1 μm which is below the lower sensing limit of the available OPC and APS, no direct comparison of the results could be made in the proximity of the most penetrating particle size. But for particles in the range of 0.2 and 0.5 μm in diameter, the agreement between CNC and OPC results is quite good, while for larger particles, the results of the OPC and APS are in satisfactory agreement. Figure 6.29 shows the penetration values of monodisperse DOP particles passing through the respirator M at the rate of 28 liters per minute as measured by the CNC and OPC. This was the only respirator among those tested for which the most penetrating particle size at the above flow rate was within the operating range of the OPC. In addition, since the response of any OPC is strongly dependent upon the index of refraction and shape of particles among other factors, the penetration of the atmospheric aerosol which contains particles of various material, shape, and size was obtained to determine the effect of the above parameters on the penetration measurements. The atmospheric aerosol was drawn through the respirator filter at the rate of 28 liters per minute and the penetration values were determined from the

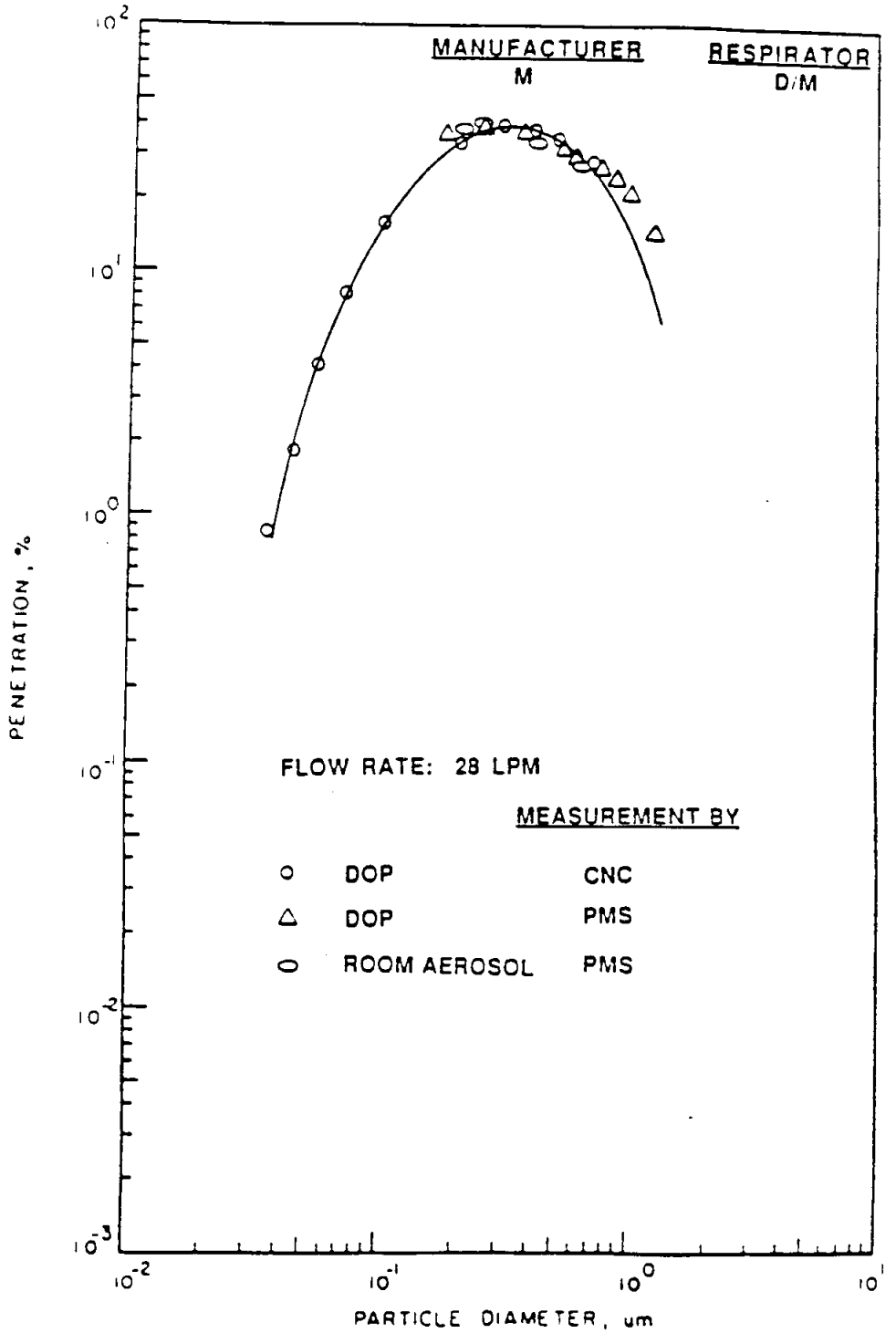

Figure 6.29 Penetration of room aerosol and monodisperse DOP particles through respirator M at 28 liters per minute as measured by TSI condensation nucleus counter and PMS ASAS-300X laser optical particle counter

measured upstream and downstream particle size distributions. The results are presented also in Figure 6.29. First, notice the excellent agreement between the CNC and OPC measurement results over their overlapping particle size range for the DOP particles. Both instruments predict nearly the same value of approximately 39% for the maximum penetration occuring at a particle diameter of 0.33 μm. Secondly, notice also the excellent agreement between the penetration values of the room aerosol particles and those of the DOP as measured by the OPC, which suggests that the index of refraction and/or shape of particles in the room aerosol had no significant effect on the measured penetration values.

Therefore, based on foregoing, the use of optical particle counters in the filtration studies is recommended if the instruments are well calibrated and have particle size sensitivity of 0.1 to 0.3 μm in diameter. The same can be stated also for the APS but as mentioned earlier, its use in the filtration studies is limited except for low efficiency filters which may have appreciable penetration values for particles above 0.5 μm in diameter.

Chapter 7

CONCLUSIONS

An experimental study of filtration performance of respirator filter composed of charged and uncharged fibers was conducted in conjunction with a numerical study of filtration characterisitcs of charged rectangular fibers. The studies were carried out independent of one another mainly because of unknown surface charge density of real electret fibers, random orientation, size and space distribution of fibers within a filter, and unknown and very complicated electric field within a real electret filter which limit the accuracy of the numerical model in approximating the filtration performance of an eletret filter. Thus, no attempt was made to compare or correlate the experimental measurements with the numerical results obtained in the present work.

The following are the major conclusions of this study:

1. The most penetrating particle diameter through considered respirator filters was found to lie in the vicinity of 0.1 μm for filters containing charged fibers and around 0.3 to 0.4 μm for mechanical filters.

2. The peak penetration of both solid NaCl particles and liquid DOP particles through respirator filters was found to range from approximately 1.2% to 30% at 16 Lpm, 3.5% to 37% at 28 Lpm, and 6% to 45% at 48 lpm.

3. No significant difference in penetration characterisitc of NaCl and DOP particles was found.

4. The test method developed in the present study for evaluation of filtration performance of respirator filters does not cause loading of the filters and yields very repeatable results as opposed to the NIOSH's test method.

5. The most penetrating particle diameter through one of the selected filters was found to be unaffected by the loading conditions of the filter as it was loaded with NaCl particles to 2, 3, and 4 times the pressure drop corresponding to the clean filter at 28 Lpm.

6. The peak penetration decreased from 14% for a clean respirator filter of manufacturer L to 2.7%, 0.64%, and 0.40% for loading steps corresponding to 2, 3, and 4 times the pressure drop of the clean filter at 28 Lpm, respectively.

7. The penetration measurements obtained by different aerosol instruments such as condensation nucleus counter, laser optical particle counter, and aerodynamic particle sizer tend to be in reasonable agreement in the overlapping region of the particle size range of the instruments.

8. The optical particle counters can be used in the filtration studies to predict the penetration characteristics of moderate to high efficiency filters if the instruments are well calibrated and have a particle size sensitivity of 0.1 to 0.3 μm in diameter.

9. The viscous flow field in a staggered array of rectangular or cylindrical fibers was found to be independent of the Reynolds number for $Re \leq 0.2$.

10. The dimensionless viscous drag on rectangular fibers with aspect ratios greater than 1 was found to be independent of the fiber aspect ratio and a function of the filter solid-volume fraction, which correlated well with the Kuwabara analytical results for cylindrical fibers.

11. For fiber aspect ratios below or equal to 1, the dimensionless drag was a function of both the aspect ratio and solid-volume fraction.

12. Collection efficiency of a single electret fiber was proportional to -2/3, 1.55, 0.92, and 0.47 powers of Peclet number, Interception parameter, Coulombic, and induced force parameters, respectively, when individual collection mechanism prevailed.

13. The single electret fiber efficiency due to pure diffusion was proportional to the square root of the fiber aspect ratio.

14. The single electret fiber efficiency was proportional to 0.278, 0.54, and 0.15 powers of the solid-volume fraction, respectively, for pure diffusion, interception, and Coulombic force interaction when each mechanism prevailed individually.

BIBLIOGRAPHY

1. Agarwal, J. K. and Sem, G. J. (1980), "Continuous Flow, Single-Particle-Counting Condensation Nucleus Counter", J. Aerosol Sci. 11: 343-357.

2. Ahlberg, J. H., Nilson, E. N., and Walsh, J. L.(1967), The theory of Splines and Their Applications, Academic Press, New York.

3. Ariman, T., Tang, L. (1976), "Collection of Aerosol Particles by Fabric Filters in an Electrostatic Field", Atmos. Environ. 10: 205-210.

4. Berglund, R. N. and Liu, B. Y. H. (1973), "Generation of Monodisperse Aerosol Standards", Environ. Sci. Technol. 7: 147-153.

5. Brown, R. C. (1981), "Capture of Dust Particles in Filters by Line-Dipole Charged Fibers", J. Aerosol Sci. 12: No. 4, 349-356.

6. Brown, R. C. (1982), "The Behavior of Electrostatic Filters Made of Fibers or Sheets Arranged Parallel to the Air Flow", J. Aerosol Sci. 12: No. 3, 249-257.

7. Brown, R. C. (1984), "A Many-Fiber Model of Air Flow Through a Fibrous Filter", J. Aerosol Sci., 583-593.

8. Buckingham, E. (1915), "Model Experiments and the Form of Empirical Equations", Trans. ASME 37: 263-296.

9. Burgess, W. A., Silverman, L., and Stein, F. (1961), "A New Technique for Evaluating Respirator Performance", Am. Ind. Hyg. Assoc. J., December, 422-429.

10. Cadle, R. D. and Thuman, W. C. (1960), "Filters from Submicron-Diameter Organic Fibers", Ind. Eng. Chem. 52: 315-316.

11. Cooper, D. W., Hinds, W. C., and Price, J. M. (1983), "Emergency Respiratory Protection with Common Materials", Am. Ind. Hyg. Assoc. J. 44: No. 1, 1-6.

12. Davies, C. N. (1973), Air Filtration, Academic Press, London.

13. Dorman, R. G. (1974), Dust Control and Air Cleaning Pergamon press, Oxford.

14. Dorman, R. G. and Pich, J. (1966), Aerosol Science (Davies, C. N. ed.), Academic Press, London.

15. Emi, H., Kanaoka, C., Otani, Y., and Ishiguro, T., Partic. Sci. Technol., in press.

16. Ferber, B. I., Brenenborg, F. J., and Rhode, A. (1970), "Respirator Filter Penetration Using Sodium Chloride Aerosol", Report of Investigations 7403, U.S. Dept. of the Interior, Bureau of Mines.

17. Ferber, B. I., Brenenborg, F. J., and Rhode, A. (1972), "Penetration of Sodium Chloride Aerosol through Respirator Filters", Am. Ind. Hyg. Assoc. J., December, 791-796.

18. Fergin, G. S. (1984), "Respirator Evaluation for Carbon Setters with Beards", Am. Ind. Hyg. Assoc. J. 45: No. 8, 533-537.

19. Fissan, H., Lathrache, R. (1986), "Investigation of Collection Behavior of Electrostatically Charged Fibrous Filters,", University of Duisburg, process and Aerosol Measurement Technology, Duisburg, West Germany.

20. Gillespie, T. (1955), "The Role of Electric Forces in the Filtration of Aerosols by Fiber Filter," J. Colloid. Sci. 10: 299-314.

21. Happel, J. (1959), "Viscous Flow Relative to Arrays of Cylinders", AICHE J. 5: 174-177.

22. Harris, H. E., DeSieghardt, W. C. (1974), "Field Testing of Throw-away Half-mask Dust Respirators", Am. Ind. Hyg. Assoc. J., September, 546-551.

23. Henry, F., Ariman, T. (1981), "The Effect of Neighboring Fibers on the Electric Field in a Fibrous Filter", J. Aerosol Sci. 12: No. 2, 137-149.

24. Henry, F., Ariman, T. (1981) "Cell Model of Aerosol Collection by Fibrous Filters in an Electrostatic Field", J. Aerosol Sci. 12: No. 2, 91-103.

25. Hochrainer, D. (1969) "Aerosol Deposition on a Single Fiber Under the Influence of Electrical Forces" Staub-Reinhalt. Luft 29: No. 2, 28-32.

26. Hyatt, E. C., Pritchard, J. A., and Richards, C. P. (1972), "Respirator Efficiency Measurement Using Quantitative DOP Man Tests", Am. Ind. Hyg. Assoc. J., October, 635-643.

27. Imai, I. (1951), "On the asymptotic behavior of viscous fluid flow at a great distance from a cylindrical body, with special reference to Filon's paradox", Proc. R. Soc. A 208: 487.

28. Japuntich, D. A., Johnson, B. D. (1983), Aerosols in the Mining and Industrial Work Stations (Marple, V. A., Liu, B. Y. H. ed.), Vol. 2, Chapter 37, Ann Arbor Science, Ann arbor, Michigan.

29. Jodeit, H., Loffler, F. (1984), "The Influence of Electrostatic Forces Upon Particle Collection in Fibrous Filters", J. Aerosol Sci. 15: 311-317.

30. Kanaoka, C., Emi, H., Otani, Y., and Iiyama, T. (1987), "Effect of Charging State of Particles on Electret Filtration", Aerosol Science and Technology 7: 1-13.

31. Katz, S. H., Smith, G. W., and Meiter, E. G. (1926a), "Dust Respirators: Their Construction and Filtering Efficiency", Technical Paper 394, Dept. of Commerce, Bureau of Mines.

32. Katz, S. H., Smith, G. W., and Meiter, E. G. (1926b), "Tests and Characteristics of Dust Respirators", Serial No. 2745, Dept. of Commerce, Bureau of Mines.

33. Kirsch, A. A. and Fuchs, N. A. (1967), "The Fluid Flow in a System of Parallel Cylinders Perpendicular to the Flow Direction at Small Reynolds Numbers", J. Phys. Soc. Japan 22: 1251-1255.

34. Kirsch, A. A. and Fuchs, N. A. (1968), "Studies on Fibrous Aerosol Filters-III. Diffusional Deposition of Aerosols in Fibrous Filters", Ann. Occup. Hyg. 11: 299-304.

35. Kirsch, A. A. (1972), "The Influence of an External Electric Field on the Deposition of Aerosols in Fibrous Filters", J. Aerosol Sci. 3: 25-29.

36. Knutson, E. O. and Whitby, K. T. (1975), "Accurate Measurement of Aerosol Electric Mobility Moments", J. Aerosol Sci. 6: 453.

37. Kraemer, H. F. and Johnstone, H. F. (1955), "Collection of Aerosol Particles in Presence of Electrostatic Fields", Ind. Eng. Chem. 47: No. 12, 2426-2434.

38. Kuwabara, S. (1959), "The Forces Experienced by Randomly Distributed Parallel Circular Cylinders or Spheres in Viscous Flow at Small Reynolds Numbers", J. Phys. Soc. Japan 14: 527-532.

39. Lamb, H. (1932), Hydrodynamics, 6th edition, p. 77, Cambridge University Press, London.

40. Lathrache, R. and Fissan, H. (1986), "Fractional Penetrations for Electrostatically Charged Fibrous Filters in the Submicron Particle Size Range", Part. Charact. 3: 74-80.

41. Lathrache, R. and Fissan, H. (1986), "Enhancement of Particle Deposition in Filters Due to Electrostatic Effects", Proc. 4th World Filtration Congress, Ostend, Belgium.

42. Lathrache, R., Fissan, H., and Neumann, S. (1986), "Deposition of Submicron Particles on Electrically Charged Fibers", J. Aerosol Sci. 17: 3, 446-449.

43. Lee, K. W. (1977), "Filtration of Submicron Aerosols by Fibrous Filters", Ph.D. Thesis, Mechanical Engineering Department, University of Minnesota, Minneapolis, Minnesota.

44. Liu, B. Y. H. and Pui, D. Y. H. (1974a), "Electrical Neutralization of Aerosols", J. Aerosol Sci. 5: 465-472.

45. Liu, B. Y. H. and Pui, D. Y. H. (1974b), "A Submicron Aerosol Standard and the Primary, Absolute Calibration of the Condensation Nucleus Counter", J. Colloid Interface Sci. 47: 155-171.

46. Liu, B. Y. H. and Lee, K. W. (1975), "An Aerosol Generator of High Stability", Am. Ind. Hyg. Assoc. J. 36: 861-865.

47. Liu, B. Y. H. and Lee, K. W. (1976), "Efficiency of Membrane and Nuclepore Filters for Submicrometer Aerosols", Environ. Sci. Technol. 10: 345-350.

48. Liu, B. Y. H. (1977), "Aerosol Instrumentation: Generation, Standards, Measurement Techniques and Data Reduction", Presented at the Annual Meeting of the Assoc. for Aerosol Research, Karlsruhe, Germany, October 26-28.

49. Liu, B. Y. H., Szymanski, W. W. , and Pui, D. Y. H. (1984), "Response of a Laser Optical Particle Counter to Transparent and Light-Absorbing Particles", Report to the American Society of Heating, Refrigerating and Air Conditioning Engineers, Particle Technology Laboratory, University of Minnesota, Minneapolis, Minnesota.

50. Liu, B. Y. H., Szymanski, W. W., and Ahn, K. H. (1985), "On Aerosol Size Distribution Measurement by Laser and White Light Optical Particle Counters", J. Environ. Sciences 28: 19-24.

51. Liu, B. Y. H. and Japuntich, D. A. (1987), "Respirator", McGraw-Hill Encyclopedia of Science and Technology, 6th ed., 15: 395-397.

52. Lowry, P. L., Hesch, P. R., and Revoir, W. H. (1977), "Performance of Single-use Respirators", Am. Ind. Hyg. Assoc. J. 38: September, 462-467.

53. Lowry, P. L. and Revoir, W. H. (1978), "Comparison of a Sodium Chloride Aerosol Filter Test Method to Silica-dust and Silica-mist Filter Test Methods", Am. Ind. Hyg. Assoc. J. 39: September, 709-716.

54. Lundgren D. A. and Whitby K. T. (1965), "Effect of Paticle Electrostatic Charge on Filtration by Fibrous Filters", I & E.C. process Design and Development 4: October, 345-349.

55. Luxon, S. G. (1973), "Harmonization of Respirator Standards in Europe", Am. Ind. Hyg. Assoc. J., April, 143-149.

56. Mitchell, R. N., Bevis, D. A., and Hyatt, E. C. (1971), "Comparison of Respirator Filter Penetration by Dioctyl Phthalate and Sodium Chloride", Am. Ind. Hyg. Assoc. J., June, 357-364.

57. Natanson, G. L. (1957), "Diffusion Precipitation of Aerosols on a Streamlined Cylinder with a Small Capture Coefficient", Dokl. Acad. Nauk. SSSR 112: 100-103; Proc. Acad. Sci. USSR, Phys. Chem. Sec. 112: 21-25 (English Translation).

58. Patankar, S. V., Liu, C. H., and Sparrow, E. M. (1977), "Fully Developed Flow and Heat Transfer in Ducts having Streamwise-Periodic Variations of Cross-Sectional Area", ASME Journal of Heat Transfer 99: 180-186.

59. Patankar, S. V. (1980), Numerical Heat Transfer and Fluid Flow, McGraw-Hill, New York.

60. Pich, J. (1965), "The Filtration Theory of Highly Dispersed Aerosols", Staub 25: May, 16-23 (English Translation).

61. Pich, J. (1966), "Theory of Aerosol Filtration by Fibrous and Membrane Filters", in Aerosol Science (C. N. Davies, ed.), Chapter 9, Academic Press, London.

62. Pui, D. Y. H. and Liu, B. Y. H. (1976), "Electrical Aerosol Analyzer: Calibration and Performance", Presented at Aerosol Measurement Workshop, University of Florida, Gainesville, Florida, March 24-26.

63. Rao, K. S., Ariman, T., Yang, K. T., and Hosbein, R. L. (1973), "Collection of Dust by Fabric Filtration in an Electrostatic Field", Proceedings of the 2nd Annual Environmental Engineering and Science Conference, pp. 555-571, University of Louisville.

64. Remiarz, R. J., Agarwal, J. K., Quant, F. R., and Sem, G. J. (1983), "A Real-Time Aerodynamic Particle Size Analyzer", Aerosols in the Mining and Industrial Work Environments (V. A. Marple and B. Y. H. Liu, ed.), Ann Arbor Science, Ann Arbor, Michigan, 879-895.

65. Revoir, W. H. and Yurgilas, V. A. (1968), "Performance Characteristics of Dust Respirators, Bureau of Mines Approved and Non-approved Types", Am. Ind. Hyg. Assoc. J., July-August, 322-332.

66. Rubow, K. L. (1981), "Submicron Aerosol Filtration Characteristics of Membrane Filters", Ph.D. Thesis, Mechanical Engineering Department, University of Minnesota, Minneapolis, Minnesota.

67. Schrenk, H. H. (1939), "Testing and Design of Respiratory Protective Devices", Information Circular No. 7086, U.S. Dept. of the Interior, Bureau of Mines.

68. Schurmann, G. and Fissan, H. (1984), "Fractional Efficiencies of an Electrostalically Spun Polymer Fiber Filter", The Eleventh Annual Conference of the Association for Aerosol Research, 317-320.

69. Smith, D. L., Johnston, O. E., and Lockwood, W. T. (1979), "The Efficiency of Respirator Filters in a Coke Oven Atmosphere", Am. Ind. Hyg. Assoc. J., December, 1030-1038.

70. Spielman, L. and Goren, S. (1968), "Model for Predicting Pressure Drop and Filtration Efficiency in Fibrous Media", Environ. Sci. Technol. 2: 279-287.

71. Stenhouse, J. I. T. (1974), "The Influence of Electrostatic Forces in Fibrous Filtration", Filtration & Separation, January-February, 25-26.

72. Szymanski, W. W. and Liu, B. Y. H. (1986), "On the Sizing Accuracy of Laser Optical Particle Counters", Particle Characterization 3: 1, 1-7.

73. Tuomi, T. (1985), "Face Seal Leakage of Half Masks and Surgical Masks", Am. Ind. Hyg. Assoc. J. 46: June, 308-312.

74. Van Turnhout, J. (1975), "The Use of Polymers for Electrets", J. of Electrostatics 1: 147-163.

75. Van Turnhout, J., Van Bochove, C., and Van Veldhuizen, G. J. (1976), "Electret Fibers for High-Efficiency Filtration of Polluted Gases", Staub-Reinhalt.Luft 36: 36-39.

76. Van Turnhout, J., Hoeneveld, W. J., Adamse, J.W.C., and Van Rossen, L. M. (1979), "Electret Filters for High-Efficiency and High-Flow Air Cleaning", Industry Applications Society Annual Meeting, 117-125.

77. Walkenhorst, W. and Zebel, G. (1964), "Uber ein neues Schwebstoffilter hoher Abscheideleistung und geringen Stromungswiderstandes", (in German) Staub 24: 444.

78. Walkenhorst, W. (1970), "Reflections and Research on the Filtraton of Dust from Gases with Special Consideration of Electrical Forces", J. Aerosol Sci. 1: 225-242.

79. Willeke, K., Ayer, H. E., and Blanchard, J. D. (1981), "New Methods for Quantitative Respirator Fit Testing with Aerosols", Am. Ind. Hyg. Assoc. J. 42: February, 121-125.

80. Willeke, K. and Liu, B. Y. H. (1976), "Single Particle Optical Counter: Principle and Application", in Fine Particles: Aerosol Generation, Measurement, Sampling, and Analysis (B. Y. H. Liu, ed.), Academic Press, New York.

81. Wilson, J. C. and Liu, B. Y. H. (1980), "Aerodynamic Particle Size Measurement by Laser-Doppler Velocimetry", J. Aerosol Sci. 11: 139.

82. Yeh, H. C. (1972), "A Fundamental Study of Aerosol Filtration by Fibrous Filters", Ph.D. Thesis, Mechanical Engineering Department, University of Minnesota, Minneapolis, Minnesota.

83. Yoshioka, N., Emi, H., Hattori, M. and Tamori, I. (1968) "Effect of Electrostatic Force in the Filtration Efficiency of Aerosols", Kagaka KogaKu. Chem. Eng. Japan 32: No. 8, 815-820.

84. Zebel, G. (1965), "Deposition of Aerosol Flowing Past a Cylindrical Fiber in a Uniform Electric Field", J. Colloid. Sci. 20: 522-543.

85. Zebel, G. (1969), "Aerosol deposition on a Single Fiber Under the Influence of Electrical Forces", Staub-Reinhalt. Luft 29: No. 2, 21-27.

APPENDIX A

NIOSH's Respirator Test Procedures and Approval Requirements

The following is a copy of the sub-part K of Part 11 in Title 30, code of federal regulations, which contains the procedures and requirements considered by NIOSH for testing and approving respirators and their filters. The copy was obtained from Pritchard (1976).

Subpart K—Dust, Fume, and Mist Respirators

§ 11.130 Dust, fume, and mist respirators; description.

Dust, fume, and mist respirators, including all completely assembled respirators designed for use as respiratory protection, during entry into and escape from hazardous particulate atmospheres which contain adequate oxygen to support life, are described as follows:

(a) Respirators, either with replaceable or reusable filters, designed as respiratory protection against dusts (1) having an air contamination level not less than 0.05 milligram per cubic meter of air, including but not limited to coal, arsenic, cadmium, chromium, lead, and manganese; or (2) dusts having an air contamination level not less than 2 million particles per cubic foot of air, including but not limited to aluminum, flour, iron ore, and free silica, resulting principally from the disintegration of a solid, e.g., dust clouds produced in mining, quarrying, and tunneling, and in dusts produced during industrial operations, such as grinding, crushing, and the general processing of minerals and other materials.

(b) Respirators, with replaceable filters, designed as respiratory protection against fumes of various metals having an air contamination level not less than 0.05 milligram per cubic meter, including but not limited to aluminum, antimony, arsenic, cadmium, chromium, copper, iron, lead, magnesium, manganese, mercury (except mercury vapor), and zinc, which result from the sublimation or condensation of their respective vapors, or from the chemical reaction between their respective vapors and gases.

(c) Respirators, with replaceable filters, designed as respiratory protection against mists of materials having an air contamination level not less than 0.05 milligram per cubic meter or 2 million particles per cubic foot, e.g., mists produced by spray coating with vitreous enamels, chromic acid mist produced during chromium plating, and other mists of materials whose liquid vehicle does not produce harmful gases or vapors.

(d) Respirators, with replaceable filters, designed as respiratory protection against dusts, fumes, and mists having an air contamination level less than 0.05 milligram per cubic meter, including but not limited to lithium hydride and beryllium, and against radionuclides.

(e) Respirators, with replaceable filters, designed as respiratory protection against radon daughters, and radon daughters attached to dusts, fumes, and mists.

(f) Respirators, with replaceable filters, designed as respiratory protection against asbestos-containing dusts and mists.

(g) Respirators, with replaceable filters, designed as protection against various combinations of particulate matter.

(h) Single-use dust respirators designed as respiratory protection against pneumoconiosis- and fibrosis-producing dusts, or dusts and mists, including but not limited to aluminum, asbestos, coal, flour, iron ore, and free silica.

(i) The types of dust, fume, and mist respirators in paragraphs (a) through (g) of this section may also be classified according to their design as follows:

(1) Air-purifying respirators; and

(2) Powered air-purifying respirators.

§ 11.131 Dust, fume and mist respirators; required components.

(a) Each dust, fume, and mist respirator described in § 11.130 shall, where its design requires, contain the following component parts:

(1) Facepiece, mouthpiece with noseclip, hood, or helmet;

(2) Filter unit;

(3) Harness;

(4) Attached blower; and

(5) Breathing tube.

(b) The components of each dust, fume, and mist respirator shall meet the minimum construction requirements set forth in Subpart G of this part.

§ 11.132 Breathing tubes; minimum requirements.

(a) Flexible breathing tubes used in conjunction with respirators shall be designed and constructed to prevent:

(1) Restriction of free head movement;

(2) Disturbance of the fit of facepieces, mouthpieces, hoods, or helmets;

(3) Interference with the wearer's activities; and

(4) Shutoff of airflow due to kinking, or from chin or arm pressure.

§ 11.133 Harnesses; installation and construction; minimum requirements.

(a) Each respirator shall, where necessary, be equipped with a suitable harness designed and constructed to hold the components of the respirator in position against the wearer's body.

(b) Harnesses shall be designed and constructed to permit easy removal and replacement of respirator parts, and, where applicable, provide for holding a full facepiece in the ready position when not in use.

§ 11.134 Respirator containers; minimum requirements.

(a) Except as provided in paragraph (b) of this section each respirator shall be equipped with a substantial, durable container bearing markings which show the applicant's name, the type of respirator it contains, and all appropriate approval labels.

(b) Containers for single-use respirators may provide for storage of more than one respirator, however, such containers shall be designed and constructed to prevent contamination of respirators which are not removed, and to prevent damage to respirators during transit.

§ 11.135 Half-mask facepieces, full facepieces, hoods, helmets, and mouthpieces; fit; minimum requirements.

(a) Half-mask facepieces and full facepieces shall be designed and constructed to fit persons with various facial shapes and sizes either: (1) By providing more than one facepiece size, or (2) by providing one facepiece size which will fit varying facial shapes and sizes.

(b) Full facepieces shall provide for optional use of corrective spectacles or lenses, which shall not reduce the respiratory protective qualities of the respirator.

(c) Hoods and helmets shall be designed and constructed to fit persons with various head sizes, provide for the optional use of corrective spectacles or lenses, and insure against any restriction of movement by the wearer.

(d) Mouthpieces shall be equipped with noseclips which are securely attached to the mouthpiece or respirator and provide an airtight seal.

(e) Facepieces, hoods, and helmets shall be designed to prevent eyepiece fogging.

(f) Half-mask facepieces shall not interfere with the fit of common industrial safety corrective spectacles, as determined by the Bureau's facepiece tests in §§ 11.140–1 and 11.140–2.

§ 11.136 Facepieces, hoods, and helmets; eyepieces; minimum requirements.

Facepieces, hoods, and helmets shall be designed and constructed to provide adequate vision which is not distorted by the eyepieces.

§ 11.137 Inhalation and exhalation valves; minimum requirements.

(a) Inhalation and exhalation valves shall be protected against distortion.

(b) Inhalation valves shall be designed and constructed and provided where necessary to prevent excessive exhaled air from adversely affecting filters, except where filters are specifically designed to resist moisture as prescribed in § 11.140–5.

(c) Exhalation valves shall be: (1) Provided where necessary; (2) protected against damage and external influence; and (3) designed and constructed to prevent inward leakage of contaminated air.

§ 11.138 Head harnesses; minimum requirements.

(a) All facepieces shall be equipped with head harnesses designed and constructed to provide adequate tension during use and an even distribution of pressure over the entire area in contact with the face.

(b) Facepiece head harnesses, except those employed on single-use respirators, shall be adjustable and replaceable.

(c) Mouthpieces shall be equipped, where applicable, with adjustable and replaceable harnesses, designed and constructed to hold the mouthpiece in place.

§ 11.139 Air velocity and noise levels; hoods and helmets; minimum requirements.

Noise levels generated by the respirator will be measured inside the hood or helmet at maximum airflow obtainable and shall not exceed 80 dBA.

§ 11.140 Dust, fume, and mist respirators; performance requirements; general.

Dust, fume, and mist respirators and the individual components of each such device shall, as appropriate, meet the requirements for performance and protection specified in the tests described in §§ 11.140–1 through 11.140–12 and prescribed in Tables 9 and 10.

§ 11.140–1 Isoamyl acetate tightness test; dust, fume, and mist respirators designed for respiratory protection against fumes of various metals having an air contamination level not less than 0.05 milligram per cubic meter; minimum requirements.

(a) The respirator will be modified in such a manner that all of the air that normally would be inhaled through the inhalation port(s) is drawn through an efficient activated charcoal-filled canister, or cartridge(s), without interference with the face-contacting portion of the facepiece.

(b) The modified respirator will be worn by persons for at least 2 minutes each in a test chamber containing 100 parts (by volume) of isoamyl-acetate vapor per million parts of air.

(c) The odor of isoamyl-acetate shall not be detected by the wearers of the modified respirator while in the test atmosphere.

§ 11.140–2 Isoamyl acetate tightness test; respirators designed for respiratory protection against dusts, fumes, and mists having an air contamination level less than 0.05 milligram per cubic meter, or against radionuclides; minimum requirements.

(a) The applicant shall provide a charcoal-filled canister or cartridge of a size and resistance similar to the filter unit with connectors which can be attached to the facepiece in the same manner as the filter unit.

(b) (1) The canister or cartridge will be used in place of the filter unit, and persons will each wear a modified half-mask facepiece for 5 minutes in a test chamber containing 100 parts (by volume) of isoamyl-acetate vapor per million parts of air.

(2) The following work schedule will be performed by each wearer in the test chamber:

(i) Two minutes walking, nodding, and shaking head in normal movements, and

(ii) Three minutes exercising and running in place.

(3) The facepiece shall be capable of adjustment, according to the applicant's instructions, to each wearer's face, and the odor of isoamyl-acetate shall not be detectable by any wearer during the test.

(c) Where the respirator is equipped with a full facepiece, hood, helmet, or mouthpiece, the canister or cartridge will be used in place of the filter unit, and persons will each wear the modified respiratory-inlet covering for 5 minutes in a test chamber containing 1,000 parts (by volume) of isoamyl-acetate vapor per million parts of air, performing the work schedule specified in paragraph (b)(2) of this section.

§ 11.140–3 Air-purifying filter tests; performance requirements; general.

Dust, fume, and mist respirators will be tested in accordance with the schedule set forth in Table 10 to determine their effectiveness as protection against the particulate hazards specified therein.

§ 11.140–4 Silica dust test; single-use or reusable filters; minimum requirements.

(a) Three respirators with single-use filters will be tested for periods of 90 minutes each at a continuous airflow rate of 32 liters per minute for air-purifying respirators, and for periods of 4 hours each at a flowrate not less than 115 liters per minute to tight-fitting facepieces, and not less than 170 liters per minute to loose-fitting hoods and helmets for powered air-purifying respirators.

(b) The relative humidity in the test chamber will be 20–80 percent, and the room temperature approximately 25° C.

(c) The test suspension in the chamber will not be less than 50 nor more than 60 milligrams of flint (99+ percent free silica) per cubic meter of air.

(d) The flint in suspension will be ground to pass 99+ percent through a 270-mesh sieve.

(e) The particle-size distribution of the test suspension will have a geometric mean of 0.4 to 0.6 micrometer, and the standard geometric deviation will not exceed 2.

(f) The total amount of unretained test suspension in samples taken during testing shall not exceed 1.5 milligrams for an air-purifying respirator, 14.4 milligrams for a powered air-purifying respirator with tight-fitting facepiece, and 21.3 milligrams for a powered air-purifying respirator with loose-fitting hood or helmet.

(g) Three respirators with reusable filters will be tested and shall meet the requirements specified in paragraphs (a) through (f) of this section; each filter shall be tested three times: Once as received; once after cleaning, and once after recleaning. The applicant's instructions shall be followed for each cleaning.

§ 11.140–5 Silica-dust test; single-use dust respirators; minimum requirements.

(a) Three respirators will be tested.

(b) As described in § 11.140–4, airflow will be cycled through the respirator by a breathing machine at the rate of 24 respirations per minute with a minute volume of 40 liters; a breathing machine cam with a work rate of 622 kg-m⁻¹-minute shall be used.

(c) Air exhaled through the respirator will be 35° ±2° C. (95° ±3° F.) with 94 ±3 percent relative humidity.

(d) Air inhaled through the respirator will be sampled and analyzed for respirator leakage.

(e) The total amount of unretained test suspension, after drying, in samples taken during testing, shall not exceed 1.8 milligrams for any single test.

§ 11.140–6 Lead fume test; minimum requirements.

(a) Three respirators will be tested for a period of 312 minutes each at a continuous airflow rate of 32 liters per minute for air-purifying respirators, and for periods of 4 hours each at a flow rate not less than 115 liters per minute to tight-fitting facepieces, and not less than 170 liters per minute to loose-fitting hoods and helmets for powered air-purifying respirators.

(b) The relative humidity in the test chamber will be 20–80 percent, and the room temperature approximately 25° C.

(c) The test suspension in the test chamber will not be less than 15 nor more than 20 milligrams of freshly generated lead-oxide fume, calculated as lead (Pb), per cubic meter of air.

(d) The fume will be generated by impinging an oxygen-gas flame on molten lead.

(e) Samples of the test suspension will be taken during each test period for analysis.

(f) The total amount of unretained test suspension in the samples taken during testing, which is analyzed and calculated as lead (Pb), shall not exceed 1.5 milligrams of lead for an air-purifying respirator, 4.2 milligrams of lead for a powered air-purifying respirator with tight-fitting facepiece, and 8.2 milligrams of lead for a powered air-purifying respirator with loose-fitting hood or helmet.

§ 11.140–7 Silica mist test; minimum requirements.

(a) Three respirators will be tested for a period of 312 minutes each at a continuous airflow rate of 32 liters per minute for air-purifying respirators, and for periods of 4 hours each at a flow rate not less than 115 liters per minute to tight-fitting facepieces, and not less than 170 liters per minute to loose-fitting hoods and helmets for powered air-purifying respirators.

(b) The room temperature in the test chamber will be approximately 25° C.

(c) The test suspension in the test chamber will not be less than 20 nor more than 25 milligrams of silica mist, weighed as silica dust, per cubic meter of air.

(d) Mist will be produced by spraying an aqueous suspension of flint (99+ percent free silica), and the flint shall be ground to pass 99+ percent through a 270-mesh sieve.

(e) Samples of the test suspension will be taken during each test period for analysis.

(f) The total amount of silica mist unretained in the samples taken during testing, weighed as silica dust, shall not exceed 2.5 milligrams for an air-purifying respirator, 6.9 milligrams for a powered air-purifying respirator with tight-fitting facepiece, and 10.2 milligrams for a powered air-purifying respirator with loose-fitting hood or helmet.

§ 11.140–8 Tests for respirators designed for respiratory protection against more than one type of dispersoid; minimum requirements.

Respirators designed as respiratory protection against more than one particulate hazard (dust, fume, or mist) shall comply with all the requirements of this part, with respect to each of the specific hazards involved.

§ 11.140–9 Airflow resistance tests; all dust, fume, and mist respirators; minimum requirements.

(a) Resistance to airflow will be measured in the facepiece, mouthpiece, hood, or helmet of a dust, fume, or mist respirator mounted on a test fixture with air flowing at a continuous rate of 85 liters per minute, both before and after each test conducted in accordance with §§ 11.140–4 through 11.140–7.

(b) The maximum allowable resistance requirements for dust, fume, and mist respirators are as follows:

MAXIMUM RESISTANCE
(mm. water-column height)

Type of respirator	Initial Inhalation	Final Inhalation	Exhalation
Single-use	12	18	15
Dust, fume and mist with single-use filter	20	30	20
Dust, fume and mist with reusable filter	20	40	20
Radon daughter	15	[1] 25	15
Asbestos dust and mist	15	25	15

[1] Measured after silica dust test described in § 11.140–4.

§ 11.140–10 Exhalation valve leakage test; minimum requirements.

(a) Dry exhalation valves and valve seats will be subjected to a suction of 25 mm. water-column height while in a normal operating position.

(b) Leakage between the valve and valve seat shall not exceed 30 milliliters per minute.

§ 11.140–11 DOP filter test; respirators designed as respiratory protection against dusts, fumes, and mists having an air contamination level less than 0.05 milligram per cubic meter and against radionuclides; minimum requirements.

(a) All single air-purifying respirator filter units will be tested in an atmosphere concentration of 100 micrograms of DOP per liter of air at continuous flow rates of 32 and 85 liters per minute for a period of 5 to 10 seconds.

(b) Where filters are to be used in pairs, the flow rates will be 16 and 42.5 liters per minute, respectively, through each filter.

(c) The filter will be mounted on a connector in the same manner as used on the respirator, and the total leakage for the connector and filter shall not exceed 0.03 percent of the ambient DOP concentration at either flow rate.

§ 11.140–12 Silica dust loading test; respirators designed as protection against dusts, fumes, and mists having an air contamination level less than 0.05 milligram per cubic meter and against radionuclides; minimum requirements.

Three respirators will be tested in accordance with the provisions of § 11.140–4 and shall meet the minimum requirements of §§ 11.140–4 and 11.140.9.

TABLE 9—FACEPIECE TEST REQUIREMENTS
(30 CFR Part 11, Subpart K, § 11.140–1, et seq.)

Respirator types	Pressure demand test [1]	Isoamyl acetate test	
		11.140–1	11.140–7
Dusts: Air Contamination Level not less than 0.05 mg/M³ or 2 mppcf	X		
Fumes: Air Contamination Level not less than 0.05 mg/M³	X	X	
Mists: Air Contamination Level not less than 0.05 mg/M³ or 2 mppcf	X		
Dusts, Fumes and Mists Air Contamination Level less than 0.05 mg/M³ or 2 mppcf, and radionuclides	X		X
Radon daughters	X	X	
Asbestos-containing dusts and mists	X		

[1] Test is required only where applicable.

TABLE 10—AIR-PURIFYING AND POWERED AIR-PURIFYING RESPIRATOR FILTER TESTS REQUIRED FOR APPROVAL
(30 CFR Part 11, Subpart K, § 11.140–4, et seq.)

Respirator types	Silica dust tests			Lead fume test	Silica mist test	DOP test
	11.140–4	11.140–6	11.140–12	11.140–6	11.140–7	11.140–11
Dusts: Air Contamination Level not less than 0.05 mg/M³ or 2 mppcf	X					
Fumes: Air Contamination Level not less than 0.05 mg/M³				X		
Mists: Air Contamination Level not less than 0.05 mg/M³ or 2 mppcf					X	
Dusts, Fumes and Mists: Air Contamination Level less than 0.05 mg/M³ or 2 mppcf, and radionuclides			X			X
Radon daughters	X[1]			X[1]		
Asbestos-containing dusts and mists	X[1]				X[1]	
Single-use dust and mist respirators		X[1]			X[1]	

[1] For resistance only.
[2] For penetration only.
[3] Test required only where applicable.

Subpart L—Chemical Cartridge Respirators

§ 11.150 Chemical cartridge respirators; description.

Chemical cartridge respirators including all completely assembled respirators which are designed for use as respiratory protection during entry into or escape from atmospheres not immediately dangerous to life and health, are described according to the specific gases or vapors against which they are designed to provide respiratory protection, as follows:

Type of chemical cartridge respirator	Maximum use concentration, parts per million
Ammonia	300
Chlorine	10
Hydrogen chloride	50
Methyl amine	100
Organic vapor [1]	[2] 1,000
Sulfur dioxide	50

[1] Not for use against organic vapors with poor warning properties or those which generate high heats of reaction with sorbent material in the cartridge.

[2] Maximum use concentrations are lower for organic vapors which produce atmospheres immediately hazardous to life or health at concentrations equal to or lower than this concentration.

NOTE: Chemical cartridge respirators for respiratory protection against gases or vapors which are not specifically listed with their maximum use concentration except pesticides, may be approved if the applicant submit a request for such approval in writing to the Bureau. The Bureau and the Institute shall consider each such application and accept or reject the application after a review of the effects on the wearer's health and safety and in the light of any field experience in use of chemical cartridge respirators as protection against such hazards.

§ 11.151 Chemical cartridge respirators; required components.

(a) Each chemical cartridge respirator described in § 11.150 shall, where its design requires, contain the following component parts:

(1) Facepiece, mouthpiece, and nose-clip, hood, or helmet;
(2) Cartridge;
(3) Cartridge with filter;
(4) Harness;
(5) Breathing tube; and
(6) Attached blower.

(b) The components of each chemical cartridge respirator shall meet the minimum construction requirements set forth in Subpart G of this part.

§ 11.152 Cartridges in parallel; resistance requirements.

Where two or more cartridges are used in parallel, their resistance to airflow shall be essentially equal.

§ 11.153 Cartridges; color and markings; requirements.

The color and markings of all cartridges or labels shall conform with the requirements of the American National Standard for Identification of Gas Mask

APPENDIX B

Numerical Solution of Flow Equations

The momentum equations (4.26) and (4.27) and convective-diffusion equation (4.76) presented earlier are particular cases of a general differential equation expressed in the cartesian-tensor form as follows,

$$\frac{\partial}{\partial x_j}(\rho u_j \phi) = \frac{\partial}{\partial x_j}(\Gamma \frac{\partial \phi}{\partial x_j}) + S \qquad (B.1)$$

where ϕ is the dependent variable representing a variety of different quantities such as enthalpy, velocity components, mass concentration, etc., Γ is called the diffusion coefficient which stands for material properties such as thermal conductivity, viscosity, diffusivity, etc., u_j represents the jth component of velocity vector and S is called the source term. The above equation basically represents the principle of conservation of quantity ϕ over an infinitesimal control volume in terms of the net tranport rate of ϕ out of the volume by the fluid flow being equal to the net rate of diffusion of ϕ into the volume plus the net generation rate of ϕ within the control volume.

In general, there is no analytical solution to equation

(B.1) and one must resort to the numerical means to obtain any information about the distribution of ϕ in the domain of interest based on given set of boundary conditions. A numerical solution of equation (B.1) is basically a set of numbers representing values of ϕ in the domain, from which the distribution of ϕ can be deduced. In other words, one replaces the continuous distribution of ϕ as the analytical solution of equation (B.1) by its discrete values obtained from the numerical solution. Such action is, in essence, discretizing the governing differential equation in the form of finite number of algebraic equations containing values of ϕ at finite number of locations in the calculation domain, commonly referred to as grids. These algebraic equations are called discretization equations which can be obtained from the differential equation under consideration in several ways.

The technique considered here for discretizing equation (B.1) is based on the control volume formulation described in detail by Patankar (1980) in his book. Below, a detail discussion of the technique is presented, which closely follows that given by Patankar (1980).

B.1 One Dimensional Diffusion Problem

For better illustration of the discretization

technique, it is best to consider a one dimensional, steady state diffusion problem without the influence of fluid flow. Thus, equation (B.1) can be simplified as

$$\frac{d}{dx}\left(\Gamma \frac{d\phi}{dx}\right) + S = 0 \qquad (B.2)$$

whose numerical solution is being seeked. A control volume formulation of this problem first involves dividing the calculation domain into a finite number of control volumes, each enclosing a grid at its center. Figure (B.1) shows three of such control volumes which have infinite dimensions in the y- and z- directions due to one dimensional consideration of the problem. The grids are denoted by W, P, and E with W and E denoting West and East neighbors of grid point P.

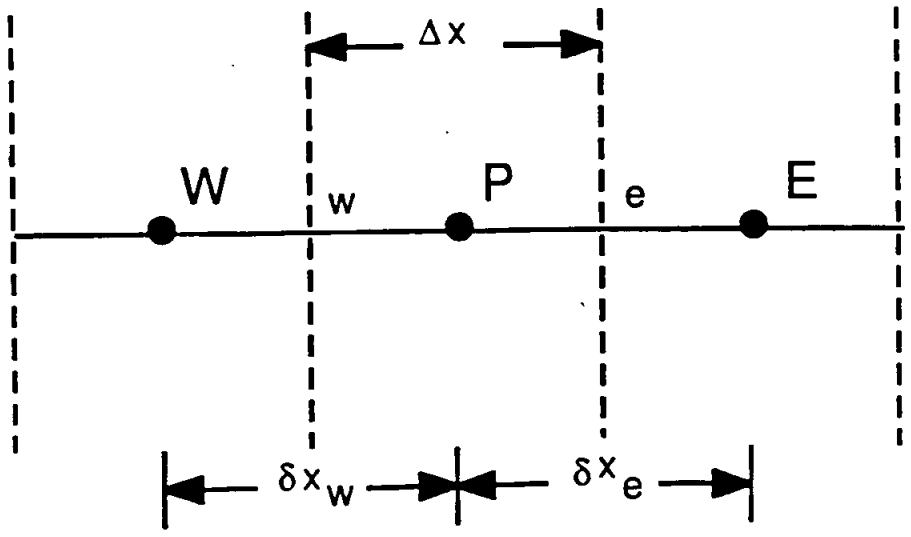

Figure B.1 Schematic diagram of one-dimensional control volumes, each enclosing a grid point

Once the control volumes are laid out, the differential equation (B.2) will be integrated over each control volume to obtain the corresponding algebraic or discretization equation. To illustrate this, let's consider the one dimensional control volume around grid P as shown in Figure (B.1). Integrating equation (B.2) over this volume yields

$$\int_w^e \frac{d}{dx}(\Gamma \frac{d\phi}{dx})dx + \int_w^e Sdx = 0 \qquad (B.3)$$

where w and e denote the location of the west and east control volume faces, respectively. Equation (B.3) can be carried one step forward as

$$(\Gamma \frac{d\phi}{dx})_e - (\Gamma \frac{d\phi}{dx})_w + \int_w^e Sdx = 0 \qquad (B.4)$$

To evaluate the terms in the above equation, one must assume a mathematical profile for variation of the dependent variable and source term in the calculation domain, in particular between adjacent grids. At this point, the view adopted by Patankar (1980) on these profiles is that their assumed form is of no consequence on the ultimate values of ϕ as, once the final grid point values of ϕ are obtained, one does not care how the dependent variable was assumed to vary in the course of reaching the final solution. Although,

it is true that different profile assumptions give rise to different discretization equations but, the final solution must be identical independent of the form of the assumed profiles. However, the derived discretization equations must satisfy certain rules which will be given below to assure that the results are physically realistic and satisfy the overall balance of the dependent variable over each control volume as well as the entire calculation domain.

Thus, based on the above view point, one may assume a linear profile for variation of ϕ along the x- direction between adjacent grids. As a result, the first and second terms in equation (B.4) can be evaluated as follows,

$$(\Gamma \frac{d\phi}{dx})_w = \Gamma_w \frac{\phi_P - \phi_W}{\delta x_w} \tag{B.5}$$

$$(\Gamma \frac{d\phi}{dx})_e = \Gamma_e \frac{\phi_E - \phi_P}{\delta x_e} \tag{B.6}$$

where Γ_w and Γ_e are values of the diffusion coefficient at the west and east loaction of the control volume faces, respectively, and δx_w and δx_e are dimensions shown in Figure (B.1).

As for the source term which is often a function of ϕ, one can not allow a dependency other than linear between S and ϕ in the present calculations since the discretization

equations will be solved by techniques for linear algebraic equations. Therefore, any non-linear relationship between S and ϕ must be linearized in the following form

$$S = S_C + S_P\phi \tag{B.7}$$

where S_C and S_P represent, respectively, the constant part and slope of the linearized relationship between S and ϕ. For more information on linearizing techniques, reference is made to Patankar (1980). Thus, the third term of equation (B.4) based on the above expression for the source term can be expressed as

$$\int_w^e S dx = \int_w^e (S_C + S_P\phi) dx \tag{B.8}$$

To evaluate the right-hand side of the integral, one may assume ϕ to be constant equal to its value at grid P, i.e. ϕ_P, for the whole control volume. Notice that this profile assumption is different from that considered for evaluation of the first and second terms of equation (B.4) due to the freedom of choice of profiles as explained above. Therefore, the integral of the source term can be expressed as

$$\int_w^e S dx = S_C \Delta x + S_P \phi_P \Delta x \tag{B.9}$$

where Δx is the width of the control volume around grid P as shown in Figure (B.1). Finally, substituting for the terms of equation (B.4) expressions given by equations (B.5), (B.6), and (B.9), one obtains the following,

$$\Gamma_e \frac{\phi_E - \phi_P}{\delta x_e} - \Gamma_w \frac{\phi_P - \phi_W}{\delta x_w} + S_C \Delta x + S_P \phi_P \Delta x = 0 \quad (B.10)$$

Rearranging terms yields

$$\left(\frac{\Gamma_e}{\delta x_e} + \frac{\Gamma_w}{\delta x_w} - S_P \Delta x\right) \phi_P = \frac{\Gamma_e}{\delta x_e} \phi_E + \frac{\Gamma_w}{\delta x_w} \phi_W + S_C \Delta x \quad (B.11)$$

Let's now introduce the following coefficients

$$a_E = \frac{\Gamma_e}{\delta x_e} \quad (B.12a)$$

$$a_W = \frac{\Gamma_w}{\delta x_w} \quad (B.12b)$$

$$a_P = a_E + a_W - S_P \Delta x \quad (B.12c)$$

and

$$b = S_C \Delta x \quad (B.12d)$$

Therefore, equation (B.11) can be written as

$$a_P \phi_P = a_E \phi_E + a_W \phi_W + b \quad (B.13)$$

This is the standard form of a discretized equation containing the value of ϕ at the central grid at the left side of the equation and its values at the neighboring grids at the right side of the equation in addition to the constant b. Such equation is obtained for each control volume considered in the calculation domain with the coefficients being determined from equations (B.12a)-(B.12d). The result is then a finite number of algebraic equations containing unknown values of ϕ at grid points, which can be determined by solving the equations simultaneously or iteratively until a converged solution is attained.

To ensure that the resulting numerical solution is physically realistic and obeys the overall balance requirements, Patankar (1980) has outlined four basic rules which, when obeyed by the discretization equations, should give rise to acceptable results. For detail discussion of these rules which are only listed below, one should refer to the Patankar's book. The rules are:

1. Flux expressions across a face common to two control volumes should be the same in the formulation of discretization equations of both control volumes.

2. The discretization coefficients a_P, a_E, and a_W must always be positive.

3. The coefficient S_p introduced in the linearized expression of the source term must always be less than or equal to zero to ensure stability of the solution.

4. The central grid discretization coefficient, a_p, must equal the sum of neighboring coefficients for situations in which ϕ and $\phi + C$ (C being a constant) both satisfy the differential equation under consideration.

B.2 One Dimensional Convective-Diffusion Problem

After describing a technique for discretizing a one dimensional diffusion equation as above, the next step is to include the fluid flow effects by considering a one dimensional convective-diffusion problem governed by the following equation

$$\frac{d}{dx}(\rho u \phi) = \frac{d}{dx}\left(\Gamma \frac{d\phi}{dx}\right) \qquad (B.14)$$

where u is the fluid velocity component in the x- direction and ρ is the fluid density. As often is the case, however, the flow field in the calculation domain under consideration is not known and one must solve the momentum and continuity equations to obtain any information about the flow field. At this point, however, it is assumed that u is known and has physically realistic values which satisfy the continuity

equation expressed as following for a steady state, one dimensional problem under consideration

$$\frac{d}{dx}(\rho u) = 0 \qquad (B.15)$$

which means

$$(\rho u) = \text{constant} \qquad (B.16)$$

In addition, as will be explained later, the numerical technique employed here determines the velocity components at the intersection of the grid lines and control volume faces instead of grid points which store values of other dependent variables involved. Figure B.2 shows u_w and u_e denoting, respectively, the u values at the west and east faces of the control volume around grid point P. It should be mentioned that the velocity is assumed to be constant along the control volume faces.

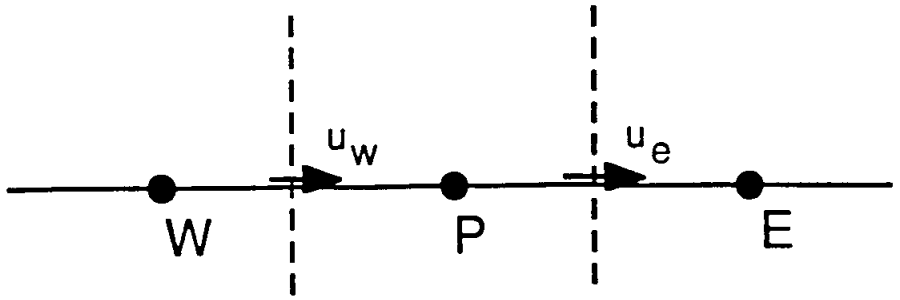

Figure B.2 Location of the u- velocity component at the control volume faces

As explained in the previous section, the discretization equations corresponding to a differential equation are the result of integration of the equation over each control volume considered in the calculation domain. Thus, integrating equation (B.14) over the control volume shown in Figure (B.2) yields

$$\int_w^e \frac{d}{dx}(\rho u\phi)dx = \int_w^e \frac{d}{dx}(\Gamma \frac{d\phi}{dx})dx \qquad (B.17)$$

or

$$(\rho u\phi)_e - (\rho u\phi)_w = (\Gamma \frac{d\phi}{dx})_e - (\Gamma \frac{d\phi}{dx})_w \qquad (B.18)$$

which, again, requires assuming a profile for variation of ϕ in order to evaluate the terms. Patankar (1980) evaluated several schemes (profiles) for ϕ and obtained the corresponding discretization equation. The advantages and disadvantages of each scheme were discussed and their results were compared with the analytical solution of equation (B.14). The scheme which gave the best comparison was the power-law scheme described in detail by Patankar (1979a). Below, only the results of application of the power-law scheme to the terms of equation (B.18) are presented and for more information, one should refer to the discussion given by Patankar (1980). Thus, the coefficients of the general discretization equation (equation (B.13))

based on the power-law scheme for the one dimensional, steady state convection-diffusion differential equation are expressed as follows,

$$a_E = D_e \, [[0 \, , \, (1 - 0.1|\frac{F_e}{D_e}|)^5]] + [[0 \, , \, -F_e]] \qquad (B.19a)$$

$$a_W = D_W \, [[0 \, , \, (1 - 0.1|\frac{F_W}{D_W}|)^5]] + [[0 \, , \, +F_W]] \qquad (B.19b)$$

$$a_P = a_E + a_W + (F_e - F_W) \qquad (B.19c)$$

where

$$D_e = \frac{\Gamma_e}{\delta x_e} \qquad (B.19d)$$

$$D_W = \frac{\Gamma_W}{\delta x_W} \qquad (B.19e)$$

$$F_e = \rho u_e \qquad (B.19f)$$

$$F_W = \rho u_W \qquad (B.19g)$$

and the symbol [[ ]] stands for the largest of the two quantities within it. Note also that the constant b in the present case is not included since there is no source term in the original differential equation.

B.3 Two Dimensional Convective-Diffusion Problem

Having taken into account the convective and diffusion mechanisms in the y- direction, the 2D, steady state convective-diffusion equation, in general, can be expressed by

$$\frac{\partial}{\partial x}(\rho u \phi) + \frac{\partial}{\partial y}(\rho v \phi) = \frac{\partial}{\partial x}(\Gamma \frac{\partial \phi}{\partial x}) + \frac{\partial}{\partial y}(\Gamma \frac{\partial \phi}{\partial y}) + S \qquad (B.20)$$

where v is the velocity component in the y- direction. Once again, it is assumed that both u and v are known.

Following the above discretization procedure, equation (B.20) can be integrated over a typical two dimansional control volume such as that shown in Figure (B.3). Using the power-law scheme for variation of ϕ in the calculation domain, the following general discretization equation is obtained

$$a_P \phi_P = a_E \phi_E + a_W \phi_W + a_S \phi_S + a_N \phi_N + b \qquad (B.21)$$

where S and N subscripts denote, respectively, the South and North neighbors of grid point P as shown in Figure (B.3).

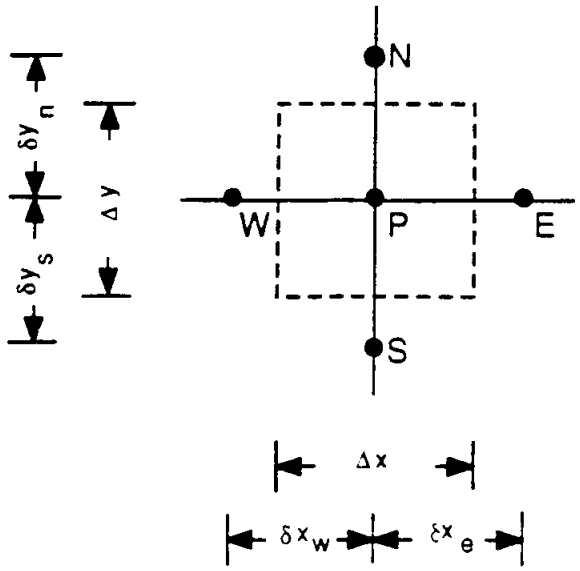

Figure B.3 Schematic diagram of a two dimensional control volume around a grid point with its immediate neighboring grids

The coefficients a_E and a_W in equation (B.21) are determined from equations (B.19a) and (B.19b) while, the other coefficients can be determined from the following expressions

$$a_N = D_n \left[\left[0 \ , \ \left(1 - 0.1\left|\frac{F_n}{D_n}\right|\right)^5\right]\right] + \left[\left[0 \ , \ -F_n\right]\right] \qquad (B.21a)$$

$$a_S = D_s \left[\left[0 \ , \ \left(1 - 0.1\left|\frac{F_s}{D_s}\right|\right)^5\right]\right] + \left[\left[0 \ , \ F_s\right]\right] \qquad (B.21b)$$

$$a_P = a_E + a_W + a_N + a_S - S_P \Delta x \Delta y \qquad (B.21c)$$

and

$$b = S_C \Delta x \Delta y \tag{B.21d}$$

where

$$D_e = \frac{\Gamma_e \Delta y}{(\delta x)_e} \tag{B.22a}$$

$$D_w = \frac{\Gamma_w \Delta y}{(\delta x)_w} \tag{B.22b}$$

$$D_n = \frac{\Gamma_n \Delta x}{(\delta y)_n} \tag{B.22c}$$

$$D_s = \frac{\Gamma_s \Delta x}{(\delta y)_s} \tag{B.22d}$$

and

$$F_e = (\rho u)_e \Delta y \tag{B.22e}$$

$$F_w = (\rho u)_w \Delta y \tag{B.22f}$$

$$F_n = (\rho v)_n \Delta x \tag{B.22g}$$

$$F_s = (\rho v)_s \Delta x \tag{B.22h}$$

The presentation of the two dimensional discretization equation as above facilitates the derivation of the momentum discretization equations as explained below.

B.4 Discretization of the Flow Equations

As emphasized, the above discretization equations were obtained assuming the velocity components were known. But most often, the velocity field is not known and must be determined by simultaneously solving the continuity and

momentum equations (4.25), (4.33), and (4.34)

$$\frac{\partial u}{\partial x} + \frac{\partial v}{\partial y} = 0 \qquad (4.25)$$

$$\rho\left(u\frac{\partial u}{\partial x} + v\frac{\partial u}{\partial y}\right) = \hat{\beta} - \frac{\partial P}{\partial x} + \mu\nabla^2 u \qquad (4.33)$$

$$\rho\left(u\frac{\partial v}{\partial x} + v\frac{\partial v}{\partial y}\right) = -\frac{\partial P}{\partial y} + \mu\nabla^2 v \qquad (4.34)$$

for the problem under consideration. The discretization procedure for the above differential equations is similar to that shown earlier for the one and two dimensional convective-diffusion problems with the exception that the control volumes considered for discretization of the flow equations are staggered with respect to those surrounding main grid points simply because the velocity components are chosen to be determined at the faces of the main control volumes. The reasons for such choice as discussed by Patankar (1980) are

1. Physically non-realistic velocity fields could satisfy the flow equations if the velocity components are specified at the main grids.
2. By specifying the velocity components at the control volume faces, one does not need to interpolate their values in order to determine the convection rate of conserved quantities such as enthalpy, mass concentration, etc. into or out of the main control volumes.

3. The concept of driving a velocity component at a control volume face by the difference in pressure values specified at two main grids immediate to that face is more comprehensible and natural.

The control volumes for the two typical velocity components u_e and v_n are shown, respectively, in Figures B.4 and B.5. Notice that since the velocity control volumes are staggered with respect to the main control volumes, they will be referred to as staggered control volumes from hereinafter. Integrating equations (4.33) and (4.34) over corresponding staggered control volumes shown, respectively, in Figures (B.4) and (B.5) yields the following general discretization equations for the two velocity components,

$$a_e u_e = \Sigma a_{nb} u_{nb} + (P_P - P_E)A_e + \hat{\beta}\Delta y \qquad (B.23)$$

$$a_n v_n = \Sigma a_{nb} v_{nb} + (P_P - P_N)A_n \qquad (B.24)$$

where subscript nb denotes neighbor, a's are the discretization coefficients given by equations (B.19a), (B.19b), and (B.21a)-(B.21c), P is pressure, A_e and A_n are the areas of the control volume faces normal to u_e and v_n, respectively. Had the pressure field been known, the above

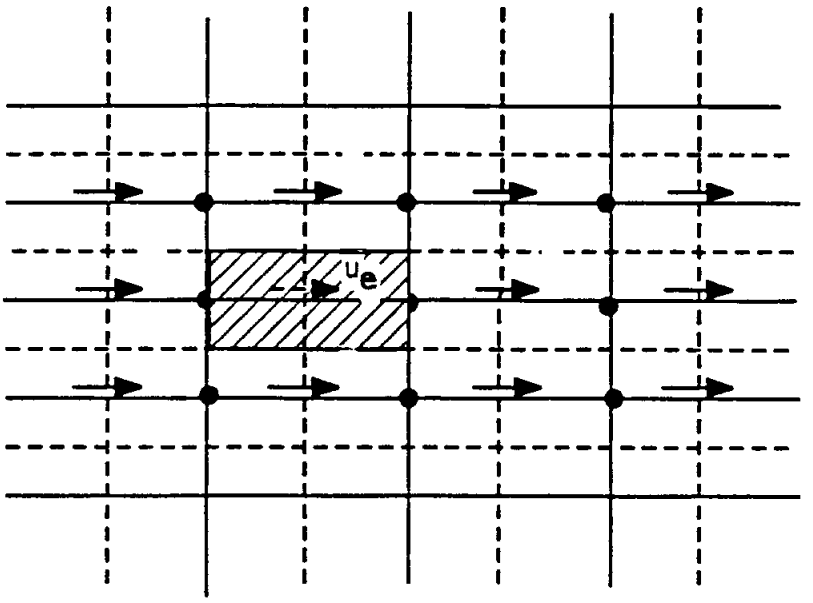

Figure B.4 Staggered control volume for calculation of the u- velocity component

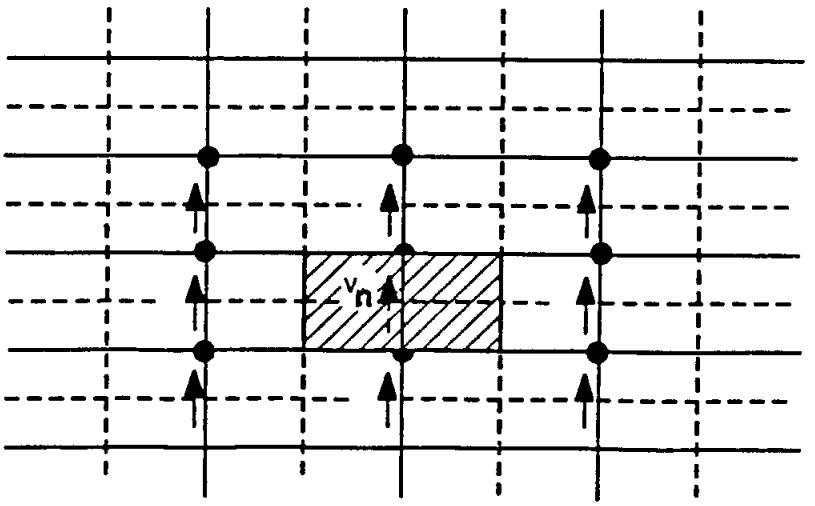

Figure B.5 Staggered control volume for calculation of the v- velocity component

equations could have been solved iteratively starting with a gussed velocity field until a converged solution would have been obtained. But, of course, in most cases the pressure field is not known and must be determined prior to or in conjunction with solution of equations (B.23) and (B.24). There is, however, another important flow equation, namely, the continuity equation which must be satisfied by the velocity components resulting from solution of equations (B.23) and (B.24). In other words, except for the correct pressure field, the continuity equation will not be satisfied by the solution of the discretized momentum equations.

But in the absence of the correct pressure field, one may start with a guessed pressure field, P^*, for solution of the momentum equations. In that case, the velocity components resulting from this pressure field must satisfy the following equations

$$a_e u_e^* = \Sigma a_{nb} u_{nb}^* + (P_P^* - P_E^*)A_e + \hat{\theta}\Delta x \qquad (B.25)$$

$$a_n u_n^* = \Sigma a_{nb} v_{nb}^* + (P_P^* - P_N^*)A_n \qquad (B.26)$$

where the starred veocity components constitute the imperfect velocity field obtained as a result of the guessed

pressure field, P^*. Note that equations (B.23) and (B.24) give rise to the correct velocity field when the correct pressure field, P, is used. Hence, the guessed pressure field must be modified by a correction pressure field, P', to yield the perfect or correct pressure field as follows,

$$P = P^* + P' \tag{B.27}$$

Similarly, the imperfect velocity components will also be corrected to the right values by corresponding correction terms as follows

$$u = u^* + u' \tag{B.28}$$

$$v = v^* + v' \tag{B.29}$$

where u' and v' are the resulting corrections to the starred velocity components when P^* is corrected by P'. In other words, u' and v' must satisfy the following equations obtained by subtracting equations (B.25) and (B.26) from equations (B.23) and (B.24), respectively,

$$a_e u'_e = \Sigma a_{nb} u'_{nb} + (P'_P - P'_E)A_e \tag{B.30}$$

$$a_n v'_n = \Sigma a_{nb} v'_{nb} + (P'_P - P'_N)A_n \tag{B.31}$$

At this point, the summation terms in the above equations will be dropped following the Patankar's approach based on the following reasons: 1- that equations (B.30) and (B.31) are only auxiliary means to obtaining a solution to the continuity equation and therefore, if a satisfactory solution can still be obtained from use of a simplified version of these equation, one should not be concerned about details of the simplifications; 2- that if the summation terms are kept, they will bring the effect of the pressure correction values at all the grid points in the calculation domain into the pressure correction equation, as will be derived below, thus making the problem unmanageable.

In any event, equations (B.30) and (B.31) are simplified as

$$a_e u'_e = (P'_P - P'_E)A_e \tag{B.32}$$

$$a_n v'_n = (P'_P - P'_N)A_n \tag{B.33}$$

Solving for u'_e and v'_n yields

$$u'_e = (P'_P - P'_E)d_e \tag{B.34}$$

$$v'_n = (P'_P - P'_E)d_n \tag{B.35}$$

where

$$d_e = \frac{A_e}{a_e} \tag{B.36}$$

$$d_n = \frac{A_n}{a_n} \tag{B.37}$$

Thus, the correct values of u_e and v_n are then given by

$$u_e = u_e^* + (P_P' - P_E')d_e \tag{B.38}$$

$$v_n = v_n^* + (P_P' - P_N')d_n \tag{B.39}$$

Notice that similar expressions can also be written for u_w, the u-component at the west face, and v_n, the v-component at the south face, as follows,

$$u_w = u_w^* + (P_W' - P_P')d_w \tag{B.40}$$

$$v_s = v_s^* + (P_S' - P_P')d_s \tag{B.41}$$

where

$$d_w = \frac{A_w}{a_w} \tag{B.42}$$

$$d_s = \frac{A_s}{a_s} \tag{B.43}$$

Meanwhile, the expressions for the velocity components at four faces of a main control volume must satisfy the mass

conservation or continuity equation expressed by the following equation for the finite control volume shown in Figure (B.2),

$$[(\rho u)_e - (\rho u)_w] + [(\rho v)_n - (\rho v)_s] = 0 \qquad (B.44)$$

Notice that the above equation results from integration of equation (4.25) over the finite control volume. Substituting the expressions for the velocity components given by equations (B.38)-(B.41) into equation (B.44), one obtains the following after rearrangement,

$$a_P P'_P = a_E P'_E + a_W P'_W + a_N P'_N + a_S P'_S + b \qquad (B.45)$$

where

$$a_E = \rho_e d_e \Delta y \qquad (B.46a)$$

$$a_W = \rho_w d_w \Delta y \qquad (B.46b)$$

$$a_N = \rho_n d_n \Delta x \qquad (B.46c)$$

$$a_S = \rho_s d_s \Delta x \qquad (B.46d)$$

$$a_P = a_E + a_W + a_N + a_S \qquad (B.46e)$$

and

$$b = (\rho_w u^*_w - \rho_e u^*_e) + (\rho_s v^*_s - \rho_n v^*_n) \qquad (B.46f)$$

Note that the fluid density in the above equations is expressed at the control volume faces, which can be

interpolated from its grid point values if the density is not constant. Equation (B.45) is the discretized equation for the pressure correction field P', which can be solved numerically since its coefficients are based on the guessed (starred) velocity components. The resulting pressure correction field is then used to update values of pressure and velocity components according to equations (B.27), (B.38), and (B.39). The freshly calculated pressure field is then treated as a new guessed pressure field and the above steps and calculations are repeated until a converged solution is obtained. Note that the parameter b expressed by equation (B.46f) is a measure of satisfaction of the continuity equation by the starred velocity components. In other words, its value will be zero or more realistically close to zero (of the order of 10^{-7}) for each control volume in the calculation domain only when a converged flow field is obtained. Therefore, the change in maximum value of b within the calculation domain from one iteration to another is a measure of the convergance rate of the solution while, the absolute value of the maximum b value at the end of each iteration can be used as a convergance criteria.

In conclusion, the above procedure for calculating the flow field has been given the name SIMPLE, which stands for Semi-Implicit Method for Presuure-Linked Equations and consists of the following steps:

1. Start with a guessed pressure distribution.

2. Solve the momentum equations (B.25) and (B.26) to obtain u^* and v^*.

3. Solve the pressure correction equation (B.45) with the obtained u^* and v^* values.

4. Update the pressure and velocity values using equations (B.27), (B.38), and (B.39).

5. Treat the new pressure as a new guessed pressure and return to step 2 and repeat the whole procedure until a converged solution is obtained.

B.4.1 Calculation Procedure

As described in Chapter 4, the flow equations were subjected to periodic boundary conditions given by equations (4.29a) and (4.29b). Expressing these conditions in discretized form for the general variable ϕ results in the following equations,

$$\phi_{0,j} = \phi_{m-1,j} \qquad \text{(B.47a)}$$

$$\phi_{1,j} = \phi_{m,j} \qquad \text{(B.47b)}$$

$$\phi_{2,j} = \phi_{m+1,j} \qquad \text{(B.47c)}$$

where $\phi_{i,j}$ denotes value of ϕ at a grid point whose x- and y- coordinates in the calculation domain are signified by

integers i and j, and i = 1 and i = m refer to grid points located at the inflow and outflow boundaries, respectively. The point to be noticed in the above expressions is that the ϕ values at grid lines i = 0 and i = m+1, which are outside the calculation domain, are, respectively, equal to those at grid lines i = m-1 and i = 2, which are inside the calculation domain, based on the assumption that the flow field in each periodic module is identical. Thus, when the discretization equations are written for the inflow and outflow boundary grid points, the $\phi_{0,j}$ and $\phi_{m+1,j}$ quantities in those equations are replaced, respectively, by $\phi_{m-1,j}$ and $\phi_{2,j}$ to ensure that the discretized equations do not contain unknowns from region outside the calculation domain and the number of unknowns will be equal to the number of equations.

The resulting equations were solved by the Cyclic Tridiagonal Matrix Algorithm which is a special case of Guassian elimination technique. This method is especially well suited for solving algebraic equations subject to periodic conditions such as those considered in the present study. A detaile explanation of the algorithm is given by Ahlberg et al. (1967).

B.4.2 Calculation Program

The general computer program developed by

Patankar (1980) for numerical solution of the differential equations which are similar to or a form of the general differential equation given by equation (B.1), can be basically divided into two major parts referred to as Main and User.

The Main part of the program, in general, deals with calculation of the coefficients of discretized equations for all the dependent variables under consideration and contains also a numerical algorithm for solving the equations. This part of the program is written in a general form meaning that it can be applied to all the problems whose unknown dependent variables satisfy equation (B.1) or a form of it.

On the other hand, the User part of the program is problem-dependent and designed to convey the necessary information specific to a given problem to the Main part. A copy of the user's program developed for the present study of fluid flow in a staggered array of cylinders or rectangles is included at the end of the appendix. It basically consists of six subroutines containing specific type of information about the problem under consideration. The subroutine names in the order by which they are called by the Main program are GRID, START, DENSE, BOUND, OUTPUT, and GAMSOR. A brief description of the type of information being supplied to each subroutine is as follows:

GRID : This is the first subroutine called by the Main program. As the name implies, it must contain information about the grid layout in the calculation domain, such as number and location of grid points and their surrounding control volume faces as well as dimensions of the domain and type of coordinate system considered appropriate for the problem under consideration. The latter is specified by choosing one of the following values for the variable MODE,

MODE = 1	Cartesian Coordinate System
MODE = 2	Axisymmetric Coordinate System
MODE = 3	Polar Coordinate System

Except for MODE = 1, the radius associated with the bottom boundary of the domain must also be specified in this subroutine. The Main program is capable of calculating the coefficients of discretized equations in each of the above coordinate systems.

START : The initial or guess values for all unknown dependent variables as well as boundary conditions associated with the problem under consideration are given in this subroutine.

DENSE : When dealing with problems involving fluid flow,

this subroutine calculates the fluid density if it happens to be a function of one of the dependent variables of the problem and thus, its values in the domain must be updated from one iteration to the next. But if the density is constant, its value can be given in the subroutine START and leave this subroutine empty.

BOUND : Any work related to the boundary conditions such as calculating heat or mass flux through bondaries is performed in this subroutine.

OUTPUT : This subroutine can be used to display value of any of the dependent variables at the end of each iteartion to check the convergance behavior of the solution. Also, a full two dimensional display of values of each variable can be obtained by calling subroutine PRINT which is part of the MAIN program.

GAMSOR : This subroutine supplies to the MAIN program the values of Γ, S_C , and S_P for each dependent variable considered. The Γ values are specified at all grid points including those at the boundaries while, the S_C and S_P values are specified only for the internal grids.

For a specified number of iterations, the subroutines GRID

and START are called only once while, the subroutines DENSE, BOUND, and OUTPUT are called once per iteration by the MAIN program. The subroutine GAMSOR, however, is called at least once per iteration depending on the dependent variable. A list of major variables employed in the USER program along with their definition precedes the program listing.

List of Fortran Variables in the Flow Field USER program

ALPHA	Solid-volume fraction
AMU	Fluid viscosity
AMWALL	Viscosity of fiber (Very large number)
AN	Step angle
CON(I,J)	The constant term b in the discretization equation; also stands for S_C in GAMSOR
DH	Hydraulic diameter
DPDX	Stands for $\hat{\beta}$ in the flow equations
GAM(I,J)	Denotes fluid or fiber viscosity in the calculation domain
I	Index denoting the position in x
ITER	A counter for iterations
J	Index denoting position in Y
LAST	Maximum number of iterations allowed by the user
LBLK	When .TRUE., activates the block correction subprogram in the MAIN program
LINPUT	When .TRUE., Values of the desired variable are inputted to the program
LPRINT	When .TRUE., prints the desired variable
LSOLVE	When .TRUE. solves for the desired variable
LSTOP	When .TRUE., Computation stops
L1	Value of I for the last grid location in the x direction

L2	L1 - 1
L3	L2 - 1
MODE	Index for the coordinate system
M1	Value of J for the last grid location in the y direction
M2	M1 - 1
M3	M2 - 1
NF	Index denoting a particular variable
RE	Reynolds number
RELAX	Relaxation factor
RHO(I,J)	Density ρ
RHOCON	Value of ρ for a constant-density problem
RNR	Value of interception parameter
RP	Particle Radius
SMAX	The largest absolute value of the "mass source" in the p' equation
SSUM	Algebraic sum of all "mass sources" in the p' equation
TITLE	Alphanumeric title of the desired variable
U(I,J)	x-direction velocity u
UBAR	Average u velocity at the domain entrance
V(I,J)	y-direction velocity v
WIDTH	Half width of rectangular fiber
X(I)	Value of x at grid points
XCV(I)	x-direction widths of main control volumes

XDIF(I)	Difference X(I) - X(I-1)
XL	x-direction length of the calculation domain
XL1	Distance between entrance of the domain and center of the rectangular fiber in the domain
XLENGTH	Length of the rectangular fiber in the calculation domain
XU(I)	Locations of the control volume faces in the x-direction
Y(J)	Values of y at grid points
YCV(J)	y-direction widths of main control volumes
YDIF(J)	Difference Y(J) - Y(J-1)
YL	y-direction length of the calculation domain
YV(J)	Locations of the control volume faces

```
      SUBROUTINE USER
C*****************************************************************
C
C
C              ___________________________________
C             I                                   I
C             I                                   I
C             I                                   I
C             I          ____________             I
C             I         I            I            I
C              ___________________________________
C
C
C*****************************************************************
      IMPLICIT DOUBLE PRECISION (A-H),(O-Z)
      CHARACTER*40 INPUTF,SAVEF,LISFIL,DUMMY,GIVEFIL
      PARAMETER (ID=55,JD=55,IMX=64)
      PARAMETER (LIV=4)
      PARAMETER (LV=LIV+3)
      COMMON/FILE/INPUTF,SAVEF,LISFIL
      LOGICAL  LSOLVE,LPRINT,LBLK,LSTOP,LINPUT,LSAVE,LCHECK
      COMMON F(ID,JD,LV),CON(ID,JD),
     1 AIP(ID,JD),AIM(ID,JD),AJP(ID,JD),AJM(ID,JD),AP(ID,JD),
     2 X(ID),XU(ID),XDIF(ID),XCV(ID),XCVS(ID),
     3 Y(JD),YV(JD),YDIF(JD),YCV(JD),YCVS(JD),
     4 YCVR(JD),YCVRS(JD),ARX(JD),ARXJ(JD),ARXJP(JD),
     5 R(JD),RMN(JD),SX(JD),SXMN(JD),XCVI(ID),XCVIP(ID)
      COMMON  DU(ID,JD),DV(ID,JD),  FV(JD),FVP(JD),
     1 FX(ID),FXM(ID),FY(JD),FYM(JD),PT(IMX),QT(IMX)
      COMMON/INDX/NF,NFMAX,NP,NRHO,NGAM,L1,L2,L3,M1,M2,M3,
     +  XP,YP,LP,MP,Z,DZ,LL,LR,LM,LC,
     1 IST,JST,ITER,LAST,TITLE(LV),RELAX(LV),TIME,DT,XL,YL,
     2 IPREF,JPREF,LSOLVE(LV),LPRINT(LV),MODE,NTIMES(LV),GVAR,
     3 RHOCON,LINPUT(LV),LSAVE(LV),LBLK(LV)
      COMMON/CNTL/LSTOP,LCHECK
      COMMON/SORC/SMAX,SSUM
      COMMON/COEF/FLOW,DIFF,ACOF
      DIMENSION U(ID,JD),V(ID,JD),PC(ID,JD)
      DIMENSION P(ID,JD),RHO(ID,JD),GAM(ID,JD)
      EQUIVALENCE(F(1,1,LIV+1),P(1,1)),(F(1,1,LIV+2),RHO(1,1)),
     1 (F(1,1,LIV+3),GAM(1,1))
      EQUIVALENCE(F(1,1,1),U(1,1)),(F(1,1,2),V(1,1)),(F(1,1,3),PC(1,1))
      DIMENSION TH(ID),THU(ID),THDIF(ID),THCV(ID),THCVS(ID)
      EQUIVALENCE(X,TH),(XU,THU),(XDIF,THDIF),(XCV,THCV)
     1  ,(XCVS,THCVS),(XL,THL)
C*****************************************************************
C
C_____________ FILTER FLOW FIELD CALCULATION  _____________
C_____________ RECTANGULAR GEOMETRY _____________
C*****************************************************************
      DATA TITLE(1),TITLE(2),TITLE(3),TITLE(LIV+1)
     1   /7H  VEL U,7H  VEL V,7H STR FN,8HPRESSURE/
      DATA LSAVE(1),LSAVE(2),LSAVE(LIV+1)/3*.TRUE./
      DATA LINPUT(1),LINPUT(2),LINPUT(LIV+1)/3*.TRUE./
      DATA (LSOLVE(I),I=1,3),LSOLVE(5)/4*.TRUE./
      DATA LBLK(1),LBLK(2),LBLK(3)/3*.TRUE./
      DATA LAST/10/
      DATA RHOCON/1.206/

C*****START OF SUBROUTINE 'GRID' FOR SPECIFYING LOCATION OF CONTROL
C*****VOLUME FACES AND GRID POINTS
C
      ENTRY GRID
C
C     THIS PROGRAM SOLVES A NUMBER OF DIFFERENT CASES AS LONG AS
C     THEIR CORRESPONDING FILE NAMES ARE GIVEN IN 'FILNAME.DAT' BELOW.
C     EACH FILE CONSISTS OF NAMES OF THE INPUT,SAVE,AND OUTPUT
C     FILES,AND THE VALUES OF THE DIFFERENT PARAMETERS AS REQUIRED
C     BELOW.
C
      OPEN (UNIT=7,FILE='FILNAME.DAT',STATUS='OLD')
      READ(7,640,END=598)GIVEFIL
  640 FORMAT(A40)
      GO TO 597
  597 OPEN (UNIT=8,FILE=GIVEFIL,STATUS='OLD')
      READ(8,610)INPUTF
  610 FORMAT(A40)
      READ(8,610)SAVEF
      READ(8,610)LISFIL
C     ENTER LENGTH OF CALCULATION DOMAIN, XL
      READ(8,*)XL
C      ENTER WIDTH OF CALCULATION DOMAIN, YL :
      READ(8,*)YL
C      ENTER HALF OF WIDTH OF WHOLE RECTANGLE :
      READ(8,*)WIDTH
C      ENTER LENGTH OF WHOLE RECTANGLE :
      READ(8,*)XLENGTH
C      ENTER INTERCEPTION PARAMETER :
      READ (8,*) RNR
```

```
C      DOMAIN AND CENTER OF RECTANGLE)
       READ(8,*)XL1
C       ENTER VALUE OF DPDX :
       READ(8,*)DPDX
C      RELAXATION FACTOR TO CONTROL CONVERGANCE RATE
       READ(8,*)RELAX(1),RELAX(2),RELAX(LIV+1)
C       ENTER THE NUMBER OF ITERATIONS :
       READ(8,*)LAST
C       START FROM STORED FILE ? YES=1 '
       READ(8,*)IINPUT
C       WISH TO PRINT U,V,SF,P DISTRIBUTIONS ? YES=1 '
       READ(8,*)IPRINT
C
CALCULATE HYDRAULIC DIAMETER OF RECTANGLE AND INTERCEPTION
C      WIDTH ACCORDING TO VALUE OF RNR
C
       DH=(4.0*WIDTH*XLENGTH)/(2.*WIDTH+XLENGTH)
       RH=DH/2.
       RP=RNR*WIDTH
       PI=3.1415926
       RAD=PI/180.0
       AN=11.25*RAD
       RR=XLENGTH/2.
C
       XU(2)=0.0
       MULX=3
       XX=RR+RP
       XR=XL1-XX-0.050
       IB=7
       DO 10 I=3,IB
  10   XU(I)=XU(I-1)+XR/(IB-2)
       DX=0.01
       IF (MULX.NE.0) THEN
       DO 1000 I=1,MULX
 1000  XU(IB+I)=XL1-XX-(MULX-I+1)*DX
       ENDIF
       IPP=IB+MULX+1
       XU(IPP)=XL1-XX
C
       IF (RP.EQ.0.0) THEN
       GO TO 13
       ENDIF
       IBEG=IB+MULX+1
C
       ICON=2*IBEG-1
       IP=0
       DO 1001 I=IBEG,IBEG+3
       I1=2*I-ICON
       IP=IP+1
       IF (I.EQ.IBEG) IP=I+1
       XU(IP)=(XL1-RR)-RP*COS(I1*AN)
 1001  CONTINUE
       IPP=IP+1
       XU(IPP)=XL1-RR
  13   CONTINUE
       DO 12 I=IPP+1,IPP+6
       XU(I)=XU(I-1)+RR/7.0
       IP=I
  12   CONTINUE
       DO 14 I=1,IP-2
       IPP=I+IP
       XU(IPP)=XL1-XU(IP+1-I)+XL1
  14   CONTINUE
       L1=IPP+1
       XU(L1)=XL
       DX1=XL1-RR
       DX2=XL1+RR
C
C      THIS LOOP DETERMINES THE 'I' VALUE CORRESPONDING TO
C      BEGINNING AND END LOCATIONS OF THE
C      SOLID RECTANGLE FOR LATER USE IN GAMSOR WHERE A LARGE GAMMA
C      IS ASSIGNED TO THE SOLID DOMAIN.
C
       DO 22 I=IB,L1
       IF ((XU(I)-DX1).LE.0.00000001) IBGAM=I
       IF ((XU(I)-DX2).LE.0.00000001) IEGAM=I-1
  22   CONTINUE
C
C      SPECIFY C.V. FACES IN THE Y- DIRECTION
C
       YV(2)=0.0
       JE=7
       DO 15 J=3,JE
       YV(J)=YV(J-1)+WIDTH/5.0
  15   CONTINUE
       MULY=0
       DY=0.01
```

```
      IF (MULY.NE.0) THEN
      DO 16 J=1,MULY
   16 YV(JE+J)=WIDTH+J*DY
      ENDIF
      JDD=JE+MULY+1
      YV(JDD)=WIDTH+0.050
      GO TO 25
      ENDIF
C
      JP=0
      DO 1003 J=1,4
C      DO 1003 J=1,3
      JP=JP+1
      IF (J.EQ.1) JP=JE+1
      YV(JP)=WIDTH+RP*SIN(2*J*AN)
 1003 CONTINUE
   26 CONTINUE
      IF (MULY.NE.0) THEN
      DO 1002 J=JP+1,JP+MULY
      YV(J)=YV(J-1)+DY
 1002 CONTINUE
      ENDIF
      JDD=JP+MULY+1
      YV(JDD)=YV(JP)+0.050
   25 CONTINUE
C
      DYY=(YL/2.)-YV(JDD)
      DO 17 J=JDD+1,JDD+3
      YV(J)=YV(J-1)+DYY/3.
      JPP=J
   17 CONTINUE
      YHAF=YL/2.
      DO 18 J=1,JPP-3
      JP=JPP+J
      YV(JP)=(YHAF-YV(JPP-J))+YHAF
   18 CONTINUE
      M1=JP+1
      YV(M1)=YL
  705 CONTINUE
C
      IF(IPRINT.EQ.1) THEN
      LPRINT(1)=.TRUE.
      LPRINT(2)=.TRUE.
      LPRINT(3)=.TRUE.
      LPRINT(5)=.TRUE.
      ENDIF
      RETURN
C
C     START OF SUBROUTINE 'START' FOR INITIALIZING VARIABLES
C
      ENTRY START
      IF(IINPUT.EQ.1) CALL INPUT
  120 AMU=18.30
      AMWALL=1.0D+15
      ALPHA=WIDTH*XLENGTH/(XL*YL)
      RETURN
C
C     SUBROUTINE 'DENSE' DEALS WITH VARIABLE DENSITY PROBLEMS
C
      ENTRY DENSE
      RETURN
C
C     SUBROUTINE 'BOUND' DEALS WITH BOUNDARY CONDITIONS
C
      ENTRY BOUND
      USUM=0.0
CALCULATE MEAN VELOCITY AT THE DOMAIN ENTRANCE
C
      DO 200 J=2,M2
  200 USUM=USUM+U(2,J)*YCV(J)
      UBAR=USUM/YL
CALCULATE REYNOLDS NUMBER
C
      RE=RHOCON*UBAR*DH/AMU
      RETURN
C
C     SUBROUTINE 'OUTPUT' LISTS THE RESULTS OF CALCULATIONS
C
      ENTRY OUTPUT
      IF(ITER.NE.0) GO TO 400
      WRITE(1,421)
C      PRINT 421
      WRITE(1,408)INPUTF,SAVEF,LISFIL
C      PRINT 408,INPUTF,SAVEF,LISFIL
      WRITE(1,409)(I,RELAX(I),I=1,3)
C      PRINT 409,(I,RELAX(I),I=1,3)
      WRITE(1,410)DPDX
```

```
      WRITE(1,422)XL,YL,ALPHA
C      PRINT 422,XL,YL,ALPHA
      WRITE(1,423)WIDTH,XLENGTH
C      PRINT 423,WIDTH,XLENGTH
C      PRINT 401
      WRITE(1,482) RP
      WRITE(1,401)
  400 WRITE(1,403),ITER,SMAX,SSUM,U(14,7),V(14,7),RE
C      PRINT 403,ITER,SMAX,SSUM,U(14,7),V(14,7),RE
C  400 WRITE(1,463)ITER,T(2,3),T(4,5),T(10,10),T(6,8),T(12,12)
C  463 FORMAT(I5,1P5E15.3)
  401 FORMAT(//,'  ITER',7X,'SMAX',11X,'SSUM',10X,'U(14,7)',
     1 8X,'V(14,7)',5X,' RE#')
C  401 FORMAT(//,'  ITER',7X,'T(2,3)',10X,'T(4,5)',8X,'T(10,10)'
C     +       ,6X,'T(6,8)',5X,'T(12,12)')
  403 FORMAT(I5,1P5E15.3)
  408 FORMAT(//,2X,'INPUT DATA FILE :',A40,/,2X,'OUTPUT
     +DATA FILE :',A40,/,2X,'LIST FILE :',A40)
  409 FORMAT(/,(2X,'RELAX(',I2,') :'F5.2))
  410 FORMAT(/,2X,'DPDX :'F10.2,/)
  421 FORMAT(/,30X,'RECTANGULAR GEOMETRY')
  422 FORMAT(/,2X,'XL=',F6.2,5X,'YL=',F6.2,5X,'ALPHA=',F8.4)
  482 FORMAT(/,2X,'PARTICLE RADIUS : ',E10.5)
  423 FORMAT(/,2X,'HALF OF WIDTH OF RECTANGLE :',F10.5,/,2X,
     +       'LENGTH OF RECTANGLE :'F10.5)
      IF(ITER.EQ.LAST) THEN
         CALL PRINT
         CALL SAVE
      ENDIF
      RETURN
C
C     SUBROUTINE 'GAMSOR' PROVIDES INFORMATION ABOUT THE DIFFUSION
C     COEFFICIENT DISTRIBUTION FUNCTION IN THE CALCULATION DOMAIN
C
      ENTRY GAMSOR
C
C     NF=1 DENOTES U, NF=2 DENOTES V AND NF=3 DENOTES PRESSURE
C     CORRECTION FUNCTION
C
      IF(NF.EQ.3) RETURN
      DO 500 J=1,M1
      DO 500 I=1,L1
      GAM(I,J)=AMU
  500 CONTINUE
      IF(NF.EQ.1)THEN
C
C     THE FLOW IS SYMMETRIC WITH RESPECT TO U COMPONENT OF THE
C     VELOCITY AT THE TOP AND THE BOTTOM BOUNDARIES.
C
      DO 506 I=1,L1
      GAM(I,1)=0.
      GAM(I,M1)=0.
      DO 506 J=1,M1
      CON(I,J)=DPDX
  506 CONTINUE
      ENDIF
C
C     THE SOLID REGION GAMMA VALUES ARE ASSIGNED HERE.
C
      DO 60 J=1,JE-1
      DO 60 I=IBGAM,IEGAM
   60 GAM(I,J)=AMWALL
  708 CONTINUE
      RETURN
      END
```

APPENDIX C

Numerical Solution of the Convective-Diffusion Equation

The differential equation expressing the balance between the convection and diffusion rate of particles into and out of an infinitesimal control volume as given by equation (4.76) is a particular form of the general two dimensional convective-diffusion equation (equation (B.20)) with the general variable ϕ being equal to the particle concentration, N, and the source term, S, being equal to zero.

The procedure for numerical solution of equation (4.76) as described in detail in Appendix B, is summerized as follows: a calculation domain with known boundary conditions is first chosen around the fiber toward which the diffusion rate of particles is to be determined. The domain is then divided into a finite number of control volumes, each enclosing a grid point at its center. Equation (4.76) is then integrated over each control volume, assuming a profile for variation of N between adjacent grid points, to yield a finite number of algebraic equations containing unknown values of N at grid points. Subsequently, these equations are solved to obtain the distribution of particle

concentration in the domain for the specified boundary conditions and thus, determine the diffusion rate of particles towards the fiber.

Similar to the case of momentum equations, the calculation program for determining coefficients of the algebraic equations and their subsequent solution is composed of two major parts, MAIN and USER, as explained previously in Appendix B.

The formulation of coefficients and the solution algorithm in the MAIN program corresponding to the present calculations are slightly different from those in the MAIN program corresponding to the calculation of the flow equations since the periodicity conditions were not applied to the particle concentration values at the inflow and outflow boundaries of the domain.

The USER program developed for providing information about the boundary conditions and other necessary known parameters to the MAIN program basically consists of six subroutines called GRID, START, DENSE, BOUND, OUTPUT, and GAMSOR, each explained previously in Appendix B. A printout of the USER program for calculation of particle concentration along with a list of its major variables in addition to those listed in Appendix B is enclosed at the end.

It should be mentioned that since, the previoussly

calculated velocity components must be used in achieving a numerical solution to eqaution (4.76), the domain considered for calculation of the particle concentration for a given fiber aspect ratio and solid-volume fraction must be identical to that used for the flow calculations corresponding to the same parameters. Therefore, the infomation about the size of the domain around a given rectangular fiber and number and location of control volumes within the domain as specified in the subroutine GRID is the same as that provided to the flow calculation program for similar fiber aspect ratio and solid-volume fraction values.

The previously calculated velocity components are read into the program in the subroutine START where the particle concentration variable CCON(I,J) is initialized to zero everywhere in the domain except at the entrance where a value of 1 is assumed for the incoming particle concentration. The values of other relevant parameters are specified also in this subroutine.

The subroutine DENSE which deals with variation of the fluid density is left empty since it does not play a role in the present calculations.

The next two subroutines, BOUND and OUTPUT, deal with boundary conditions and printing out of the results, respectively.

Finally, in the last subroutine, GAMSOR, the value of

the diffusion coefficient of particles, DIFCOF, is assigned to the grid points. Note that the diffusion coefficient at the outflow boundary (I = L1) is set equal to zero in response to the absence of information about the particle concentration at that boundary. Such action, in effect, eliminates the influence of unknown conditions at the outflow boundary on the rest of the domain if the boundary does not cross any flow-recirculation region. This, according to Patankar (1980), is the price that one has to pay in order to obtain a solution despite of unknown outflow boundary conditions. Such consideration is perhaps a good approximation to the real case when dealing with large Peclet numbers, but in the case of relatively small values of the Pectlet number, the above consideration will generate some error in the calculated values of particle concentration. It is assumed here, however, that the effect of such error on the calculated values of the single fiber efficiency is minimal as one deals with the concentration gradients and fraction of number of particles captured.

List of Major Variables in the Particle

Concentration USER program

ANO	Particle concentration value at the domain entrance
RHOAIR	Air viscosity
CCON(I,J)	Particle concentration variable
DIFCOF	Diffusion coefficient of particles
PE	Peclet number
WALDIF	Diffusion coefficient within fiber (very large)

```
      SUBROUTINE USER
C*****************************************************************
C
C     THIS PROGRAM CALCULATES THE DIFFUSION RATE OF POINT-LIKE
C     PARTICLES TOWARD SURFACE OF A RECTANGULAR FIBER.
C     THE FLOW FIELD (U AND V COMP. OF VELOCITY) HAS
C     BEEN DETERMINED ALREADY AND IS INPUTTED TO THIS PROGRAM.
C
C
C              ___________________________________
C             I                                   I
C             I                                   I
C             I                                   I
C             I          ___________              I
C             I         I           I             I
C             I_________I           I_____________I
C
C
C*****************************************************************
      IMPLICIT DOUBLE PRECISION (A-H),(O-Z)
      CHARACTER*40 INPUTF,SAVEF,LISFIL,DUMMY,GIVEFIL
      PARAMETER (ID=55,JD=55,IMX=64)
      PARAMETER (LIV=4)
      PARAMETER (LV=LIV+3)
      COMMON/FILE/INPUTF,SAVEF,LISFIL
      LOGICAL  LSOLVE,LPRINT,LBLK,LSTOP,LINPUT,LSAVE,LCHECK
      COMMON F(ID,JD,LV),CON(ID,JD),
     1 AIP(ID,JD),AIM(ID,JD),AJP(ID,JD),AJM(ID,JD),AP(ID,JD),
     2 X(ID),XU(ID),XDIF(ID),XCV(ID),XCVS(ID),
     3 Y(JD),YV(JD),YDIF(JD),YCV(JD),YCVS(JD),
     4 YCVR(JD),YCVRS(JD),ARX(JD),ARXJ(JD),ARXJP(JD),
     5 R(JD),RMN(JD),SX(JD),SXMN(JD),XCVI(ID),XCVIP(ID)
      COMMON  DU(ID,JD),DV(ID,JD),  FV(JD),FVP(JD),
     1 FX(ID),FXM(ID),FY(JD),FYM(JD),PT(IMX),QT(IMX)
      COMMON/INDX/NF,NFMAX,NP,NRHO,NGAM,L1,L2,L3,M1,M2,M3,
     1 IST,JST,ITER,LAST,TITLE(LV),RELAX(LV),TIME,DT,XL,YL,
     2 IPREF,JPREF,LSOLVE(LIV),LPRINT(LV),LBLK(LIV),MODE,NTIMES(LIV),
     3 RHOCON,LINPUT(LV),LSAVE(LV)
      COMMON/CNTL/LSTOP,LCHECK
      COMMON/SORC/SMAX,SSUM
      COMMON/COEF/FLOW,DIFF,ACOF
      DIMENSION U(ID,JD),V(ID,JD),PC(ID,JD)
      DIMENSION P(ID,JD),RHO(ID,JD),GAM(ID,JD)
      EQUIVALENCE(F(1,1,LIV+1),P(1,1)),(F(1,1,LIV+2),RHO(1,1)),
     1 (F(1,1,LIV+3),GAM(1,1))
      EQUIVALENCE(F(1,1,1),U(1,1)),(F(1,1,2),V(1,1)),(F(1,1,3),PC(1,1))
      DIMENSION TH(ID),THU(ID),THDIF(ID),THCV(ID),THCVS(ID)
      EQUIVALENCE(X,TH),(XU,THU),(XDIF,THDIF),(XCV,THCV)
     1   ,(XCVS,THCVS),(XL,THL)
C*****************************************************************
C
C---------------- DIFFUSION FLUX CALCULATION  ----------------
C_________________ RECTANGULAR GEOMETRY _____________________
C*****************************************************************
      DIMENSION CCON(ID,JD)
      EQUIVALENCE (F(1,1,4),CCON(1,1))
      DATA TITLE(1),TITLE(2),TITLE(4)
     1   /7H  VEL U,7H  VEL V,7H CONCN./
C
C     START OF SUBROUTINE 'GRID' FOR SPECIFYING LOCATION OF
C     CONTROL VOLUMES AND GRID POINTS
C
      ENTRY GRID
C
C     LINPUT(1) AND LINPUT(2) CORRESPOND TO U AND V VELOCITIES
C
      LINPUT(1)=.TRUE.
      LINPUT(2)=.TRUE.
C
C     LSOLVE(4) CORRESPONDS TO PARTICLE CONCENTRATION
C
      LSOLVE(4)=.TRUE.
      LBLK(4)=.TRUE.
      LPRINT(4)=.TRUE.
C
 597  OPEN (UNIT=8,FILE='RECDIF.D',STATUS='OLD')
C
C     ENTER LENGTH OF CALCULATION DOMAIN, XL
      READ(8,*)XL
C     ENTER WIDTH OF CALCULATION DOMAIN, YL :'
      READ(8,*)YL
C      ENTER HALF OF WIDTH OF WHOLE RECTANGLE :'
      READ(8,*)WIDTH
C      ENTER LENGTH OF WHOLE RECTANGLE :'
      READ(8,*)XLENGTH
C      ENTER VALUE OF XL1 (DISTANCE BETWEEN DOMAIN ENTRY AND
C      CENTER OF RECTANGLE) :'
      READ(8,*)XL1
```

```
      READ(8,*) DIFCOF
C      ENTER THE NUMBER OF ITERATIONS :'
      READ(8,*)LAST
C      WISH TO PRINT U,V DISTRIBUTIONS ? YES=1 '
      READ(8,*)IPRINT
C
CALCULATE HYDRUALIC DIAMETER
C
      DH=(4.0*WIDTH*XLENGTH)/(2.0*WIDTH+XLENGTH)
      RR=XLENGTH/2.
      RP=0.0
C
      XU(2)=0.0
      MULX=3
      XX=RR+RP
      XR=XL1-XX-0.050
      IB=7
      DO 10 I=3,IB
   10 XU(I)=XU(I-1)+XR/(IB-2)
      DX=0.01
      IF (MULX.NE.0) THEN
      DO 1000 I=1,MULX
      XU(IB+I)=XL1-XX-(MULX-I+1)*DX
 1000 CONTINUE
      ENDIF
      IPP=IB+MULX+1
      XU(IPP)=XL1-XX
C
   13 CONTINUE
      DO 12 I=IPP+1,IPP+6
      XU(I)=XU(I-1)+RR/7.0
      IP=I
   12 CONTINUE
      DO 14 I=1,IP-2
      IPP=I+IP
      XU(IPP)=XL1-XU(IP+1-I)+XL1
   14 CONTINUE
      L1=IPP+1
      XU(L1)=XL
      DX1=XL1-(RR+RP)
      DX2=XL1+(RR+RP)
C
C     THIS LOOP DETERMINES THE 'I' BEGIN AND END LOCATIONS OF THE
C     SOLID RECTANGLE FOR LATER USE IN GAMSOR WHERE A LARGE GAMMA
C     IS ASSIGNED TO THE SOLID DOMAIN.
C
      DO 22 I=IB,L1
      IF ((XU(I)-DX1).LE.0.00000001) IBGAM=I
      IF ((XU(I)-DX2).LE.0.00000001) IEGAM=I
   22 CONTINUE
C
C     SPECIFY C.V. FACES IN THE Y- DIRECTION
C
      YV(2)=0.0
      JE=7
      DO 15 J=3,JE
      YV(J)=YV(J-1)+WIDTH/5.0
   15 CONTINUE
C
      MULY=3
      DY=0.01
      IF (MULY.NE.0) THEN
      DO 16 J=1,MULY
   16 YV(JE+J)=WIDTH+J*DY
      ENDIF
      JDD=JE+MULY+1
      YV(JDD)=WIDTH+0.050
      GO TO 25
      ENDIF
C
   25 CONTINUE
      DYY=(YL/2.)-YV(JDD)
      DO 17 J=JDD+1,JDD+3
      YV(J)=YV(J-1)+DYY/3.
      JPP=J
   17 CONTINUE
      YHAF=YL/2.
      DO 18 J=1,JPP-3
      JP=JPP+J
      YV(JP)=(YHAF-YV(JPP-J))+YHAF
   18 CONTINUE
      M1=JP+1
      YV(M1)=YL
C
      IF(IPRINT.EQ.1) THEN
      LPRINT(1)=.TRUE.
      LPRINT(2)=.TRUE.
```

```
      RETURN
C
C     SUBROUTINE 'START' FOR INITIALIZING VARIABLES
C
      ENTRY START
      CALL INPUT
C     ANO IS THE INCOMING PARTICLE CONCENTRATION
C
      ANO=1.
      AMU=18.38
      RHOAIR=1.206
      WALDIF=1.0E30
      ALPHA=WIDTH*XLENGTH/(XL*YL)
      USUM=0.0
      DO 74 J=2,M2
 74   USUM=USUM+U(2,J)*ARX(J)
      UAVG=USUM/YL
C
CALCULATE REYNOLDS AND PECLET NUMBERS
C
      RE=RHOAIR*UAVG*DH/AMU
      PE=DH*UAVG/(DIFCOF+1.0E-15)
      DO 100 J=1,M1
      CCON(1,J)=ANO
      DO 99 I=2,L1
      CCON(I,J)=0.0
  99  CONTINUE
 100  CONTINUE
      RETURN
C
C     SUBROUTINE 'DENSE' DEALS WITH VARIABLE DENSITY PROBLEMS
C
      ENTRY DENSE
      RETURN
C
C     SUBROUTINE 'BOUND' DEALS WITH MODIFICATIONS OF OR CALCULATION
C     AT THE BOUNDARIES OF DOMAIN
C
      ENTRY BOUND
      RETURN
C
C     SUBROUTINE 'OUTPUT' LIST THE RESULTS
C
      ENTRY OUTPUT
      IF(ITER.NE.0) GO TO 400
      WRITE(1,421)
C      PRINT 421
      WRITE(1,408)INPUTF,SAVEF,LISFIL
C      PRINT 408,INPUTF,SAVEF,LISFIL
      WRITE(1,422)XL,YL,ALPHA
C      PRINT 422,XL,YL,ALPHA
      WRITE(1,423)WIDTH,XLENGTH
C      PRINT 423,WIDTH,XLENGTH
      WRITE (1,482)RP
C     PRINT 482,RP
      WRITE (1,424) RE,PE
C     PRINT 424,RE,PE
C      PRINT 401
      WRITE(1,401)
 400  WRITE(1,403),ITER,CCON(4,5),CCON(10,10),CCON(14,7)
C      PRINT 403,ITER,CCON(4,5),CCON(10,10),CCON(14,7)
 401  FORMAT(//,'  ITER',8X,'C(4,5)',7X,'C(10,10)',8X,'C(14,7)')
 403  FORMAT(I5,1P3E15.3)
 408  FORMAT(//,2X,'INPUT DATA FILE :',A40,/,2X,'OUTPUT
     +DATA FILE :',A40,/,2X,'LIST FILE :',A40)
 421  FORMAT(/,30X,'RECTANGULAR GEOMETRY')
 422  FORMAT(/,2X,'XL=',F6.2,5X,'YL=',F6.2,5X,'ALPHA=',F8.4)
 482  FORMAT(/,2X,'PARTICLE RADIUS : ',E10.5)
 423  FORMAT(/,2X,'HALF OF WIDTH OF RECTANGLE :',F10.5,/,2X,
     +       'LENGTH OF RECTANGLE :'F10.5)
 424  FORMAT(//,'  RE # =',E10.5,/,'  PE # =',E10.5)
      IF(ITER.EQ.LAST) THEN
         CALL PRINT
C         CALL SAVE
      ENDIF
      RETURN
C
C     SUBROUTINE 'GAMSOR' DEALS WITH SPECIFICATION OF DIFFUSION
C     COEFFICIENT AND SOURCE TERM AT GRID POINTS
C
      ENTRY GAMSOR
      DO 500 J=1,M1
      DO 500 I=1,L1
      GAM(I,J)=DIFCOF
 500  CONTINUE
C
C     DUE TO SYMMETRY CONDITIONS AT THE TOP AND BOTTOM
```

```
C
      DO 506 I=1,L1
      GAM(I,1)=0.
      GAM(I,M1)=0.
  506 CONTINUE
C
C     DUE TO ABSENCE OF INFORMATION AT THE DOMAIN OUTFLOW
C     BOUNDARY:
C
      DO 502 J=2,M2
  502 GAM(L1,J)=0.0
C
C     THE SOLID REGION GAMMA VALUES ARE ASSIGNED HERE.
C
      IF (RP.EQ.0.0) THEN
      DO 60 J=1,JE-1
      DO 60 I=IBGAM,IEGAM-1
   60 GAM(I,J)=WALDIF
      RETURN
      ENDIF
C
      IF (LCHOCE.EQ.0) THEN
      DO 1006 I=IBGAM,IEGAM-1
      DO 1006 J=1,JEND-1
      GAM(I,J)=WALDIF
 1006 CONTINUE
      RETURN
      ENDIF
C
      DO 800 I=IBGAM,IEGAM-1
      DO 800 J=1,JE
  800 GAM(I,J)=WALDIF
      ISTRT=IBGAM
      IFINSH=IEGAM-1
      DO 801 J=JE,JEND-1
      ISTRT=ISTRT+1
      IFINSH=IFINSH-1
      DO 802 I=ISTRT,IFINSH
      GAM(I,J)=WALDIF
  802 CONTINUE
  801 CONTINUE
      RETURN
      END
```

APPENDIX D

Particle Trajectory Calculation Program

The trajectory equations governing the behavior of a particle subject to electrostatic forces in a viscous flow around a rectangular fiber were derived in section 4.8.3. To integrate those equations in order to determine the particle position at any time during its travel in the calculation domain, a computer program was developed to perform the integrations using the Runge-Kutta method. A listing of the program is enclosed at the end of the appendix.

Prior to describing the program, a few words about the region around the fiber under consideration, within which the particle trajectories are to be determined are in order. This region or domain could be of any reasonable size and shape if the fluid flow in the domain could be expressed analytically. But since, the fluid velocity components in the case of viscous flow around a rectangular fiber are only available in discrete form at certain locations around the fiber (control volume faces), as obtained previously in this study, the domain considered for the trajectory calculations must be identical to that used for the flow field calculations including the same control volume layout so that the previously calculated fluid velocity components corresponding to a given fiber aspect ratio and solid-volume

fraction can be used.

The trajectory program basically consists of two main subroutines named GRID which deals with setting up the calculation domain and IMPINGE which integrates the trajectory eqautions in that domain.

In the subroutine GRID, the program user should specify the dimensions of the calculation domain and rectangular fiber according to the desired values of b/w and α, number and distribution of grid points, computer file name containing the previously calculated values of the fluid velocity components corresponding to the specified values of b/w and α, type of electrostatic interaction, Coulombic or inductive, and value of the corresponding dimensionless electrostatic force parameter N_C or N_I. The computer then calculates the x- and y- locations of the control volume faces according to the user's specifications so that the resulting control volume distribution is identical to that used for the flow field calculations corresponding to the given values of b/w and α. Further, the origin of the cartesian coordinate system is moved from the lower left corner of the domain to the center of the fiber for the present calculations and all the length parameters are non-dimensionalized by the fiber width, w, in compliance with the non-dimensional trajectory expressions given by equations (4.112) and (4.113) or (4.114) and (4.115)

depending on the type of electrostatic interaction. Next, the stored values of the fluid velocity components are read into the corresponding variables, u and v, which are subsequently non-dimensionalized by the mean fluid velocity normal to the inflow boundary. At this point, the computer returns control to the main program and immediately calls the subroutine IMPINGE.

The calculation of trajectory of a point-mass particle is initiated by supplying to the program the x- and y-coordinates of the starting travel point of the particle along with i and j values of the control volume which contains the starting point. The x- and y- coordinates of the starting point are stored, respectively, in YP(1) and YP(2). Next, in order to determine the fluid velocity at the particle position, it is assumed that the fluid velocity components, UF and VF, vary linealy between adjacent control volume faces with the slope and intercept signified, respectively, by CU2 and CU1 for the u- component and CV2 and CV1 for the v- component, being calculated in the subroutine CONSTS. Having obtained UF and VF at the particle location, its velocity components UP and VP can be calculated according to equations (4.112) and (4.113) or (4.114) and (4.115), respectively, depending on the assumed electrostatic interaction. These starting UP and VP values are necessary for calculating the approximate time that

takes the particle to travel through the starting control volume. This travel time is then divided into many small intervals along which, the trajectory equations are integrated continuously until the particle exits the starting or "old" control volume and enters a new one as verified by checking the particle position at the end of each integration step against the location of the "old" control volume faces in the direction of motion of the particle. The travel time calculations are performed in the subroutine TIMCOR in which, the direction of motion of the particle is determined by the sign of its velocity components and the shortest time taken to cross either the vertical or horizontal face of the "old" control volume is considered as the travel time, TX.

As mentioned, the integrations are carried out using the Runge-Kutta method which was formulated and programmed by the University of Minnesota Computer Center and attached to the present program as subroutine RK which is described in detail below.

At the end of each itegration step, the new particle position is checked to see if it has entered a new control volume and/or "penetrated" through the fiber which is an indication of the particle being captured by the fiber. In the event that the particle is found in a new control volume, its current position is treated as its starting

position in the new control volume and the procedure described above is repeated. The calculations continue until the particle is either captured by the fiber or exits the calculation domain. Of course, the objective of trajectory calculations is to determine the starting y- coordinate of the critical trajectory which, as described in section 4.8.3, is used to determine the single fiber efficiency due to electrostatic forces.

D.1 Runge-Kutta Integration Method

The trajectory equations were integrated using a subroutine from the library of the University of Minnesota Computer Center entitled "Runge-Kutta differential equation solver with variable integration step and automatic error control". This subroutine used Runge-Kutta formulas of fourth order accuracy.

The Runge-Kutta subroutine is called by the following statement

```
CALL RK (TI, TF, YP, F, DERIV, N, EPS, ETA, IDRK, TEMP, DT)
```

where

TI The beginning of time step with which the integaration begins.

TF The end of time step to which the system of equations are to be integrated.

YP An input array of N elements containing unknown dependent variables.

F An output array of N elements containing the derivatives of elements of array YP. For example, in the case of present study,

$$F(1) = \frac{dx^*_p}{dt^*} = u^* - N_C \cdot \sum_{i=1}^{n_c} \left[\frac{x^*_{p_i}}{r^{*2}_{p_i}} - \frac{x^*_{n_i}}{r^{*2}_{n_i}}\right]$$

$$F(2) = \frac{dy^*_p}{dt^*} = v^* - N_C \cdot \sum_{i=1}^{n_c} \left[\frac{y^*_{p_i}}{r^{*2}_{p_i}} - \frac{y^*_{n_i}}{r^{*2}_{n_i}}\right]$$

for the case of Coulombic forces and

$$F(1) = \frac{dx^*_p}{dt^*} = u^* - N_I \cdot \sum_{i=1}^{n_c} \left[\frac{x^*_{p_i}}{r^{*4}_{p_i}} - \frac{x^*_{n_i}}{r^{*4}_{n_i}}\right]$$

$$F(2) = \frac{dy^*_p}{dt^*} = v^* - N_I \cdot \sum_{i=1}^{n_c} \left[\frac{y^*_{p_i}}{r^{*4}_{p_i}} - \frac{y^*_{n_i}}{r^{*4}_{n_i}}\right]$$

for the case of induced forces.

DERIV — Name of a subroutine with 3 parameters in the order of T, YP, F, which computes elements of array F based on given values of T and YP.

N — Number of equations (N = 2 for the present case).

EPS — The relative error allowed in the YP elements in any integration step. A value of 10^{-7} was chosen for EPS in the present calculations.

ETA — An array of N numbers which serves as the absolute error criterion in the automatic stepping process. Each ETA element applies to the corresponding YP element. Both ETA elements in this study were set equal to 10^{-6}.

ID — An input control parameter which is positive for the first call to RK and negative for subsequent calls. When ID is negative, RK uses the same DT (see below) for each portion of the interval to satisfy the error criteria.

TEMP — Temporary storage array which must be dimensioned at least 4*N elements.

DT — The integration step size in the Runge-Kutta equations. When RK is finished, it is the step size for which the system of equations was last being integrated. This is not necessarily (TF - TI) since RK chooses an appropriate DT for each portion of the interval to satisfy the error criteria.

The RK method used here first integrates over the whole time interval in one step, then in two steps and compares the results using the error parameters to see whether or not the interval should be halved and the integration attempted again. If 5 successful steps are made without halving, RK attempts to double the step size. Both relative and absolute error criteria are used and if either is satisfied for all YP elements, integration resumes.

Thus, the accuracy of RK is not governed by the time interval (TF - TI), but rather is governed by the values of EPS ans ETA used. Marple (1970) investigated the effects of values of EPS and ETA on his results by considering the following two cases:

CASE	ETA	EPS
1	10^{-6}	10^{-7}
2	10^{-12}	10^{-12}

He found his results for both cases to be identical up to 6 to 7 significant digits but the computer run time for case 2 was about 16 times longer than that for case 1. Note that the values of case 1 are same as those considered in this study.

```
c*****************************************************************
      call grid
      call impinge
      stop
      end
c*****************************************************************
      subroutine grid
c*****
      parameter (id=40,jd=40)
      common/gridd/xl,x(id),xu(id),xcv(id),xdif(id),l1,l2,l3
     &            ,yl,y(jd),yv(jd),ycv(jd),ydif(jd),m1,m2,m3
      common/const/pi,dp,qch,ichek,xmid,ddis,width,rr,qcharge
      common/flow/u(id,jd),v(id,jd)
c*****************************************************************
c
 597  open (unit=8,file='relec.d',status='OLD')
c      print *,'enter length of calculation domain, xl :'
c      read *,xl
      read(8,*)xl
c      print *,'enter width of calculation domain, yl :'
c      read *,yl
      read(8,*)yl
c      print *,'enter half of width of whole rectangle :'
c      read *,width
      read(8,*)width
c      print *,'enter length of whole rectangle :'
c      read *,xlength
      read(8,*)xlength
c      print *,'enter value of xmid :'
c      read *,xmid
      read(8,*)xmid
c
      open(unit=1,file='es.out',status='UNKNOWN')
      open(unit=9,file='es2.out',status='UNKNOWN')
c*****************************************************************
c
c      print *,'is this run for induction forces or coulombic
c     &        forces (enter "1" for ind. & other for col.)'
      read(8,*)ichek
      if (ichek.eq.1) then
c        print *,'enter the value for dimensionless ind. paramter'
        read(8,*)qcharge
      else
c        print *,'enter value for dimensionless coulombic parameter:'
        read(8,*)qcharge
      endif
c
      qch=qcharge
      dh=(4.0*width*xlength)/(2.*width+xlength)
      pi=3.1415926
      rhoo=1.206
      amu=18.30
      amwall=1.0e15
      rr=xlength/2.
c
c
      xu(2)=0.0
      mulx=3
      xx=rr
      xr=xmid-xx-0.050
      ib=7
      do 10 i=3,ib
  10  xu(i)=xu(i-1)+xr/(ib-2)
      dx=0.01
      if (mulx.ne.0) then
      do 1000 i=1,mulx
 1000 xu(ib+i)=xmid-xx-(mulx-i+1)*dx
      endif
      ipp=ib+mulx+1
      xu(ipp)=xmid-xx
c
  13  continue
       do 12 i=ipp+1,ipp+8
        xu(i)=xu(i-1)+rr/9.0
      ip=i
  12  continue
      do 14 i=1,ip-2
      ipp=i+ip
      xu(ipp)=xmid-xu(ip+1-i)+xmid
  14  continue
      l1=ipp+1
      xu(l1)=xl
      dx1=xmid-rr
      dx2=xmid+rr
c
c     this loop determines the 'l' begin and end locations of the
c     solid rectangle for later use in gamsor where a large gamma
```

```
c
      do 22 i=ib,i1
      if ((xu(i)-dx1).le.0.00000001) ibgam=i
      if ((xu(i)-dx2).le.0.00000001) iegam=i-1
   22 continue
c
      yv(2)=0.0
      je=9
      do 15 j=3,je
      yv(j)=yv(j-1)+width/(je-2)
   15 continue
      muly=3
      dy=0.01
      if (muly.ne.0) then
      do 16 j=1,muly
   16 yv(je+j)=width+j*dy
      endif
      jdd=je+muly+1
      yv(jdd)=width+0.050
      dyy=(yl/2.)-yv(jdd)
      do 17 j=jdd+1,jdd+4
      yv(j)=yv(j-1)+dyy/4.
      jpp=j
   17 continue
      yhaf=yl/2.
      do 18 j=1,jpp-3
      jp=jpp+j
      yv(jp)=(yhaf-yv(jpp-j))+yhaf
   18 continue
      m1=jp+1
      yv(m1)=yl
  705 continue
c
      alpha=width*xlength/(xl*yl)
C
      l2=i1-1
      l3=l2-1
      m2=m1-1
      m3=m2-1
      ddis=width
      x(1)=xu(2)
      do 5 i=2,l2
    5 x(i)=0.50*(xu(i+1)+xu(i))
      x(i1)=xu(i1)
      do 6 i=2,i1
    6 xu(i)=(xu(i)-xmid)/ddis
      do 7 i=1,i1
    7 x(i)=(x(i)-xmid)/ddis
      xl=xl/ddis
c
      y(1)=yv(2)
      do 2001 j=2,m2
 2001 y(j)=0.50*(yv(j+1)+yv(j))
      y(m1)=yv(m1)
c
      do 2005 j=1,m1
      yv(j)=yv(j)/ddis
 2005 y(j)=y(j)/ddis
      yl=yl/ddis
c
      do 2002 i=2,i1
 2002 xdif(i)=x(i)-x(i-1)
      do 2003 i=2,l2
 2003 xcv(i)=xu(i+1)-xu(i)
c
      do 35 j=2,m1
   35 ydif(j)=y(j)-y(j-1)
      do 2004 j=2,m2
 2004 ycv(j)=yv(j+1)-yv(j)
c***
calculate fiber aspect ratio
c
      bovera=xlength/(2.*width)
c     print grid locations
      write(1,148)
      write(1,149)
      write(1,150)
      write(1,151)
c***
      if (ichek.eq.1) write(1,483)
      if (ichek.ne.1) write(1,484)
      write(1,485)qch
c      write(1,421)
      write(1,422)xl,yl,alpha
      write(1,423)width,xlength
      write(1,486)bovera,dh
c
```

```
1001 if (lend.eq.l1) go to 1010
     ibeg=iend+1
     iend=iend+9
     iend=min0(lend,l1)
     write(1,50)
     write(1,51)(i,i=ibeg,iend)
     write(1,56)(xu(i),i=ibeg,iend)
     go to 1001
1010 jend=0
     write(1,50)
1011 if (jend.eq.m1) go to 1020
     jbeg=jend+1
     jend=jend+9
     jend=min0(jend,m1)
     write(1,50)
     write(1,54)(j,j=jbeg,jend)
     write(1,57)(yv(j),j=jbeg,jend)
     go to 1011
1020 continue
c
c      print *,'enter name of velocity data file :'
     open(unit=3,file='ruvbal4.02',status='UNKNOWN')
c
c     read the u and v velocity values already calculated and
c     stored in the above data file
c
     do 40 nf=1,2
     if (nf.eq.1)read(3,420)((u(i,j),i=1,l1),j=1,m1)
     if (nf.eq.2)read(3,420)((v(i,j),i=1,l1),j=1,m1)
 420 format(1x,10(e12.5,1x))
  40 continue
     close(unit=3)
c
c     modify boundary conditions according to periodic flow
c     assumption
c
     do 2791 j=2,m2
2791 u(l1,m2-j+2)=u(2,j)
     do 2792 j=3,m2
2792 v(l1,m2-j+3)=-v(1,j)
c
     usum=0.0
     do 41 j=2,m2
  41 usum=usum+u(2,j)*ycv(j)
     uavg=usum/yl
     re=rhoa*uavg*dh/amu
c
c     non-dimensionalize velocity components by mean velocity
c
     do 2006 i=2,l1
     do 2006 j=2,m1
     u(i,j)=u(i,j)/uavg
     v(i,j)=v(i,j)/uavg
2006 continue
c
c     write(9,*)((u(2,j),u(l1,j)),j=2,m2)
c
     write(1,487)
     write(1,488)re
     write(1,487)
  50 format(1x,1h )
  51 format(1x,'i =',2x,9(i4,8x))
  54 format(1x,'j =',2x,9(i4,8x))
  56 format(1x,'xu =',1p9e12.4)
  57 format(1x,'yv =',1p9e12.4)
 148 format('calculation of particle trajectory around a rectan.')
 149 format('fiber under influence of electrostatic field')
 150 format('*****************************************************')
 151 format(' ')
c
 421 format(/,30x,'rectangular geometry')
 422 format(/,2x,'xi=',f6.2,5x,'yi=',f6.2,5x,'alpha=',f8.4)
 482 format(/,2x,'particle radius : ',e10.5)
 423 format(/,2x,'half of width of rectangle :',f10.5,/,2x,
    +       'length of rectangle :'f10.5)
 483 format(/,2x,'electrostatic forces due to induction charging')
 484 format(/,2x,'electrostatic forces due to coulombic charging')
 485 format(/,2x,'corresponding dimensionless parameter :',e12.4)
 486 format(/,2x,'b/a ratio :',f10.4,10x,'hyd. diameter :',f10.4)
 487 format('*****************************************************')
 488 format(2x,'reynolds # :',f12.4)
c
     return
     end
c
c*****************************************************************
     subroutine impinge
```

```
      parameter (id=40,jd=40)
      common/gridd/x1,x(id),xu(id),xcv(id),xdif(id),l1,l2,l3,
     &             y1,y(jd),yv(jd),ycv(jd),ydif(jd),m1,m2,m3
      common/const/pi,dp,qch,ichek,xmid,ddis,width,rr,qcharge
      common/flow/u(id,jd),v(id,jd)
      common/flocon/cu1,cu2,cv1,cv2
      common/user/iinit,jinit
      dimension yp(2),f(2),eta(2),temp(20)
      dimension ypv(50),ynv(50)
      common xpc(50),xnc(50),yc(50)
      dimension xpv(50),xnv(50),rp(50),rn(50)
      external deriv
c*****************************************************************
      data eta/2*1.e-6/
c
      print *,'enter starting x-location of particle in
     &dimensional form :'
      read*,xpinit
      print *,'enter starting y-location of particle in
     &dimensional form :'
      read*,ypinit
c
c     non-dimensionalize length parameters by width of rectangle
c
      xpinit=(xpinit-xmid)/ddis
      ypinit=ypinit/ddis
c
      write(1,3000)xpinit,ypinit
      print *,'enter i & j values for the c.v. of start :'
      print *,'enter i :'
      read *,i
      print *,'enter j :'
      read *,j
      write(1,3001)i,j
 3001 format(/,2x,'starting i value :',i5,/,2x,'starting
     &       j value',i5)
 3000 format(/,2x,'initial x-location of particle in dimension-
     &       less form :',f10.4,/,2x,'initial y-location of
     &       particle in dimension-less form:',f10.4)
c
      nstep=0
      tf=0.0
      yp(1)=xpinit
      yp(2)=ypinit
      call consts(i,j)
c
calculate fluid velocity at particle position
c
      uf=cu1+cu2*yp(1)
      vf=cv1+cv2*yp(2)
c
cplace line charges on fiber and calculate their coordinates
c
      nc=50
      do 4501 ik=1,nc
       xpc(ik)=-rr/ddis
       xnc(ik)=rr/ddis
 4501 continue
      yinc=width/(nc-1)
      do 4502 jk=1,nc
       yc(jk)=(jk-1)*yinc/ddis
 4502 continue
c
      x1=0.0
      x2=0.0
      xsum=0.0
      do 3500 ik=1,nc
       rp(ik)=(yp(1)-xpc(ik))**2+(yp(2)-yc(ik))**2
       rn(ik)=(yp(1)-xnc(ik))**2+(yp(2)-yc(ik))**2
      xpv(ik)=yp(1)-xpc(ik)
      xnv(ik)=yp(1)-xnc(ik)
        if (ichek.eq.1) then
         rp(ik)=rp(ik)**2
         rn(ik)=rn(ik)**2
         x1=x1+(xpv(ik)/rp(ik))
         x2=x2+(xnv(ik)/rn(ik))
         go to 3500
        endif
      xsum=xsum+(xpv(ik)/rp(ik))-(xnv(ik)/rn(ik))
 3500 continue
      if (ichek.eq.1) then
       if (yp(1).lt.xu(11).or.yp(1).gt.xu(28)) then
        if (abs(x1).ge.abs(x2)) xsum=x1-x2
        if (abs(x1).lt.abs(x2)) xsum=x2-x1
       else
         xsum=x1+x2
       endif
```

```
c
      y1=0.0
      y2=0.0
      ysum=0.0
      do 3501 jk=1,nc
       ypv(jk)=yp(2)-yc(jk)
       ynv(jk)=yp(2)-yc(jk)
       if (ichek.eq.1) then
         y1=y1+(ypv(jk)/rp(jk))
         y2=y2+(ynv(jk)/rn(jk))
         go to 3501
       endif
       ysum=ysum+(ypv(jk)/rp(jk))-(ynv(jk)/rn(jk))
 3501 continue
      if (ichek.eq.1) then
        if (abs(y1).ge.abs(y2)) ysum=y1-y2
        if (abs(y1).lt.abs(y2)) ysum=y2-y1
      endif
c
c     write(1,3502)((xpc(k),xnc(k),yc(k),rp(k),rn(k)
c    &,xpv(k),xnv(k)),k=1,nc)
 3502 format(1x,1p7e10.3)
c     write(1,3503)xsum,ysum
 3503 format(/,'xsum = ',f12.4,10x,'ysum = ',f12.4)
c
calculate particle velocity components
c
      up= uf+qch*xsum
      vp=vf+qch*ysum
c
      write(1,3002)
      write(1,25)i,j,yp(1),yp(2),uf,vf,up,vp
      write(1,3007)
c     write(9,3007)
 3007 format(/,2x,'i',2x,'j',11x,'x',11x,'y',10x,'tf',
     &       10x,'tx',10x,'dt',10x,'step')
   25  format(2i3,1p6e12.3)
 3002 format(/,2x,'i',2x,'j',11x,'x',11x,'y',10x,'uf',
     &       10x,'vf',10x,'up',10x,'vp')
c
   26  call consts(i,j)
      idrk=1
      call timcor(i,j,tx,yp)
   30  ti=tf
      tf=ti+0.01*tx
      if (ichek.eq.1.and.yp(2).lt.1.0) then
      if (yp(1).gt.xu(10).and.yp(1).lt.xu(11)) tf=ti+tx
      if (yp(1).gt.xu(28).and.yp(1).lt.xu(29)) tf=ti+tx
      endif
      nstep=nstep+1
c
call the runge-kutta subroutine to begin integrations
c
      call rk(ti,tf,yp,f,deriv,2,1.e-7,eta,idrk,temp,dt)
c
      idrk=-1
      iold=i
      jold=j
c*****check if particle has crossed grid lines.
c
      if (yp(1).ge.xu(i+1)) i=i+1
      if (yp(1).lt.xu(i)) i=i-1
      if (yp(2).ge.yv(j+1))j=j+1
      if (yp(2).lt.yv(j)) j=j-1
c
c*****following valid for point-mass particles.
c
      if (iold.eq.i.and.jold.eq.j) go to 30
      write(1,3003) i,j,yp(1),yp(2),tf,tx,dt,nstep
c     write(9,3004)i,j,yp(1),yp(2)
 3004 format(2i3,1p2e12.4)
      print *,i,j,yp(1),yp(2)
 3003 format(2i3,1p5e12.4,i14)
c
c*****check if particle hits rectangle
c
      xlimit=rr/ddis
      ylimit=width/ddis
c      print *,xlimit,ylimit,yp(1),yp(2)
      if (abs(yp(1)).le.xlimit.and.yp(2).le.ylimit) then
         write(1,170)
         print *,'particle impacts on the fiber'
         go to 168
      endif
      if (yp(2).le.1.0) then
      if (yp(1).gt.xu(10).and.yp(1).le.xu(11)) then
       write(1,170)
```

```
c
      y1=0.0
      y2=0.0
      ysum=0.0
      do 3501 jk=1,nc
       ypv(jk)=yp(2)-yc(jk)
       ynv(jk)=yp(2)-yc(jk)
       if (ichek.eq.1) then
         y1=y1+(ypv(jk)/rp(jk))
         y2=y2+(ynv(jk)/rn(jk))
         go to 3501
       endif
       ysum=ysum+(ypv(jk)/rp(jk))-(ynv(jk)/rn(jk))
 3501 continue
      if (ichek.eq.1) then
        if (abs(y1).ge.abs(y2)) ysum=y1-y2
        if (abs(y1).lt.abs(y2)) ysum=y2-y1
      endif
c
c     write(1,3502)((xpc(k),xnc(k),yc(k),rp(k),rn(k)
c    &,xpv(k),xnv(k)),k=1,nc)
 3502 format(1x,1p7e10.3)
c     write(1,3503)xsum,ysum
 3503 format(/,'xsum = ',f12.4,10x,'ysum = ',f12.4)
c
calculate particle velocity components
c
      up= uf+qch*xsum
      vp=vf+qch*ysum
c
      write(1,3002)
      write(1,25)i,j,yp(1),yp(2),uf,vf,up,vp
      write(1,3007)
c     write(9,3007)
 3007 format(/,2x,'i',2x,'j',11x,'x',11x,'y',10x,'tf',
     &       10x,'tx',10x,'dt',10x,'step')
  25  format(2i3,1p6e12.3)
 3002 format(/,2x,'i',2x,'j',11x,'x',11x,'y',10x,'uf',
     &       10x,'vf',10x,'up',10x,'vp')
c
  26  call consts(i,j)
      idrk=1
      call timcor(i,j,tx,yp)
  30  ti=tf
      tf=ti+0.01*tx
      if (ichek.eq.1.and.yp(2).lt.1.0) then
      if (yp(1).gt.xu(10).and.yp(1).lt.xu(11)) tf=ti+tx
      if (yp(1).gt.xu(28).and.yp(1).lt.xu(29)) tf=ti+tx
      endif
      nstep=nstep+1
c
call the runge-kutta subroutine to begin integrations
c
      call rk(ti,tf,yp,f,deriv,2,1.e-7,eta,idrk,temp,dt)
c
      idrk=-1
      iold=i
      jold=j
c*****check if particle has crossed grid lines.
c
      if (yp(1).ge.xu(i+1)) i=i+1
      if (yp(1).lt.xu(i)) i=i-1
      if (yp(2).ge.yv(j+1))j=j+1
      if (yp(2).lt.yv(j)) j=j-1
c
c*****following valid for point-mass particles.
c
      if (iold.eq.i.and.jold.eq.j) go to 30
      write(1,3003) i,j,yp(1),yp(2),tf,tx,dt,nstep
c     write(9,3004)i,j,yp(1),yp(2)
 3004 format(2i3,1p2e12.4)
      print *,i,j,yp(1),yp(2)
 3003 format(2i3,1p5e12.4,i14)
c
c*****check if particle hits rectangle
c
      xlimit=rr/ddis
      ylimit=width/ddis
c      print *,xlimit,ylimit,yp(1),yp(2)
      if (abs(yp(1)).le.xlimit.and.yp(2).le.ylimit) then
         write(1,170)
         print *,'particle impacts on the fiber'
         go to 168
      endif
      if (yp(2).le.1.0) then
      if (yp(1).gt.xu(10).and.yp(1).le.xu(11)) then
       write(1,170)
```

```
       go to 168
      endif
c
      if (yp(1).ge.xu(28).and.yp(1).lt.xu(29)) then
       write (1,170)
       print *,'particle impacted on the fiber'
       go to 168
      endif
      endif
c
      if (yp(1).gt.xu(11).and.yp(1).lt.xu(28)) then
         if (yp(2).le.1.0) then
            write (1,170)
            print *,'particle impacted on the fiber'
            go to 168
         endif
      endif
c
      if (yp(1).gt.xu(11))write(1,172)
      if (yp(2).gt.yv(m1))write(1,173)
      if (yp(2).lt.yv(2))write(1,174)
c****check for error in grid location indexing
      if (yp(1).gt.xu(i+1).or.yp(1).lt.xu(i)) go to 160
      if (yp(2).gt.yv(j+1).or.yp(2).lt.yv(j)) go to 161
      go to 26
  160 write(1,165)
      go to 168
  161 write(1,166)
c
 165  format('incorrect grid indexing in x-direction')
 166  format('incorrect grid indexing in y-direction')
 170  format('particle impacted on rectangle')
 171  format('particle impacted on top of rectangle.')
 172  format('particle exiting domain from right')
 173  format('particle exiting domain from left')
 174  format('particle exiting domain from bottom')
c
 168  return
      end
c
c*************************************************************
c    assuming a linear variation of u and v between adjacent c.v.
c    faces, this subroutine calculates the slope and intercept for
c    calculation of fluid velocity at particle position
c*****
      subroutine consts(i,j)
c*****
      parameter (id=40,jd=40)
      common/gridd/xl,x(id),xu(id),xcv(id),xdif(id),l1,l2,l3
     &           ,yl,y(jd),yv(jd),ycv(jd),ydif(jd),m1,m2,m3
      common/const/pi,dp,qch,ichek,xmid,ddis,width,rr,qcharge
      common/flow/u(id,jd),v(id,jd)
      common/flocon/cu1,cu2,cv1,cv2
      dimension yp(2),f(2),eta(2),temp(20)
c*****
      dx=xu(i+1)-xu(i)
      dy=yv(j+1)-yv(j)
      dudx=(u(i+1,j)-u(i,j))/dx
      dvdy=(v(i,j+1)-v(i,j))/dy
      cu1=u(i,j)-dudx*xu(i)
      cu2=dudx
      cv1=v(i,j)-dvdy*yv(j)
      cv2=dvdy
c*****
      return
      end
c*****************************************************************
c     this subroutine approximates the minimum time taken by particle
c     to cross a control volume
c
      subroutine timcor(i,j,tx,yp)
c*****
      parameter(id=40,jd=40)
      common/gridd/xl,x(id),xu(id),xcv(id),xdif(id),l1,l2,l3,
     &           yl,y(jd),yv(jd),ycv(jd),ydif(jd),m1,m2,m3
      common/const/pi,dp,qch,ichek,xmid,ddis,width,rr,qcharge
      common/flow/u(id,jd),v(id,jd)
      common/flocon/cu1,cu2,cv1,cv2
      dimension yp(2),f(2),eta(2),temp(20)
      dimension ypv(50),ynv(50)
      common xpc(50),xnc(50),yc(50)
      dimension xpv(50),xnv(50),rp(50),rn(50)
c*****
      uf=cu1+cu2*yp(1)
      vf=cv1+cv2*yp(2)
c      r=yp(1)**2+yp(2)**2
c      if (ichek.eq.1) r=r**2
```

```
c      vp=vf+qch*yp(2)/r
       nc=50
       x1=0.0
       x2=0.0
       xsum=0.0
       do 3500 ik=1,nc
        rp(ik)=(yp(1)-xpc(ik))**2+(yp(2)-yc(ik))**2
        rn(ik)=(yp(1)-xnc(ik))**2+(yp(2)-yc(ik))**2
       xpv(ik)=yp(1)-xpc(ik)
       xnv(ik)=yp(1)-xnc(ik)
         if (ichek.eq.1) then
          rp(ik)=rp(ik)**2
          rn(ik)=rn(ik)**2
          x1=x1+(xpv(ik)/rp(ik))
          x2=x2+(xnv(ik)/rn(ik))
          go to 3500
         endif
       xsum=xsum+(xpv(ik)/rp(ik))-(xnv(ik)/rn(ik))
 3500 continue
       if (ichek.eq.1) then
         if (yp(1).lt.xu(11).or.yp(1).gt.xu(28)) then
          if (abs(x1).ge.abs(x2)) xsum=x1-x2
          if (abs(x1).lt.abs(x2)) xsum=x2-x1
         else
          xsum=x1+x2
         endif
       endif
c
       y1=0.0
       y2=0.0
       ysum=0.0
       do 3501 jk=1,nc
        ypv(jk)=yp(2)-yc(jk)
        ynv(jk)=yp(2)-yc(jk)
        if (ichek.eq.1) then
          y1=y1+(ypv(jk)/rp(jk))
          y2=y2+(ynv(jk)/rn(jk))
          go to 3501
        endif
        ysum=ysum+(ypv(jk)/rp(jk))-(ynv(jk)/rn(jk))
 3501 continue
       if (ichek.eq.1) then
         if (abs(y1).ge.abs(y2)) ysum=y1-y2
         if (abs(y1).lt.abs(y2)) ysum=y2-y1
       endif
c
       up= uf+qch*xsum
       vp=vf+qch*ysum
c*****
       if (up) 1,2,2
    1  tx1=abs((xu(i)-yp(1))/up)
       go to 3
    2  tx1=abs((xu(i+1)-yp(1))/(up+1.0e-20))
    3  if (vp) 4,5,5
    4  tx2=(yv(j)-yp(2))/vp
       go to 6
    5  tx2=(yv(j+1)-yp(2))/(vp+1.0e-20)
    6  continue
       tx=amin1(tx1,tx2)
       if (tx.lt.1.0e-15) tx=1.0e-10
       if (tx.gt.0.5) tx=0.5
c*****
       return
       end
c*************************************************************
c      this subroutine is called by the rk program for calculation of
c      derivatives of particle position coordinates
c
       subroutine deriv(t,yp,f)
c*****
       parameter(id=40,jd=40)
       common/gridd/xl,x(id),xu(id),xcv(id),xdif(id),l1,l2,l3,
      &             yl,y(jd),yv(jd),ycv(jd),ydif(jd),m1,m2,m3
       common/const/pi,dp,qch,ichek,xmid,ddis,width,rr,qcharge
       common/flow/u(id,jd),v(id,jd)
       common/flocon/cu1,cu2,cv1,cv2
       dimension yp(2),f(2),eta(2),temp(20)
       dimension ypv(50),ynv(50)
       common xpc(50),xnc(50),yc(50)
       dimension xpv(50),xnv(50),rp(50),rn(50)
c*****
       uf=cu1+cu2*yp(1)
       vf=cv1+cv2*yp(2)
       nc=50
       x1=0.0
       x2=0.0
       xsum=0.0
```

```
       rp(ik)=(yp(1)-xpc(ik))**2+(yp(2)-yc(ik))**2
       rn(ik)=(yp(1)-xnc(ik))**2+(yp(2)-yc(ik))**2
      xpv(ik)=yp(1)-xpc(ik)
      xnv(ik)=yp(1)-xnc(ik)
        if (ichek.eq.1) then
         rp(ik)=rp(ik)**2
         rn(ik)=rn(ik)**2
         x1=x1+(xpv(ik)/rp(ik))
         x2=x2+(xnv(ik)/rn(ik))
         go to 3500
        endif
      xsum=xsum+(xpv(ik)/rp(ik))-(xnv(ik)/rn(ik))
 3500 continue
      if (ichek.eq.1) then
       if (yp(1).lt.xu(11).or.yp(1).gt.xu(28)) then
         if (abs(x1).ge.abs(x2)) xsum=x1-x2
         if (abs(x1).lt.abs(x2)) xsum=x2-x1
        else
        xsum=x1+x2
       endif
      endif
c
      y1=0.0
      y2=0.0
      ysum=0.0
      do 3501 jk=1,nc
       ypv(jk)=yp(2)-yc(jk)
       ynv(jk)=yp(2)-yc(jk)
       if (ichek.eq.1) then
         y1=y1+(ypv(jk)/rp(jk))
         y2=y2+(ynv(jk)/rn(jk))
         go to 3501
       endif
       ysum=ysum+(ypv(jk)/rp(jk))-(ynv(jk)/rn(jk))
 3501 continue
      if (ichek.eq.1) then
        if (abs(y1).gt.abs(y2)) ysum=y1-y2
        if (abs(y1).lt.abs(y2)) ysum=y2-y1
      endif
c
      f(1)= uf+qch*xsum
      f(2)=vf+qch*ysum
c*****
      return
      end
c**************************************************************
c
```